ment. Factor score map is shown as PL I–7–2.

As shown in Fig. I–13, it is known that the 50% value of F is the same in L_2 and L_3 and small in L_4. This is not contradictory to the geological data that dolomite is preponderantly small in amount in L_4 compared with L_2 and L_3.

1–2–5 Conclusion of Ore Genesis

It is important for the study of genetic mechanism of vein-type lead (and zinc) ore deposit that

(1) to make clear the geologic structure and

(2) to make geochemical investigation of the country rock of ore deposit,

because lead isotopes show different time of the fractures and ore deposits.

As for (1), ore deposits such as Furnas, Lageado, Espirito Santo and Pavão are distributed at the part of limbs of the Calabouço syncline and the Serra Manduri ~ Foqouilha anticline of the first order in the area as shown in PL I–4.

The characteristics of relationship of ore deposits and geologic structure are described as following.

The Furnas ore deposits are located at the place where the thickness of the host rock is extremely reduced, the Lageado deposits are located at the place where the thickness becomes maximum.

The Lageado deposit and its surrounding area are positioned at the bottom of the Lageado syncline of the second order of the area, which is overlapped by the fold structure of NNW–SSE system. The Espirito Santo deposit is located also on the limbs of the Espirito Santo anticline and the Espirito Santo syncline of the third order of the area.

The vein fractures of deposit seem to have been formed in the more competent carbonate rocks than the meta sedimentary rocks caused by buckle folding by lateral compression of the NW–SE system took place in the stage of the Brazilian Orogeny which formed the fold structure of approximate NE-SW system of the area.

It is assumed that the fractures emplacing ore deposits have been formed in the trap overlapped with fold structure of different order or direction, and in the remarkable change of thickness of the host rock.

As the result of microanalysis of carbonate rocks, factor 1 seems to indicate the sedimentary environment of the host rock, and the factor 2 is likely to be related to the mineralization, and they are overlapped on the most part of them. The known ore deposits have been confirmed in the area of the factor 2 as mentioned above.

On the basis of the facts mentioned above it can be considered that deposition of Pb–Ag–(Zn) took place simultaneously with sedimentation of carbonate rocks under the reducing environment and that Pb–Ag–(Zn) have moved and concentrated to the fractures formed in the stage of Brazilian Orogeny.

On the Lageado deposit and the copper showings in the upstream of Rio Betari are considered that the ore deposits are hydrothermal in origin associated with the activity of granitic rocks, because these deposits show a different appearance from the lead ore deposits above mentioned such as that small dykes of granitic rocks are found in the vicinity and that the gangue mineral is quartz, which has given some hydrothermal effect to the wall rocks.

1–2–6 Future Exploration

The area to be possible of existence of promising ore deposit in the survey area is limited to the surrounding area of the Furnas mine based on the geologic structure and the result of microanalysis of the carbonate rocks.

In the Furnas mine, relatively regularly arranged large ore bodies have been exploited, therefore, in the surrounding area of the mine, especially in the southwestern part is expected the existence of mineralization.

In the area of ore deposit from Lageado to Serra, a number of old adits are found though they are discontinuous, which leads to the possibility of finding new ore deposit of a small scale.

CHAPTER 2 DETAILED SURVEY AREA

As the result of survey of the second year, the Perau area and the Barinha area were selected to be carried on detailed survey.

In the survey of the Perau area, a detailed geological survey was conducted along the IP survey line carried out successively to the second year. As the result, a part of distribution of geology in the geological map (1 : 10,000) produced in the second year was modified. There is, however, no fundamental alteration in stratigraphy and structure.

In addition, drilling survey was conducted in an area close to the G-line of IP survey line which had been selected as a promising area as the result of geological survey and geophysical prospecting of the second year.

In the survey of the Barrinha area, a detailed geological survey was conducted along the survey lines of IP and SIP, and along the main road.

2–1 Geology and Ore Deposits of the Perau Area

2–1–1 Summary of the Perau Mine

The Perau mine is situated about 25 kilometers to the south of Adrianopolis. The mine office and the entrances of adits are located along the upstream of Ribeirão do Perau, a tributary of Ribeirão Grande, at about 1.5 kilometers from the confluence.

The Perau deposit in operation is a stratiform lead deposit embedded in limestone, dolomite to carbonate schists of the Açungui I formation. The main adits have been exploited on four levels of G_1 to G_4, and seven sublevels have been excavated between those main adits at a vertical interval of about 10 meters.

2–1–2 Geology

Geology of the Perau mine is composed of the Setuva formation and the Açungui I formation from the bottom upward (Fig. I–15 · I–16, PL. I–9).

The area is located in the northern part of the Agua Clara anticline which has an exis of the NE system, and has been affected by the fold structure of the Perau anticline and the Faria syncline.

(1) Setuva Formation (Sgn)

The Setuva formation is distributed in the upstream area of Ribeirão do Perau, and forms the axial part of the Agua Clara anticline, showing general strikes of N20° ~ 40°E and dips of 20° ~35°NW.

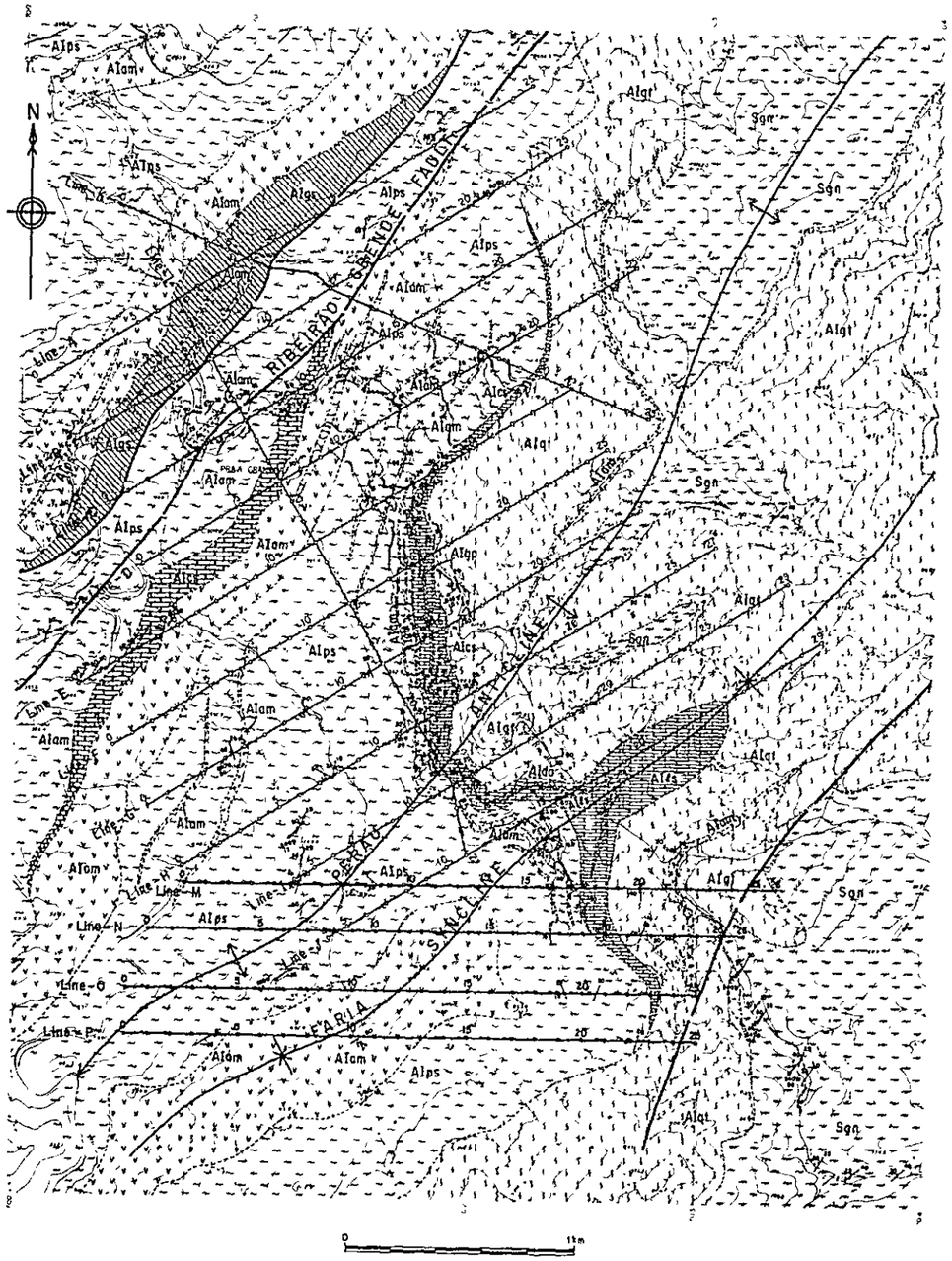

LEGEND

Apungus Formation I

- Algs — Graphite schist
- Alca — calc – schist
- Alam — Amphibolite , amphybole schist
- Alps — Mica schist
- Aldo — Dolomite layer
- Algp — Graphite schist, phyllite layer
- Alds — Limestone, dolomite, calc-silicate rock, barite and sulphides "Perau horizon"
- Algt — Quartzite, with amphibolite

Setuva Formation

- Sgn — Gneiss with minor amphibolite

- Anticlinal axis
- Synclinal axis
- Fault
- Bedding
- Schistosity
- Lineation
- Plunge of fold

Fig. I —15 Geological Map of Perau Area

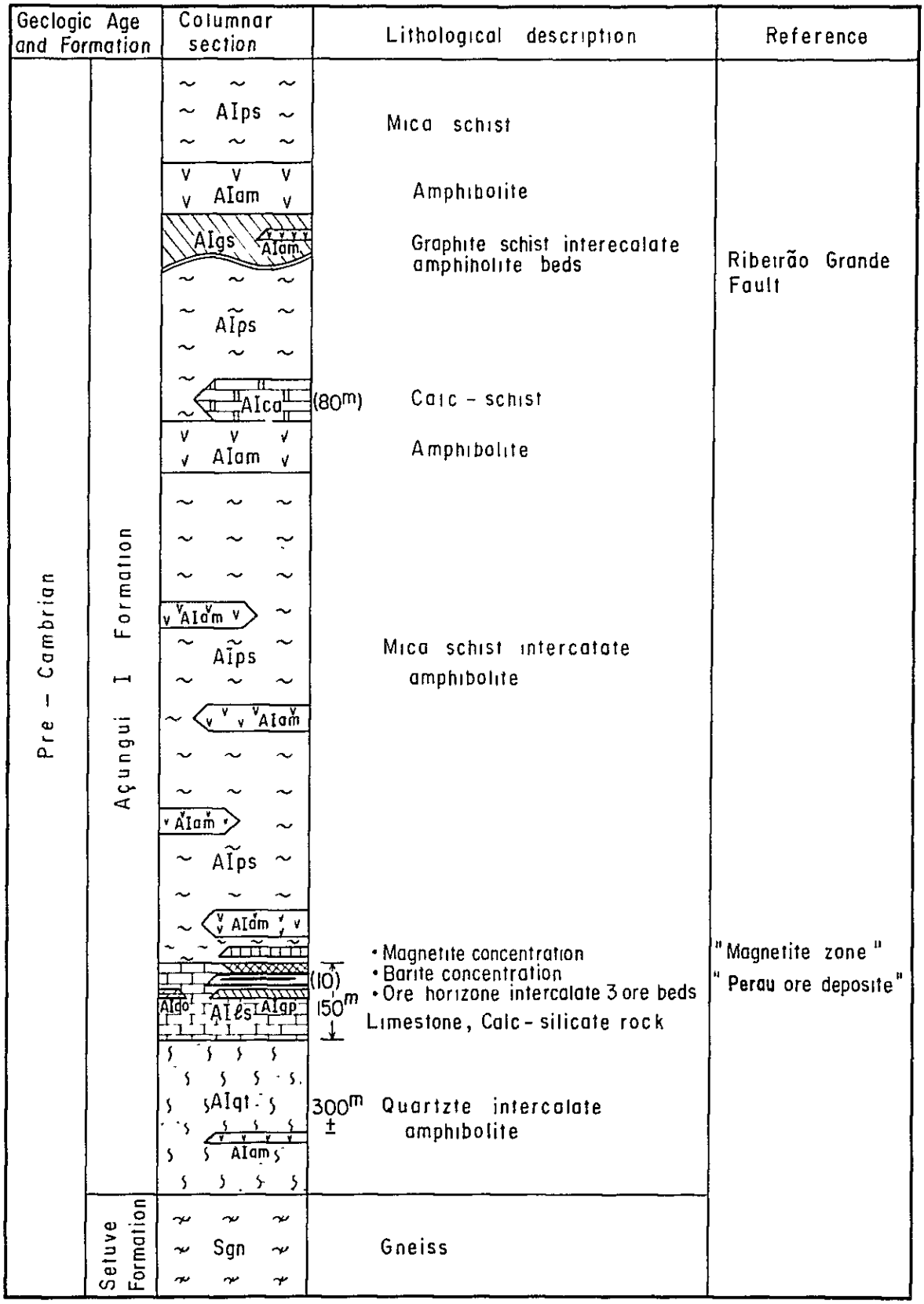

Fig. I–16 Generalized Stratigraphic Columnar Section in Perau Area

The main rock facies are gneissose rocks such as mica-biotite gneiss, and augen gneiss interbedded with biotite-epidote-hornblende-amphibole schist.

(2) Açungui I Formation

The Açungui I formation, the lowermost formation of the Açungui group is widely spread, conformably overlying the Setuva formation.

The rocks of the formation ,from the base upward, are quartzite, limestone, dolomite to carbonate schist, interbedded with the Perau deposit, mica schist and amphibolite.

(a) Quartzite (AIqt)

The rock is white to pale gray, compact and massive, and seems to be about 300 meters in thickness. It grades into limestone and dolomite to carbonate schist of the upper sequence putting the alternating beds of these rocks between them.

The drill cores (AG–01 and AG–02) showed that Quartzite formed an alternation with carbonate schist. It contains carbonate materials even in the part which is seemingly quartzite.

Very small siliceous breccias which seem to have originally deposited are observed in the drill core of the hole AG–02.

In the drill core logging, it was interpreted that the horizon of quartzite is below the top point of the alternation.

(b) Limestone·dolomite – Carbonate schist (AIlm)

The rock facies is the horizon of the Perau deposit. It is distributed from the northwest of the Perau mine toward the south showing a "S" shape, thinning out within the survey area of this year.

The main rock facies are alternating beds of limestone, dolomite, carbonate schist and pelitic to siliceous schist. The alternating beds of carbonate schist and pelitic to siliceous schist are dominant in the surrounding area of the mine.

Graphite schist forms an intertrappean bed in the footwall of the ore deposit, is an effective key bed.

A barite zone accompanied by mineralization occurs in the hanging-wall of the Perau deposit. It is distributed in lenticular to strata bound shapes with dissemination of lead and pyrite weakly in some part of the mine.

The barite zone can be observed in the drill cores (AG–01, AG–02 and AG–03), which dominantly occurs being accompanied with stratiform deposit of lead and zinc of the thickness of two to 10 meters.

A zone of magnetite concentration, five to 10 meters thick, is observed in the hanging-wall 10 to 20 meters upward from the above ore horizon as a "magnetite zone", which is

found on the surface exposure, in the underground and also in the drill cores. It is effective for a key bed on the hangingwall side of the ore deposit.

(c) Mica schist (Alps)

The rock is medium to fine-grained gray to dark gray schist with distinct schistosity.

The main constituent minerals are quartz, biotite, muscovite, accompanied by plagioclase, garnet, hornblende and tremolite. Coarse porphyroblastic garnet is often observed in the drill core.

Graphitic material is often found, and pyrite is observed in these part in the shape of film along the schistosity.

Mica schist is divided into two sub-facies of muscovite schist predominated by muscovite, and biotite schist predominated by biotite, depending on the combination of minerals described in the above.

The former occurs dominantly from the west of the mine toward the northern part, while the latter toward the southern part.

The graphitic material increases in amount more in biotite schist.

(d) Amphibolite ~ amphibole schist

Mica schist is conformably interstratified with numerous layers of amphibolite or amphibole schist. The rocks are medium to fine grained and dark gray to dark green, displaying homogeneous or heterogeneous, massive to bandded structures.

The part with dominant massive structure is considered to have been basic lava in origin, showing a very weak schistosity. The original rock of the part predominated with schistosity is considered to have been volcanic tuff, showing a rock facies of biotite-amphibole schist, being mixed with pelitic materials.

Since both rock facies are distributed in harmonious with mica schist, the original rocks of them are considered to be basic lava and volcanic effusives of the same source.

The rocks are distributed from five to 10 meters above the Perau ore horizon, showing a thickness of several meters up to more than 200 meters.

Three to four major layers are observed in the drill cores, and other several thin layers have also been confirmed in them.

Under the microscope, nematoblastic to porphyroblastic textures are characteristic. The main constituent minerals are plagioclase, actinolite, epidote and hornblende, with small amount of quartz.

2–1–3 Geologic Structure

The main geologic structure of the area surrounding the Perau mine is controlled by the Perau anticline and the Faria syncline of NE–SW system.

The fault structures are not conspicuous in the area of survey excepting the Riberão Grande fault found on the northwest of the Perau mine.

The Perau anticline and the Faria syncline are distributed in prallel with each other, having general trend of axes of N39° ~ 50°E.

The Perau horizon (AIIs) which contains ore deposit shows a distribution of "S" shape affected by both the Perau anticline and the Faria syncline. The Perau horizon pinches out toward the south in the area of survey of this year.

The Perau mine is located on the northwestern limb of the Perau anticline. Structures of minor folding and microfolding are often observed in the underground, and it has been known that the chute of the ore deposit and the directions of these small fold structure are harmonious.

Minor folding and microfolding are often observed in mica schist and carbonate schist in the drill cores. The geological cross section of drill holes shows that the Perau horizon is distributed almost in monoclinic structure and no disturbance of geologic structure is observed.

2–1–4 Ore Deposits

(1) Summary of Ore Deposits

Although only the Perau ore deposit currently in operation had been known in the Perau area, a "mineralized zone" which indicates the occurrence of new ore deposit was intersected on the west of the Perau deposit by the present drilling survey.

The Perau deposit is a lead ore deposit emplaced harmoniously in limestone and dolomite to carbonate schist (AIIs) of the Açungui I formation in a stratiform.

The extent of mineralization of about 800 meters along the strike and 120 meters along the dip, most part of the ore body has been weathered and eroded out at the surface, had been hitherto confirmed.

The "main ore body" being in operation at present which has been exploited by three main levels of G_1 to G_3 has an extent of about 350 meters along strike and pitch length of about 120 meters. The main ore body forms several ore shoots with repetition of swell and pinch, having its lower limit in the proximity of G_2 level about 120 meters below the surface.

The mineralized zone newly discovered by the present drill survey on the west of the

mine contains barite and sulphides (galena, sphalerite, pyrite, etc.) and is positioned in the same horizon with that of the Perau ore deposit. The mineralized zone was intersected by three drill holes of AG–01, AG–02 and AG–03.

The intersection of the mineralized zone are,

9.95 m. in AG–01 from 255.95 to 265.90 m.,

10.75 m. in AG–02 from 242.85 to 253.60 m., and

1.9 m. in AG–03 from 194.30 to 196.20 m.,

showing a tendency to decline toward the south. It has, however, a great potential toward the west and the north.

This mineralized zone shows a characteristic of stratiform ore deposit of concentrated dissemination of galena, sphalerite and pyrite associated with barite, showing a different character from that of the Perau "main ore body" which mainly consists of galena and pyrite.

It has been known taht there was a zone of barite in the hangingwall of the "main ore body" five to eight meters upward from the upper boundary of the ore in some parts of G_2 and G_3 levels of the Perau mine, and fine-grained galena is dissiminated in cloud shape which has not been regarded as an object of economic operation.

The prospecting by a drift on the G_2 level recently hit a high concentration of galena in the barite zone, which leads to an increasing recognition of the importance of the mineralized zone of this kind, together with the result of intersection in the drill holes mentioned above.

(2) Ore Mineral Assemblage

The characteristic of the ore mineral assemblage of the Perau deposit being currently operated is the existence of main ore minerals such as galena and pyrite and subordinate chalcopyrite and sphalerite. In addition, pyrrhotite, marcasite and tetrahedrite are observed under the microscope.

The quantitative relation between the ore minerals is characterized by a exceedingly abundant occurrence of galena and pyrite compared with other minerals.

The ore shows a stratiform shape, which is arranged harmoniously with the schistosity of wall rock.

Pyrite forms a mozaic aggregate of medium to fine-grained, subhedral to anhedral crystals, contains a small amount of euhedral crystals, accompanied with subordinate amount of galena and sphalerite.

Galena forms an aggregate of medium to coarse-grained crystals, often containing breccia and round pebble of wall rock and pyrite, though it takes a homogeneous appearance by the

naked eye.

Sometimes a phenomenon that galena has filled the cracks of the wall rock and pyrite as a remobilization. It often includes other minerals and corroded them.

The ore mineral assemblage of the barite – sulphide zone intersected by the present drilling survey shows basically no great difference from that of the Perau deposit. However, some different characterisites are shown, such as association of barite, abundance of sphalerite and concentration of mineral grains in a certain horizon in a form of dissemination without showing notable phenomenon of remobilization.

Quantitatively, galena and sphalerite are disseminated approximately in equal amount in gangue minerals including barite, carbonates and quartz, while pyrite is small in amount compared with that of the Perau deposit.

Chalcopyrite is observed under the microscope in association with sphalerite beside the minerals mentioned above. Pyrrhotite is rarely observed.

Galena displays fine to medium-grained, 5 μm ~ 1 mm, irregular form filling the interstices of the grains of gangue minerals, consistent with the trend of bedding, but some directions to cut the above trend is partly observed.

Sphalerite has almost the same grain size with that of galena, having been partly corroded by galena.

Pyrite shows fine to medium-grained crystal, 20 μm ~ 1 mm, displaying euhedral and round pebble-like to irregular crystal forms, having been distributed independently or accompanied by galena.

In the drill core of AG–01, pyrite of euhedral crystal form is generally observed.

In those of AG–2 and AG–3, however, pebble-like irregular forms are common.

Chalcopyrite is observed under the microscope in a small amount showing fine-grained anhedral crystal form. It is found throughout the mineralized zone, though small in amount, has a tendency to occur closely associated with sphalerite.

The mineral assemblage of both the Perau deposit and the barite-sulphide zone observed in the drill core shows a characteristic of polymetallic deposit composed of galena, sphalerite, pyrite and chalcopyrite as the main constituent minerals. Especially, the minerals of the Perau deposit is considered to have crystallized from the low temperature solution and harmoniously deposited with the host rock (JICA and MMAJ, 1981).

The barite-sulphide zone obtained by the drilling is considered to be a stratiform deposit distributed almost in the same horizon as that of the Perau deposit. However, since it is a characteristic of the mineral assemblage, accompanied by abundant barite and has bigger ratio

of sphalerite in quantity, it is considered that the minerals of the barite-sulphide zone was crystallized and deposited from the ore solution of different stage of the Perau deposit.

Although the stratigraphical setting of the mineralized zone can be regarded same as the Perau deposit, it is considered that the stage of mineralization of the barite-sulphide zone is a little later than the Perau deposit and positioned in a little upper part, because a mineralized zone of the Perau type was encountered in the hole AG-01 immediately below the barite-sulphide zone and because a barite-galena zone has been found in the underground of the Perau mine on the hangingwall side of the Perau deposit several meters upward.

(3) The Result of Assay of Ore Minerals

The assay result clarified difference of the ratio of quantity of the main ore minerals between the Perau deposit and the barite-sulphide zone in the drill cores.

The Perau mine produce the crude ore of lead bearing silver of 1,500 tons per month at the grade of 7-10% Pb and 80-120 g/t Ag.

JICA and MMAJ (1981) reported that the result of assay of the tip samples taken from the several places in the underground showed about 10% Pb and 200-600 g/t Ag, while copper and zinc showed less than one percent can not be treated economically.

On the other hand, the result of assay of drill cores obtained this time is as shown in the Table A-4-21.

In the AG-01, the intersection from 255 95 m. to 263.45 m. is the barite-sulphide zone, showing the grades such as 15-27% BaO, approximately 4% Pb, approx. 3% Zn and approx. 100 g/t Ag

SiO_2 showed grades of four to 10 percent in this zone, showing a very low content.

In the upper part of the barite-sulphide zone from 263.45 to 269.90 meters, SiO_2 reaches up to 35 to 50 percent, and this zone is interbedded with thin layers of cherty rock which can be observed with the naked eye.

The grade of Pb is 2.3 to 5 percent, while those of zinc and copper are very low. Silver grade is 60 ~ 100 g/t.

From these, it is clear that the latter zone shows a very similar pattern as the Perau deposit.

Mg/CaO ratio of the mineralized zone and the host rock adjacent to it are high, showing the values more than 0.5.

In the AG-02, the barite ~ sulphide zone is divided into two subzones, the upper one from 242.85 m. to 247.85m. and the lower one from 251.40 m. to 253.60 m.

In the upper subzone, lead grade is about five percent, and zinc grade is as low as less

than one percent.

Silver grade is about 90 g/t, while copper grade is 45 ~ 480 ppm, being very much varied. Copper grade is high in carbonate rock in the upper portion, partly showing 1.2% Cu.

Mg/CaO ratio and the relation of ratio of content between SiO_2 and BaO show a tendency almost the same as those of the AG–01.

In the lower subzone from 251.40 meter to 253.60 meter, the lead grade and zinc grade show almost the same value, which indicates that zinc grade of this subzone is higher than that of the upper.

In the AG–03, the mineralized zone declines showing an appearance of termination. The grades of zinc and BaO are low, while that of SiO_2 is high.

Although the relation of ratio of content between MgO and CaO is not different from that of the above, this ore zone shows a similar pattern to that of the Perau ore deposit.

Fig. I–17 shows the relation of ratio of content between the components above mentioned the Pb–Zn–Ag diagram and the BaO–SiO_2–MgO/CaO diagram.

In the AG–01, the main mineralized zone is consistent with the range of high BaO, and the proportion between lead and zinc varies broadly. However, the samples such as No.11 and No.12 are high in proportion of Pb and also rich in SiO_2, which shows that the pattern of this zone is distinctly different from that of the barite-sulphide zone. In the AG–02, the main mineralized zone is similarly consistent with the range of high BaO.

In the upper mineralized zone, Zn/Pb ratio is small, while in the lower zone, both are almost the same in quantity.

In the AG–03, the main mineralized zone corresponds to the range which is predominant with SiO_2, BaO is very small in amount, and the ratio of Zn is small.

The result of analysis of the drill cores described above is summarized as follows.

The barite-sulphide zone is observed in the hole AG–01 and AG–02, but it declines in AG–03. Especially in AG–01, lead and zinc mineralization is predominant, and it is shown that content of zinc tends to decrease toward the holes AG–02 and AG–03.

(4) Relation of Geophysical Survey and Ore Deposits

Gravity survey and electric survey, IP method and SIP method, were conducted in 1981 for geophysical survey in the surrounding area of the Perau mine and IP survey was conducted successively in this year in the southern part of the Perau area.

As the result of drill survey conducted this year on the basis of the result of analysis of the electric survey carried out in 1981, the new mineralized zone as described about was discovered.

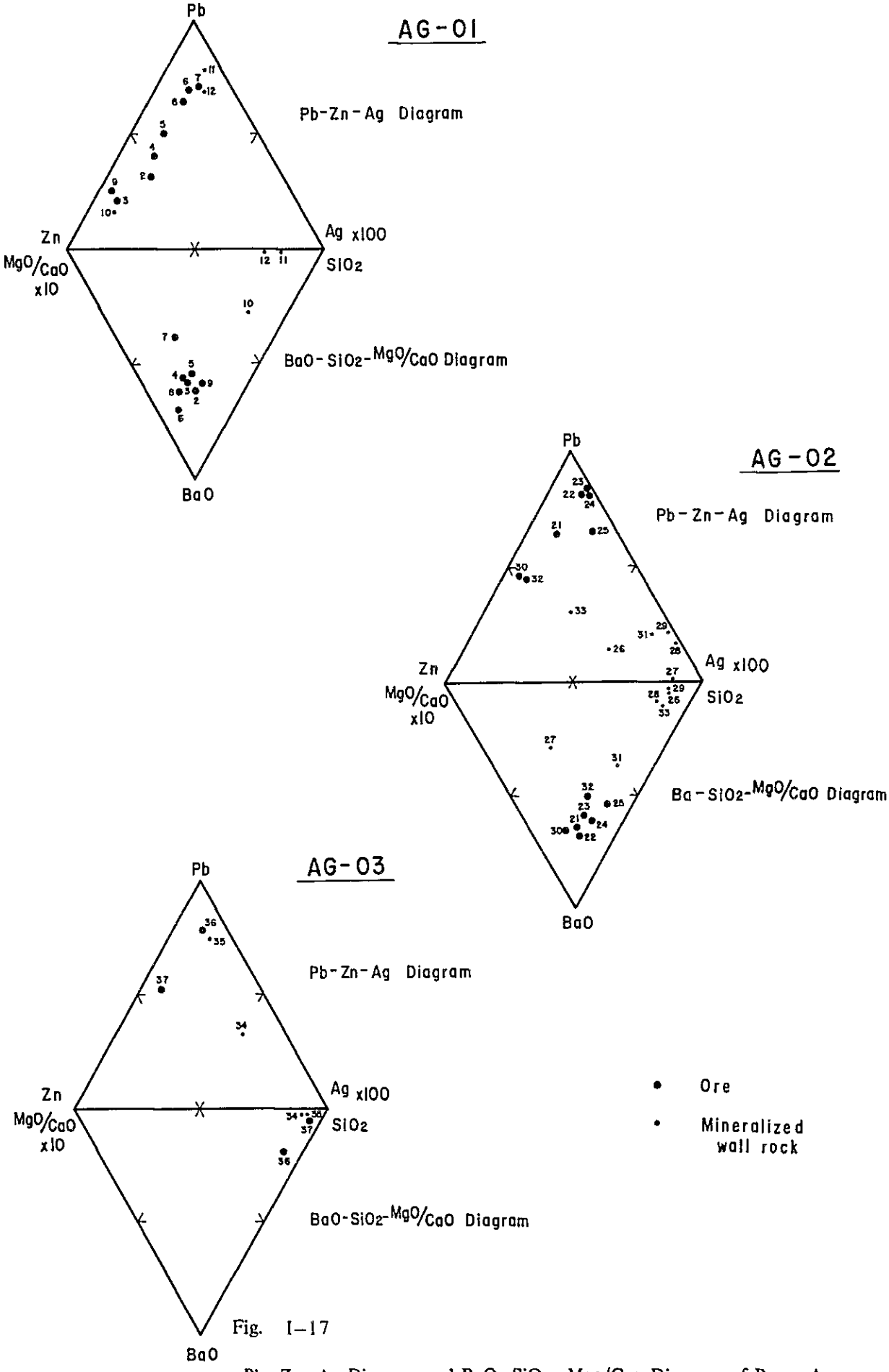

Fig. I-17

Pb–Zn–Ag Diagram and $BaO–SiO_2$–Mgo/Cao Diagram of Perau Area

The anomalous zones of electric survey have been obtained in the surrounding area of the Perau mine are classified into the following four patterns.

(1) The anomalous zone which is consistent with the distribution of graphite schist,

(2) the anomalous zone in mica schist which is interbedded with pyrite-disseminated zone and graphite schist, stratigraphically in the upper horizon than the Perau horizon,

(3) the anomalous zone consistent with the Perau horizon, and

(4) the anomalous zone which is consistent with the horizon of amphibolite, the inter-trappean in quartzite in the lower horizon than the Perau horizon.

Among these, the anomalous zone of (3) is the important target of the survey. The anomalous zones of (2) and (3) are found in the area in which the drill survey was carried out this time, and especially anomaly of (2) is dominant.

The result of drilling survey and interpretation of the electric survey showed an excellent consistency; for example, in the anomalous zone, graphitic schist occurs dominantly in mica schist.

Pyrite occurs along the schistosity in the film shape, which was the source of anomaly of electric prospecting.

In the anomalous zone (3), the barite-sulphide zone, which is the new mineralized zone, has been found.

It is also possible that the "magnetite zone" distributed in the hangingwall of the mineralized zone might have been the cause of anomaly of the electric survey.

The IP survey carried out this year resulted in to detect a part of the anomalous zone of the pattern (2), but that of (3) was not detected. It is considered, therefore, that the possibility of dominant occurrence of the mineralized zone of the Perau horizon is small in the southern part.

2–1–5 Future Exploration

As the result of comprehensive investigation of the data of geological survey, geophysical survey and drill survey, the future exploration in the area should be selected as follows.

(1) It should be followed up the survey to confirm the size and the extent of mineralization of new ore deposit intersected by the present drill survey. Especially, it is desired that further drilling survey would be conducted on the west and the north of the drill intersection of the holes AG–01 and AG–02.

(2) It is required that prospecting of the "barite zone" in the hangingwall of the ore body which has been the object of operation in the underground of the Perau mine would be conducted thoroughly.

2–2 Geology and Ore Deposits of the Barrinha Area

2–2–1 Summary of the Barrinha Mine

The Barrinha mine is situated 10 kilometers to the south of Adrianopolis. Several old pits and outcrops are found on the hill side of an altitude of 500 to 600 meters above sea level.

The Quatro deposit is the main ore deposit, and it is currently mined by underground mining beneath the old open pit. Beside it, outcrops and old pits such as Oito and São Joaquim on the north of Quatro, and Cecrisa and Laranjal on the east of the Quatro are distributed.

The drill survey is currently being carried out by the Barrinha mine itself in the adjacent area of Oito among those mentioned above.

2–2–2 Geology

Geology of the Barrinha mine consists of, from the base upward, mica schist ($AIIIS_1$), limestone to carbonate rocks ($AIIIL_2$) and phyllite to mica schist ($AIIIS_2$) of the Açungui III formation (Fig. I–18 · I–19, PL. I–10).

The survey area is located on the northern side of the Ribeira fault. The rock shows general strike of N50° ~ 80°E and dips toward north to northwest.

Because of a complicated fold structure in the surrounding area of the Barrinha mine, $AIIIL_2$ is repeatedly exposed.

The Barrinha deposit is the vein-type to irregular massive lead ore deposit emplaced in $AIIIL_2$ in the area predominant fold structure.

(1) Mica Schist ($AIIIS_1$)

The rock is distributed from the southeastern part of the survey area toward the outside of the area showing a general strike of N80°E.

The main rock facies is reddish brown to dark brown, fine-grained sericite schist, locally interbedded with sericite-biotite schist.

(2) Limestone · Carbonate Schist ($AIIIL_2$)

The member is composed mainly of limestone ($AIIIL_2$ ls) and carbonate schist or calc schist ($AIIIL_2$ cs).

The limestone ($AIIIL_2$ ls) is distributed in the southern part of the area showing the strike of approximate direction of N80°E, and also distributed at the Quatro deposit and Oito ~ São Joaquim anticlinal axis. It seems to be lain concealed beneath the anticlinal axis on the east of São Joaquim.

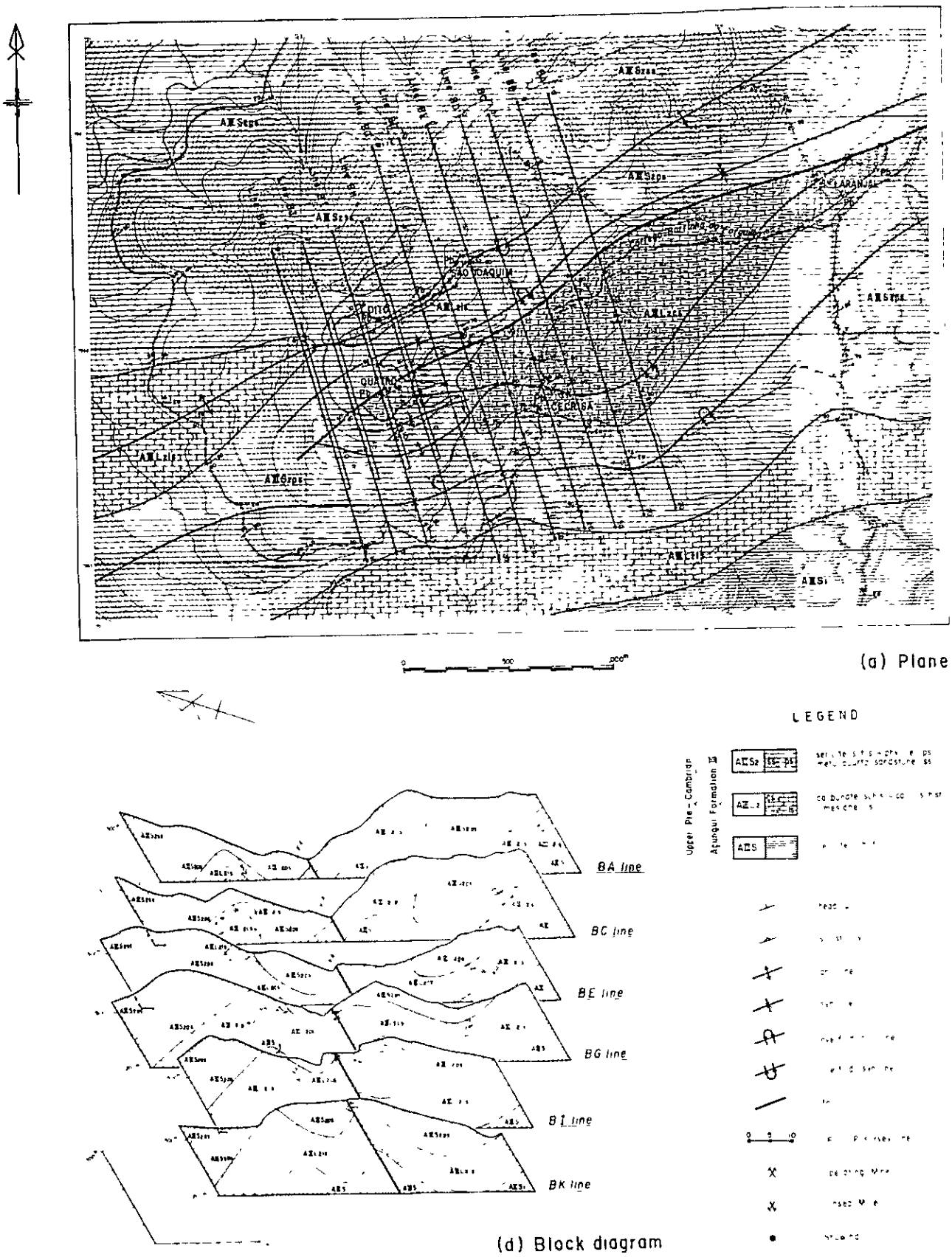

Fig. I—18 Geological Map and Geological Profile of Barrinha Area

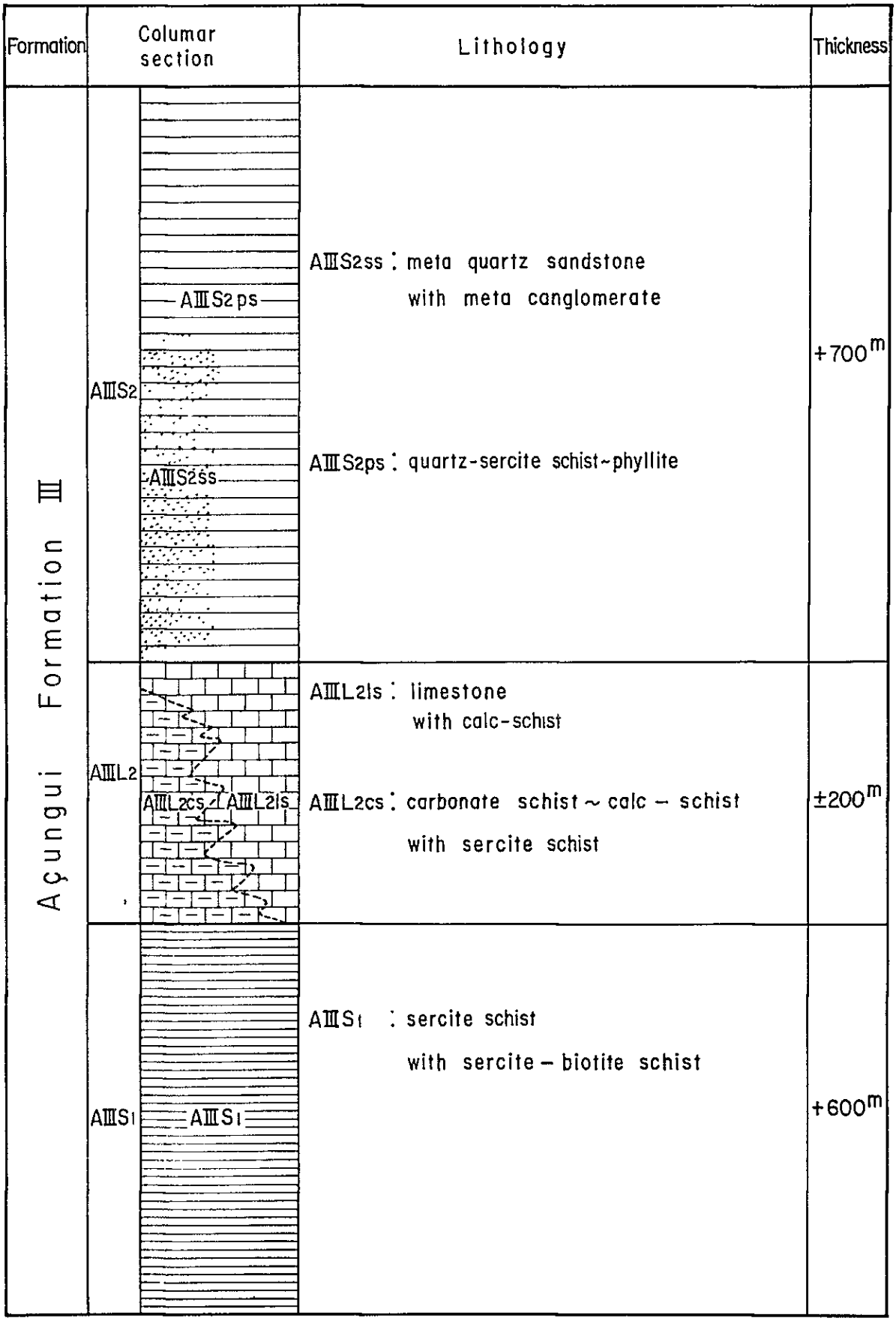

Fig 1--19 Generalized Stratigraphic Columnar Section in Barrinha Area

It shows a rock facies of dark gray, compact and massive, and is intercalated with thin layers of mica schist and carbonate schist below the boundaries between $AIIIS_1$ and $AIIIS_2$. It is often accompanied with calcite veins, especially at the entrance of the Barrinha mine road, network to breccia-like calcite veins occur predominantly.

The upper part of limestone is interbedded with more abundant carbonate schist or calc schist than other part, which seems to be because of its located closely to the carbonate schist ($AIIIL_2$ cs) member distributed from Cecrisa to Laranjal.

Carbonate schist is distributed in the crest of anticlinal structure in the central part of the area, and disappears in the vicinity of Quatro.

The rock facies are mainly dark gray carbonate schist or calc schist, interbedded with phyllite and mica schist. It contains considerable amount of tremolite, biotite and sericite, and schistosity is distinct. It is intercalated with graphite schist in the surrounding area of Cecrisa.

The rock is positioned in the same horizon with limestone ($AIIIL_2$ ls), and it is considered to have been formed correspondent to local variation of the rock facies of original rock, which leads to the assumption that it was formed form more impure carbonate rocks and pelitic rocks than limestone.

(3) Mica Schist ~ Phyllite · Meta Quartz Sandstone ($AIIIS_2$)

The rocks are broadly distributed having occupied the area about two-third of the survey area, showing general strike of N50° ~ 80°E. It shows a complicated fold structure in the surrounding area of the Barrinha mine together with the $AIIIL_2$ member above mentioned.

The main rock facies are dark gray, yellowish brown and reddish brown, medium to fine-grained sericite schist or phyllite ($AIIIS_2$ ps).

Although the rock facies shows an apparent resemblance to that of mica schist of $AIIIS_1$, the metamorphic grade is a little lower.

In the vicinity of the Barrinha mine, it displays reddish tint on the surface by oxidation.

Several pale brown meta quartz sandstone layers ($AIIIS_2$ ss), bearing conglomerate thin layers, are intercalated in the mica schist and phyllite from the northern part of the Oito ~ São Joaquim area to the State road 476 on the west.

2–2–3 Geologic Structure

The survey area is positioned, from the standpoint of regional geology, in a part of limestone and mica schist of the Açungui III formation which is widely distributed on the northern side of the Ribeira fault.

Although the rock show the general strike of N50° ~ 80°E and the general dip of 30° ~

60°N, a manifold combination of anticlines and synclines is distributed from the adjacent area of the Barrinha mine to the surrounding area of the Panelas mine.

The geologic structure of the area is controlled by the four fold axes and a fault structure running through the central part.

(1) Fold Structure

An anticline passing through Oito and São Joaquim and a syncline running on the south of Cecrisa are the main fold structures of the area. Between these main fold structures occur an anticline extending from Oito to Laranjal and a syncline running on the north of it. The axes of these folds are undulant, resulting in to show a more complicated fold structure.

A fold structure, moderate dipping, shown on the eastern side of Oito, and especially on the eastern side of a line from São Joaquim to Cecrisa, overfolds of northerly dipping are conspicuous.

(2) Fault Structure

The existence of a strike fault has been inferred in the central part of the area to run through Quatro and Laranjal. Although it is difficult to confirm the fault on the surface, it was inferred because of the occurrence of a fault breccia zone in underground of the Quatro pit and the dicontinuity of the distribution of geology.

The sense of the fault shows the depression of northern block, and the slip throws are 100 meters to 200 meters showing a tendency to be greater toward the east.

2–2–4 Ore Deposits

(1) Summary of Ore Deposits

Among many ore deposits and showings found in the Barrinha mine, Quatro, Oito, São Joaquim, Cecrisa and Laranjal are the main ones. These deposits and showings have been prospected by tunneling, trenching and drilling, among which only the Quatro deposit has been the object of economic operation.

The Quatro deposit was exploited by open pit mining, but at present, the ore at the bottom of open pit is being mined by underground.

The Quatro deposit and other deposits and showings are all emplaced in limestone (ls) and carbonate schist to calc schist (cs) of the $AIIIL_2$ member.

In terms of the shape of the ore deposits, The Quatro deposit is positioned in the axial part of anticline of the limestone member, showing irregular and massive to strata-bound forms, while the Cecrisa deposit shows a vein-type form cutting the bedding plane of carbonate schist. Although the details of other deposits and showings have not been made clear, it

may belong to either type of the aboves.

(2) Ore Mineral Assemblage

Ore minerals mainly consist of galena and pyrite, accompanied by small amount of sphalerite and chalcopyrite. Abundant cerussite and pyromorphite are observed in the oxidized zone on the surface. The microscopic observation of ore samples from the Quatro deposit showed that the ore minerals were mainly composed of galena and pyrite, with subordinate amount of sphalerite, chalcopyrite, tetrahedrite and magnetite.

Galena concentrates in a irregular form filling the interstices of carbonates and quartz, or occurs as fine-grained dissemination.

Pyrite displays medium to coarse-grained euhedral to anherdal crystal form, and often corroded by galena.

Sphalerite shows an irregular form, often covered by the film of galena and tetrahedrite.

Chalcopyrite and tetrahedrite are observed in a small amount to have been accompanied by galena and pyrite along the rim or inside of them.

Small amount of cerussite is observed along the periphery of galena. Small amount of magnetite has been replaced by hematite.

All the deposits of the Barrinha mine are vein-type to irregular and massive lead ore deposit emplaced in $AIIIL_2$, and are positioned in the part from the apex to the limb of the fold. In addition, these show a tendency to be concentrated to the boundary with $AIIIS_2$

This tendency is considered to be an effective guidance for ore finding in future exploration in the area.

(3) Relationship between Result of Geophysical Survey and Mineralization

The result of geophysical survey (IP, SIP) carried out in the area showed that the contrast of apparent resistivity was strong on every survey line, and it has well reflected the geologic structure.

The FE anomalous zone detected this time is roughly divided into the northern anomalous zone and the southern anomalous zone bounded by Corrego Barrinha do Forquilho which runs eastward in the approximately central part of the survey area. Among these, the southern anomalous zone distributed in the vicinity of Cecrisa is composed of several discontinuous anomalies of small size, and seems to reflect a vein-type mineralized zone similar to the Cecrisa deposit.

The northern anomalous zone, on the other hand, is distributed from the crest to the northern limb of the anticline which extends on the east of São Joaquim.

In this area, the limestone ($AIIIL_2$ ls) in which the mineralized zones such as Oito and

São Joaquim are emplaced, lies concealed. The anomalous zone is continuous and is distributed in harmony with the position in geologic structure of the main ore deposit of the Barrinha mine and other showings, which leads to the expectation of occurrence of any stratabound or irregular and massive mineralized zone.

The SIP anomaly was detected at the Quatro deposit and to the south-southeast of it.

The Quatro deposit which is being operated is a irregular and massive lead ore deposit in limestone, and its extention is still remained unconfirmed on all sides. It is, therefore, expected that the anomalous zone detected to the southeast of the Quatro mine would lead to the finding of the similar mineralized zone in the area.

2–2–5 Future Exploration

As result of comprehensive investigation of the result of geological survey and geophysical survey, it is recommended as follows for the future exploration of the surrounding area of the Barrinha mine.

(1) Because there is a possibility that the IP anomalous zone distributed from the axis of anticline on the east of São Joaquim to the northern limb might be related to any latent mineralization, it is desired that the drilling survey to be conducted to investigate into it.

(2) Because it is possible that the SIP anomaly detected to the southeast of the Quatro deposit would indicate the extention of the deposit, execution of drilling survey is recommended to clarify the situation.

PART Ⅱ GEOPHYSICAL SURVEY

CHAPTER 1. SUMMARY OF GEOPHYSICAL SURVEY

In the Phase III, IP and Spectral IP methods were carried out in the both areas of Perau and Barrinha.

In Perau area, for the purpose of pursuing the remarkable IP anomaly towards south detected in the Phase II IP survey in 1981, four IP survey lines, with line length of 2.5 km each, were established with line interval of 200m.

In Barrinha area, there are many ore deposits and mineralized zone. These ore deposits are the vein or network type deposits included in the same formation as Açungui III. These ore deposits are located on and near the axis of Barrinha anticline. For the purpose of detecting blind deposits, IP and Spectral IP methods were adopted. Seven IP survey lines, with the line length of 2.0 km each, were established with line interval of 150 m., and four spectral IP lines, with the line length of 1.5 km each, were set with line interval of 150 m.

CHAPTER 2. INDUCED POLARIZATION METHOD

2–1 Survey Method

IP phenomenon can be observed in time domain as well as frequency domain. It is an exceedingly complex phenomenon although it superficially resembles the discharge of a capacitor (time domain) or the variation of the impedance of an RC circuit (frequency domain).

(1) Frequency domain

In the frequency domain, the apparent resistivity of the ground is measured at two frequencies F and f (<F).

IP is expressed as an apparent frequency effect.

(2) Time domain

By supplying DC pulses of period T in the ground, the magnitude of the observed IP phenomenon is expressed as v/V, where v is the decay voltage remaining at a definite time after current off, and V is the voltage at current on.

(3) Phase domain

This is a method to measure the phase angle shift between transmitted waveform and received signal waveform.

(4) Spectral IP

By transmitting multi-frequency current into the ground, normalized amplitude and phase to the lowest frequency are measured as mentioned in chapter 3.

2–1–1 Field Measurement

Frequency domain IP method which is popularly used together with up-to-date Spectral IP method are adopted in this survey by dipole-dipole electrode configuration. Eight to ten stainless steel wire electrodes are used as a set of current electrode. Non-polarizable glazed pot which consists of Cu-CuSO4 is used as a potential electrode.

2–1–2 Line Survey

Considering the geological structure in Perau and Barrinha area, survey lines were planned and established to cut the strike perpendicularly. A pocket compass and 100 m measuring tape were used for the line-survey. Stations were established with horizontal distance of 100 m by open traverse method. The communication lines for Spectral IP were set 25 m parallel apart from the main lines. Each station of traverse lines is named as 0, 1, 2, 3, ... from the north end of the lines with 100 m. horizontally apart in Barrinha area.

Table II–2–1 List of Method and Equipments for Geophysical Survey

	PERAU AREA	BARRINHA AREA
Line Interval	200 m	150 m
Electrode Spacing (a)	200 m	100 m
Electrode Configuration	Dipole-Dipole	Dipole-Dipole
Space Factor (n)	1 to 5	1 to 5
Equipments Used	Transmitter T 7801 Receiver R-7801 R 7802	IP Survey Transmitter CHT-7801 Receiver CHR-7801 CHR-7802 SIP Survey Transmitter FT-4 Receiver GDP-12G

Table II–2–2 List of Survey Lines

PERAU AREA		BARRINHA AREA	
Name of Line	Length	Name of Line	Length
Line M	2.6 km	IP Method	
Line N	2.6 km	Line BA	2.0 km
Line O	2.5 km	Line BB	2.0 km
Line P	2.5 km	Line BC	2.0 km
		Line BD	2.0 km
		Line BE	2.0 km
		Line BF	2.0 km
		Line BG	2.0 km
		Spectral IP Method	
		Line BH	1.5 km
		Line BI	1.5 km
		Line BJ	1.5 km
		Line BK	1.5 km
TOTAL LENGTH 10.2 km		TOTAL LENGTH	IP 14.0 km SIP 6.0 km)20.0 km

2–2 Data Processing and Analysis

2–2–1 Summary

(1) IP method

IP method is conducted by supplying AC current I_{AC} into the ground through a pair of current electrodes (C_1, C_2) with another potential electrodes (P_1, P_2) detecting the potential difference V_{AC}.

In this case, the apparent resistivity ρ_{AC} of the ground is calculated by the following equation.

$$\rho_{AC} = K \cdot V_{AC} / I_{AC} \ (\Omega\text{–m})$$

K is a geometrical factor, and when an electrode spacing and an electrode spacing factor is "a" and "n" respectively, K is expressed as follows.

$$K = 2\pi / \left(\frac{1}{C_1P_1} - \frac{1}{C_1P_2} - \frac{1}{C_2P_1} + \frac{1}{C_2P_2}\right)$$

$$= \pi \, n \, (n+1) \, (n+2) \, a$$

In this survey, "a" is 200 m in Perau and 100 m in Barrinha and "n" is 1 to 5. The plotting method of the data is shown in Fig. II-2–2.

After reading the potential difference V, by keeping the current constant, and lowering the frequency closed to DC current, the deviation of the apparent resistivity due to frequency change is directly taken. This deviation is called the frequency effect (FE) and it is given by:

$$FE = \frac{V_{DC} - V_{AC}}{V_{DC}} \times 100\ (\%) = \frac{\rho_{AC} - \rho_{AC}}{\rho_{AC}} \times 100\ (\%)$$

In this survey, the frequencies used are 3.0 and 0.3 Hz.

Metallic mineral causing IP anomaly generally shows low resistivity and high FE, consequently, metal factor (MF) as defined below has been used to emphasize the anomalous zone.

$$MF = \frac{FE}{\rho_{AC}} \times 1000\ (\%/\Omega\text{m})$$

The value of apparent resistivity, FE and MF are plotted on the vertex of an equilateral triangle with a line connecting the middle point of dipole-dipole as its hypotenuse. Give a word of caution, this depth of plotting does not represent the physical property of the depth.

(2) Terrain Correction

As FE is a ratio of resistivity deviation, it is affected by topography. But as a geometrical factor K is assumed on the basis of half-infinite plane, the apparent resistivity is affected by

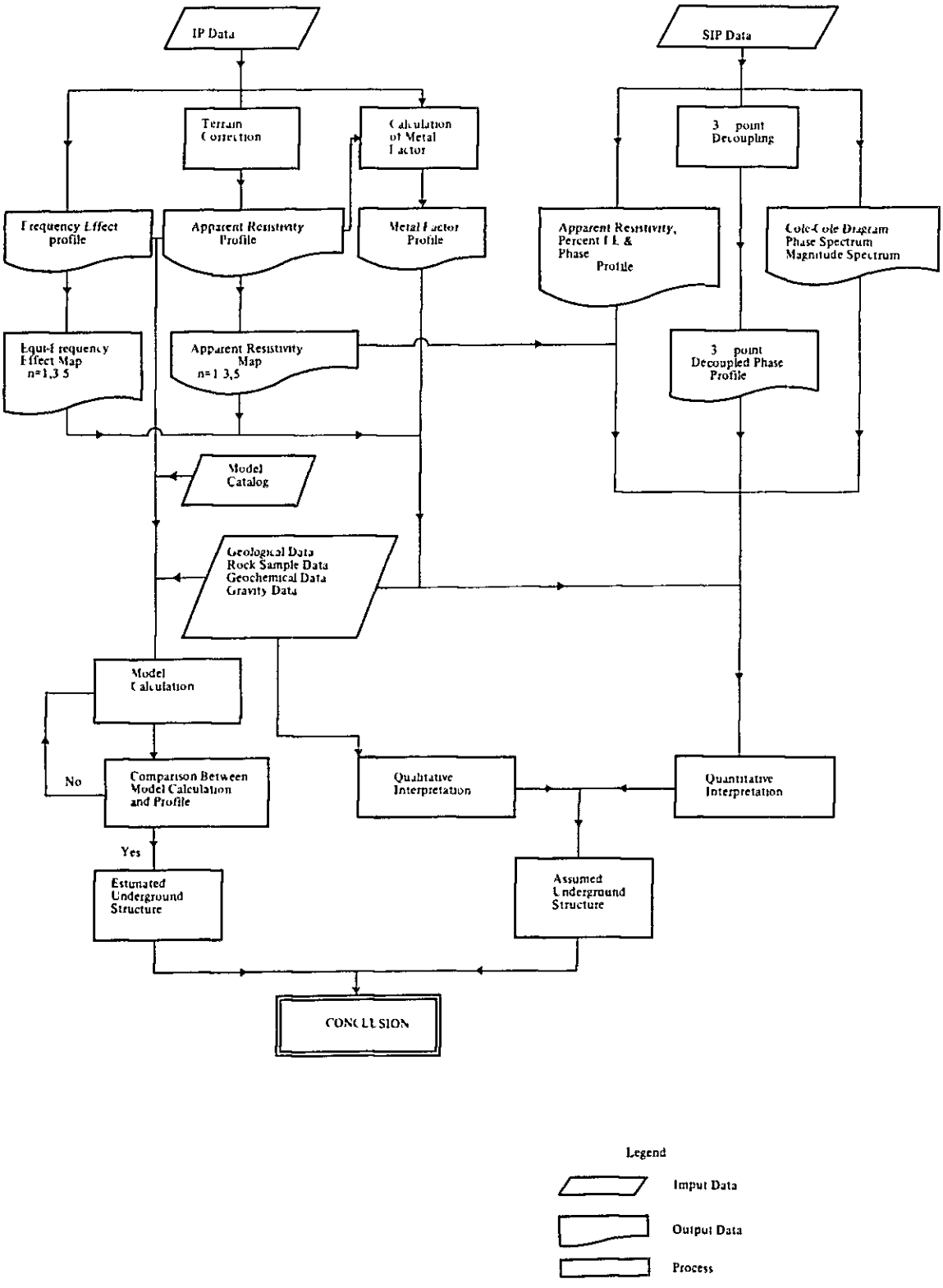

Fig. Ⅱ—2—1 Flow Chart of IP and Spectral Data Analysis

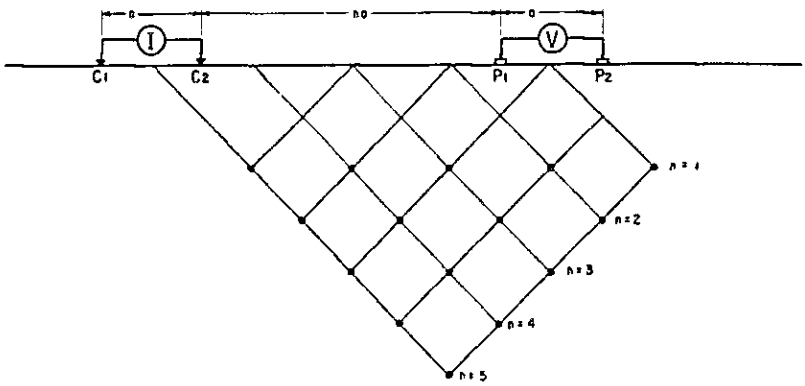

Fig. II–2–2 Plotting Method in IP Pseudo-Section

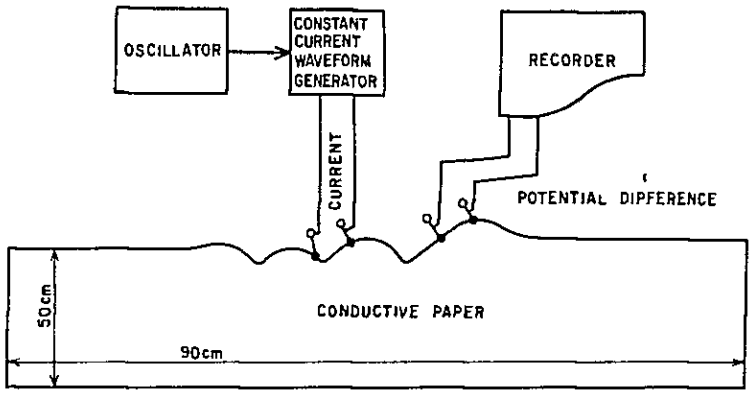

Fig. II–2–3 Block Diagram of Terrain Correction

the topography depending on the locations of electrodes. That is, resistivity will be detected as high beneath a hill and low beneath a valley.

For the purpose of rejecting the topographic effect quantitatively, a method using a conductive paper was adopted. This method is done by using a conductive paper of constant resistivity and cutting the paper simulating a scaled topography. A weak current is passed through the simulated topographic section and potential are measure (Fig. II–2–3).

As this correction is performed on the basis of the two-dimensional half-infinite plane, it is impossible to eliminate the effect in case that IP survey lines are parallel to a ridge or a creek. The effect of small topographic changes or the changes of the resistivity near the surface can not also be corrected.

In this survey area where the mountain is perpendicular to the survey lines, there are tendency that the topographic effect can possibly be eliminated.

As the topography in this survey area is very steep and so rugged, the apparent resistivity is affected by the topography. Then two-dimensional terrain correction had to be applied to all survey lines.

2–2–2 Measurement of Electrical properties

Outline

Electrical properties measured at the surface do not necessarily indicate the real properties of rocks, ore deposits, etc., because these are affected by overburden, weathered layer and underground water. Therefore, it is important to know the underground electrical properties as close as possible for electrical exploration. There are two methods to accomplish this purpose, one is the in-situ survey, and the other is the measurement of the electrical properties of rock samples in the laboratory.

In this survey area, the latter method was applied because of inadequate outcrops. Fifty rock samples were collected for the resistivity and FE measurements.

The Method of Measurement

In the laboratory, prior to the electrical property measurements, the rock samples were cut into rectangular blocks. It is desirable to have the specimens in the same condition as at the time of sampling, so the dried samples were placed in a depressurized water tank to subject all of them to similar conditions before the measurements.

The frequencies used were 0.3 and 3 Hz.

The resistivity is calculated from the following equation:

$$\rho = \frac{a_1 \cdot a_2}{\ell} \cdot \frac{V}{I}$$

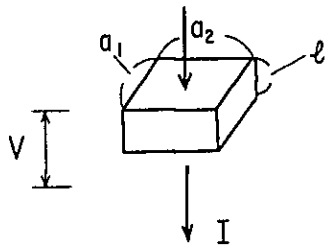

Where, ℓ is the thickness, a_1 and a_2 are the length and the width of the specimen, V is the potential difference and I is the current.

2–2–3 IP Model Simulation

In analyzing the forms and strength of the IP anomalies, the results are often checked and compared with the model simulation and also with the geological structure in order to establish a hypothesis.

For the calculation, each section was divided into 1,400 grids and the assumed FE and resistivity values were assigned in each grid. A computer of CDC 6,600 was used in the calculation by finite element method. The computer output printed out the assumed model form, and calculated FE and resistivity. By comparing the calculated and the actual values, various parameters of simulation were changed in order to approach the observed value. In this procedure it was possible to simulate the pattern of the actual structures, but they are so complicated and the combination of the assumed electrical properties are so many that it would be difficult to conduct an ideal simulation. It was then assumed that the approximate values of the FE and resistivity are close to the observed ones. For the calculation it is possible to set an assumption on the nine types of codes, but only six to seven codes were used in this case.

2–3 Results of Analysis

In this phase, the IP electrical methods were conducted in two areas, Perau and Barrinha.

Results of the observation are shown on both the section of each survey line and the plan map. Frequency effect (FE), apparent resistivity and metal conduction factor are shown on the section. Terrain corrections are conducted on the apparent resistivity. The remarkable IP anomalies detected in this survey generally show low resistivity and high FE, so that metal conduction factor shows the resemblance closely to the pattern of FE. Any comments on metal conduction factor are omitted unless deserving special mentions.

2–3–1 Perau area

(1) Section (Fig. II–2–4 ~ II–2–7)

FE values range from 0.3% to 10% in this area and they are regarded as anomaly when they exceed 3%. On the other hand, apparent resistivity are classified roughly into three groups, namely their ranges are·

low apparent resistivity : less than 30 ohm-m,

middle apparent resistivity : 300 ohm-m to 600 ohm-m,

high apparent resistivity : more than 600 ohm-m.

A) FE

The most remarkable anomalies are detected on line M within four lines conducted in this phase, which crosses with line J of Phase II.

No remarkable anomalies are detected in the southern area from line N except for the both ends of lines N, O and P where weak FE anomalies of 3% to 5% are seen.

On line M, two strong FE anomalies are detected. One is located in the depths below the western part from No. 10 and other one is seen from the surface to the depths below No. 16. Judging from the anomaly pattern, it seems that the former is due to a west dipping source and the latter to a horizontal and/or a little east dipping source. This strong anomaly varies weak anomalies in the depths on lines N, O and P.

At the west of No. 10 on line N, weak anomalies are seen, which are caused by the same source as one detected at the west from No. 10 on line M. As any anomalies are not found on lines O and P, anomalous source seems to disappear at line N or southern limts of this source may be located near line N.

B) Apparent resistivity

In this area, apparent resistivity vary from 5 ohm-m to 1,200 ohm-m and there is big contrast which may reflect the geological structure with different physical properties.

Low apparent resistivity of less than 100 ohm-m are detected from the shallows to the depths between No. 6 and No. 9 on line M, and near surface between No. 8 and No. 11 on line N. These low apparent resistivity disappear around at lines O and P, where middle to high apparent resistivity are dominantly distributed.

(2) Plan maps

Two IP anomalies are detected in the western and eastern regions of the survey area.

Western IP anomaly extends southwestward. And eastern IP anomaly extends southeastward in the shallow depth, but in the depths this anomaly becomes weak and extends to the south from the middle of the survey area.

n=1

An FE anomaly detected at the western part of the survey area have a southern limits near line O and seems to extends southwestwards beyond the survey area. A center of the anomaly seems to be located near line N, where highest FE values are detected. Low apparent resistivity zone of less than 50 ohm-m resemble closely to FE anomaly and this zone seems to extend southwestwards beyond the survey area.

On the other hand, an eastern FE anomaly extends to the south towards line N and varies its direction eastwards from line N. FE values decrease gradually southwards and westward. Middle apparent resistivity are dominantly seen in the eastern part, where the eastern FE anomaly is detected. High apparent resistivity are seen in the southern part near line P.

n=3

In this depth, three FE anomalies are found in the western, eastern and southeastern parts of the survey area, respectively.

An FE anomaly detected in the western part is broadly distributed from the middle to the west on line M, but on line N, this anomaly is found only on its both ends. And this anomaly seems to extend northwestwards in the depths beyond the survey area.

An eastern FE anomaly is seen at the east ends on lines M and N, and seems to extend northeastwards beyonds the survey area.

On the other hand, a southeastern weak FE anomaly of less than 4% can not be seen on the plan map of n=1.

Apparent resistivity show the similar pattern with the map of n=1. That is, low to middle apparent resistivity zone is detected at the western parts from No. 10 on lines M and N and at No. 19 on lines M, N and O. Western FE anomaly is located in the low apparent resistivity zone and other two FE anomalies in the middle to high apparent resistivity zones.

n=5

Two FE anomalies are seen in the western and central parts in this depth.

FE anomaly seen in the west corresponds to western FE anomalies on the maps of n=1 and n=3, but its size is the least within three depths. This anomaly shows similar pattern with FE anomalies on the maps of n=1 and n=2, and seems to extend in the depths westwards beyond the survey area.

Central FE anomaly with NS trending corresponds to FE anomalies detected in the eastern and southeastern parts on n=3 map.

Low to middle apparent resistivity are detected at both ends on lines M and O. High resistivity with NS trending are seen in the central part of the survey area.

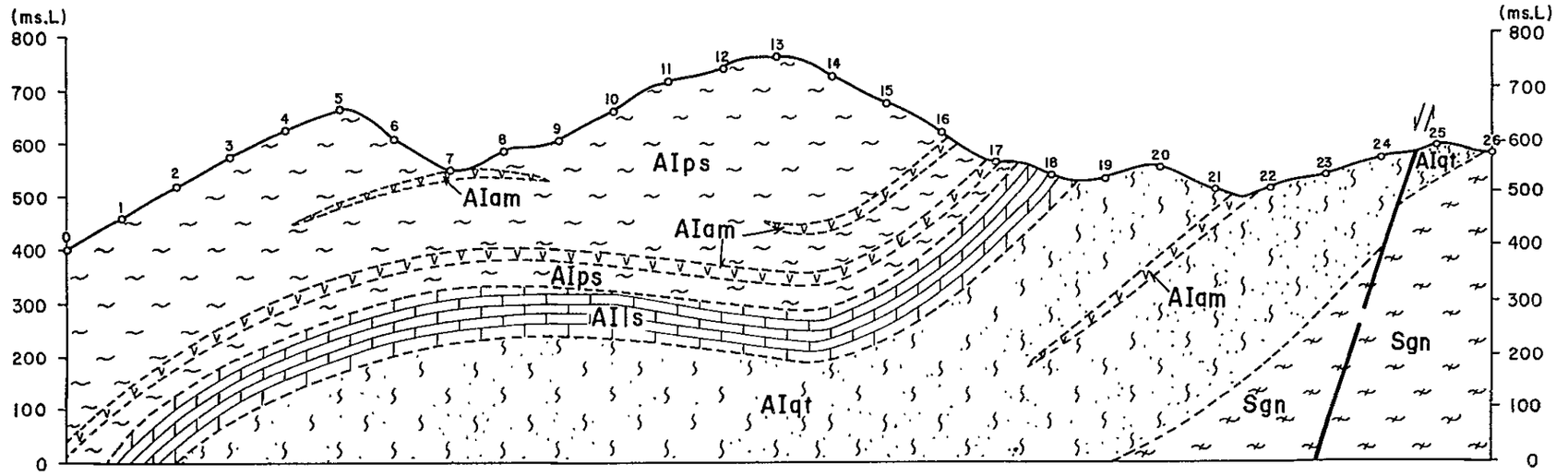

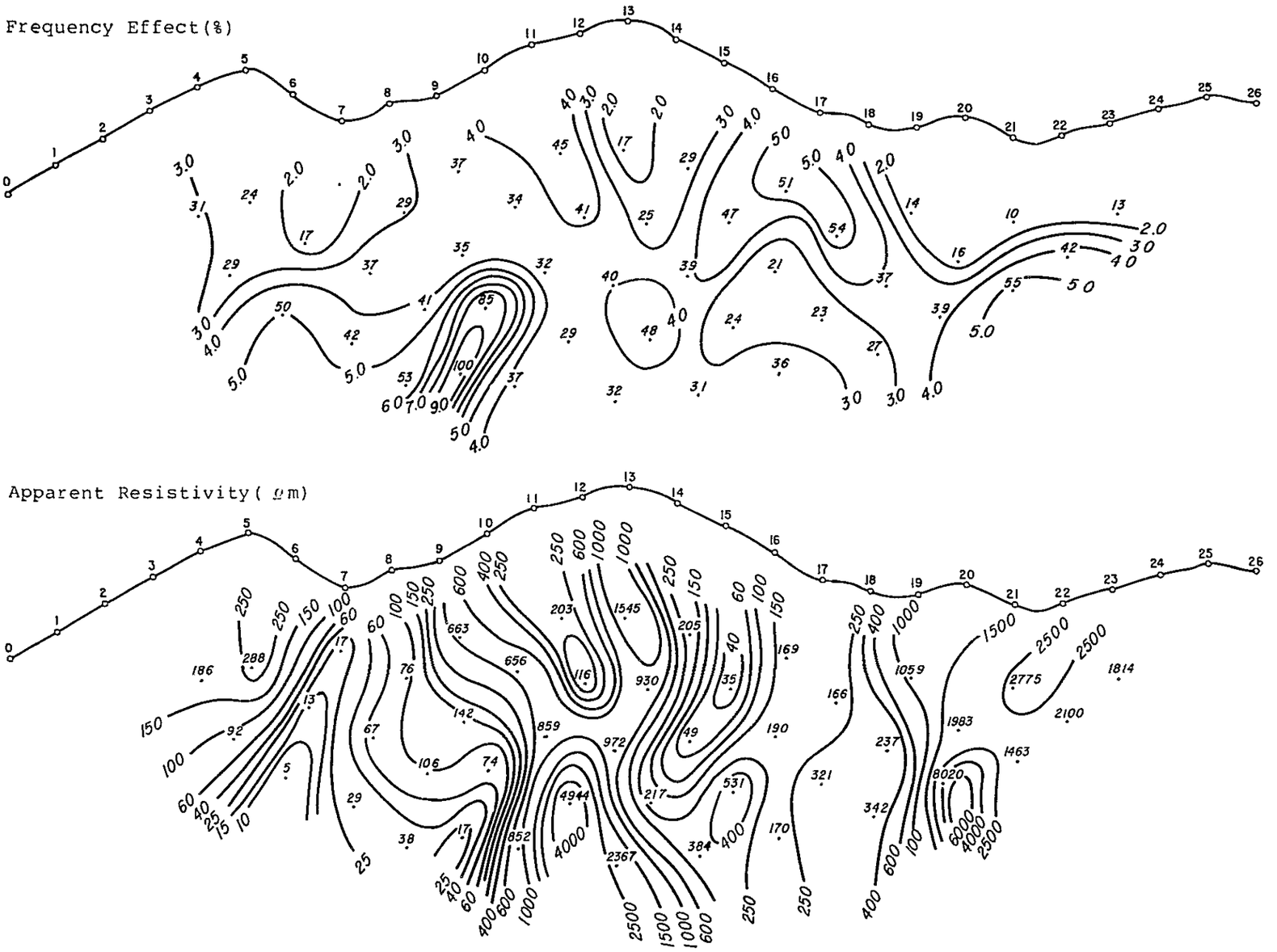

Fig. II－2－4 IP Pseudo-Section in Perau Area (Line-M)

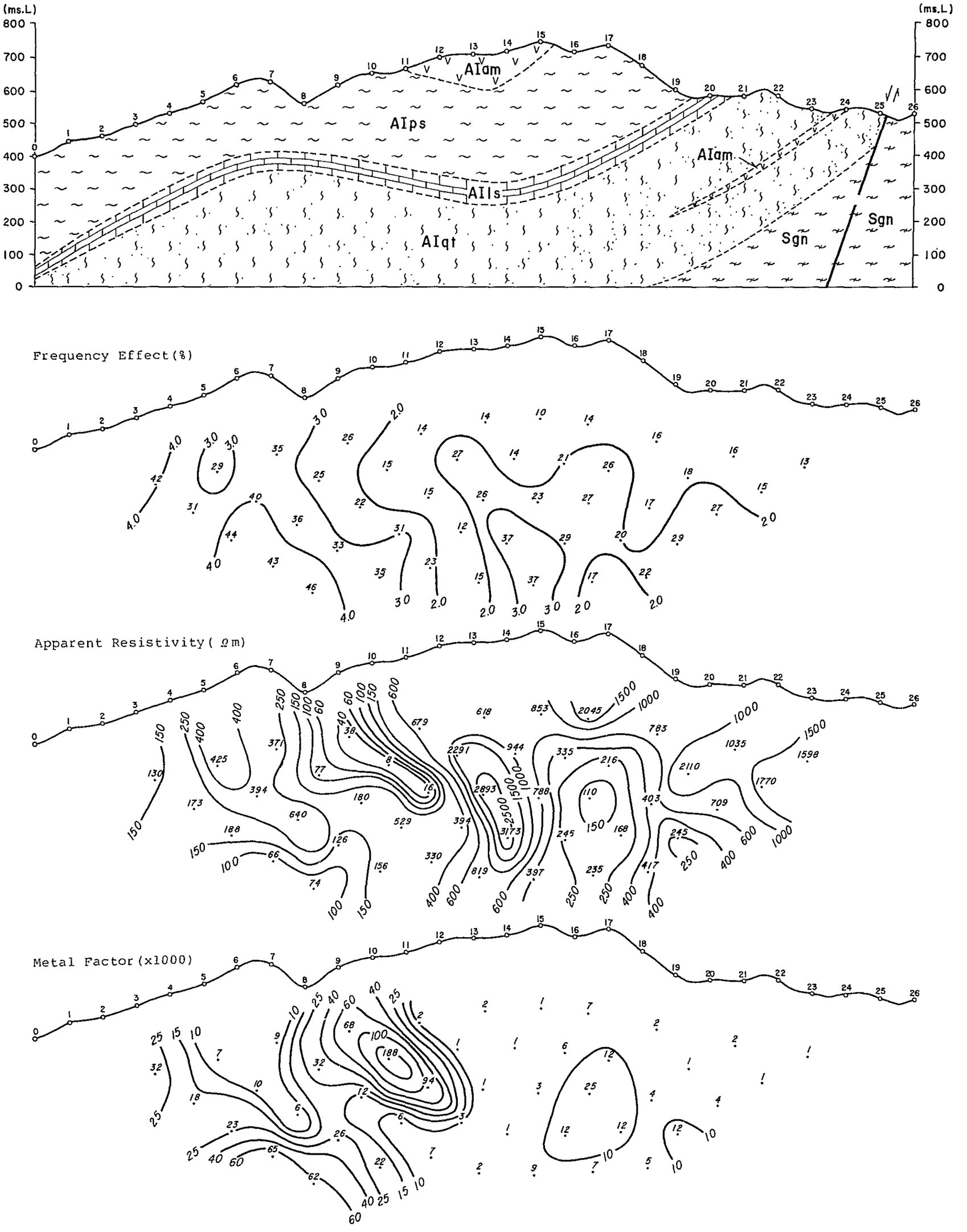

Fig. II-2-5 IP Pseudo-Section in Perau Area (Line-N)

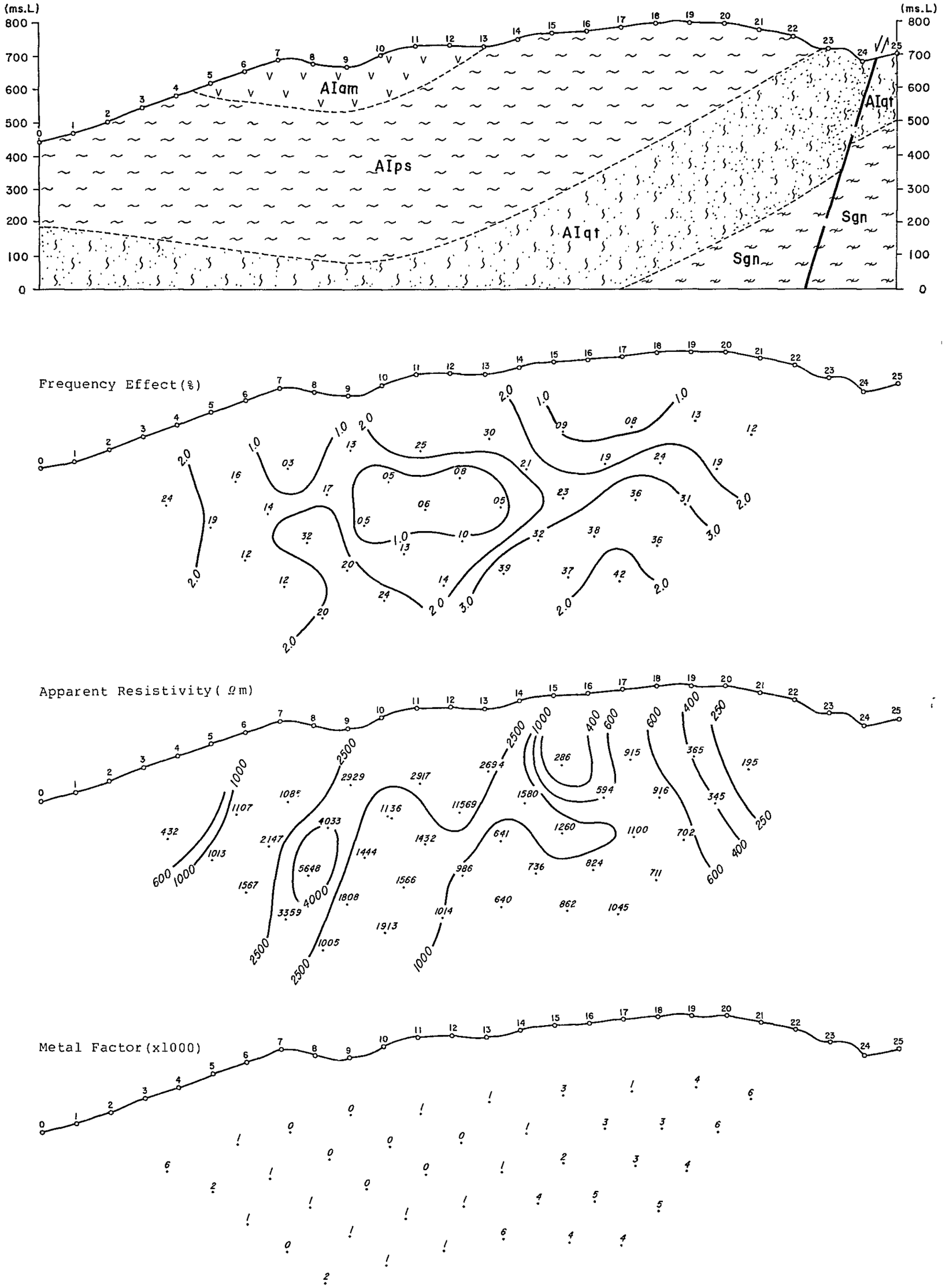

Fig. II－2－6 IP Pseudo-Section in Perau Area (Line-O)

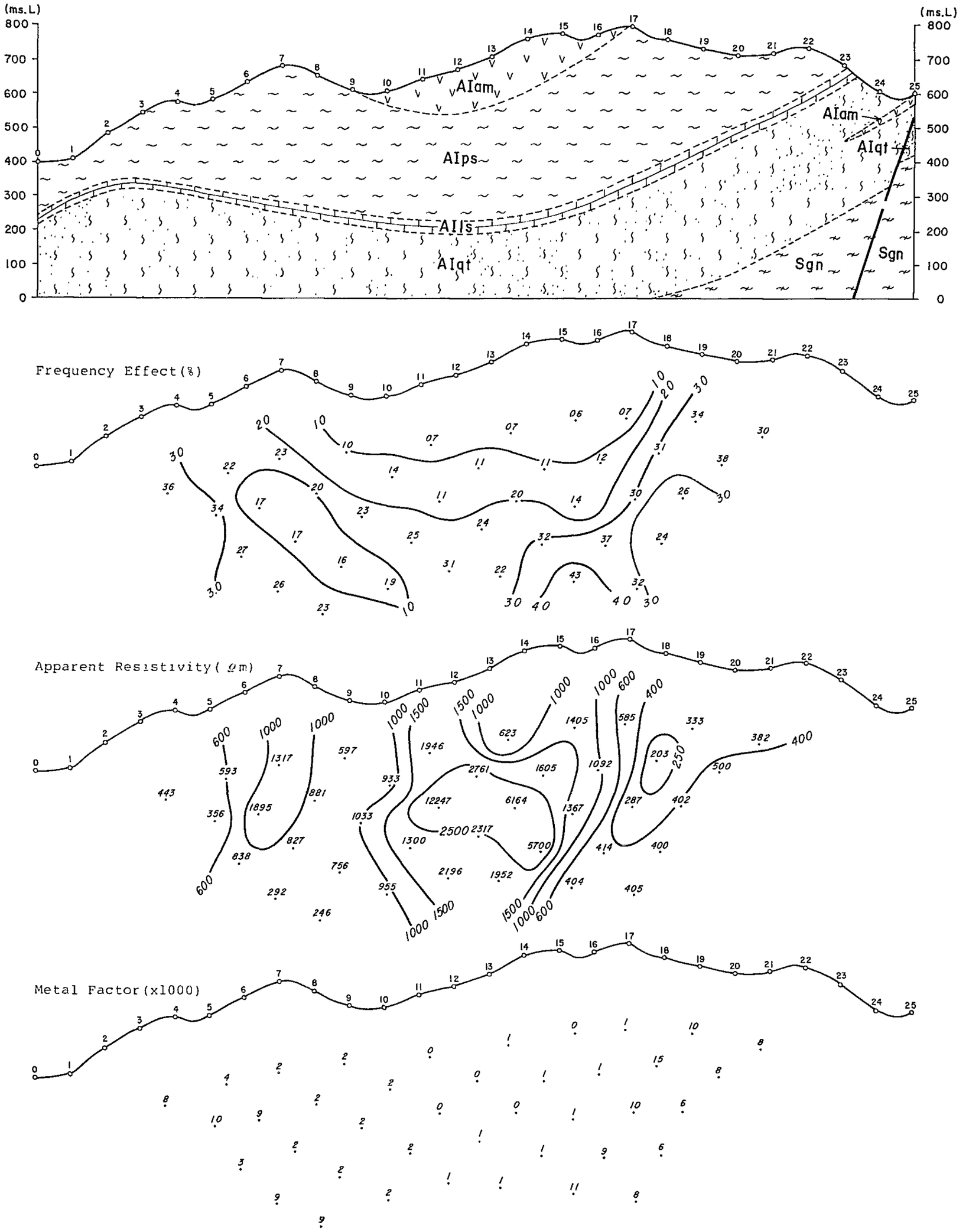

Fig. II－2－7 IP Pseudo-Section in Perau Area (Line-P)

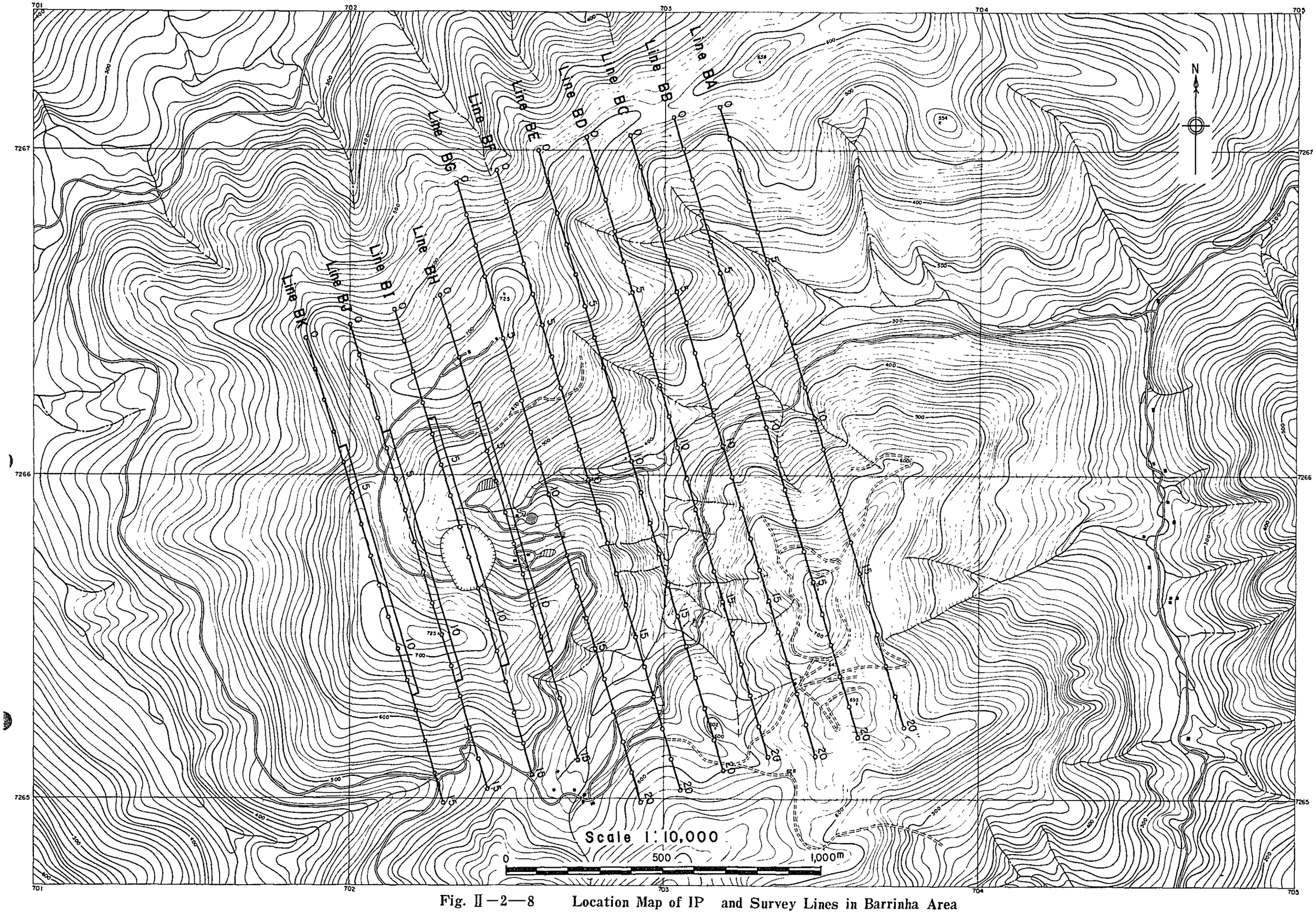

Fig. II—2—8 Location Map of IP and Survey Lines in Barrinha Area

Low to middle apparent resistivity zone detected at the western part seems to extend southwestwards beyond the survey area. Low to middle apparent resistivity zone seen in the east with a trend of SW-NE is seen broadly in the eastern part of the survey area. High apparent resistivity zone between these two low to middle apparent resistivity zones is distributed with a trend of NE-SW.

(3) Relation of FE anomaly with geology

Interpretation for the above-mentioned FE anomalies with geological survey results, taking the Phase II results into considerations, is presented below.

(i) High FE anomaly is detected on the western part and is seen from the surface to the depths. This anomaly shows a similar pattern with low apparent resistivity zone, so that this anomalous zone has low resistivity and high FE values. And this zone coincides with C anomalous zone classified at Phase II survey and is inferred to be caused by graphite schist and/or pyrite. South limits of this zone is suggested to be located near line O, judging from the shape of FE anomaly, and this zone with north dipping increases its depth to the west beyond the survey area.

(ii) FE anomaly, detected in the eastern part on n=1 and n=3 maps and in the central part on n=5 map, is distributed within a low to middle apparent resistivity zone where the Perau holizon exists Then, this anomaly seems to reflect the Perau horizon. As apparent resistivity values are a little lower than those of Phase II survey, it is suggested that this FE anomaly is due to dominant graphite schist in the lower formation and/or dominant magnetite in the upper formation of the Perau horizon

However, any remarkable anomalies are not seen in the south of line M, so it is suggested that the mineralization in the Perau horizon is very weak. Therefore, in the south of line M, although Perau horizon is distributed, the possibility of the existance of the mineralization in the Perau horizon is very little.

2–3–2 Barrinha area

(1) Sections (Fig. II–2–9 ~ II–2–15)

In this area, the background value of FE is very high, so FE values of more than 4% are treated as anomalies. On the other hand, apparent resistivity are classified roughly into three groups, namely their ranges are:

low apparent resistivity : less than 250 ohm-m,
middle apparent resistivity : 250 ohm-m to 600 ohm-m,
high apparent resistivity : more than 600 ohm-m.

A) FE

General characteristics of FE anomalies found in this area are as follows:

(i) FE anomalies, detected in the northern parts of all survey lines, show north dipping and seem to form a large FE anomalous zone.

(ii) On the other hand, FE anomalies detected in the southern part of the survey area are local or independent anomalies because there are no extentions on neighbouring survey lines.

(iii) These local FE anomalies can be seen remarkably on the lines west of line BE.

Taking above-mentioned characteristics into considerations, remarkable FE anomalies on each survey line are described below·

1) B1 anomaly

This anomaly is detected between No. 11 and No 13 on line BA.

a. The anomaly is seen from the surface to the depths, and judging from its anomaly pattern it seems to be due to south dipping anomalous source.

b. An FE anomaly detected at No. 11 to No. 12 on line BB may be caused by the same anomalous source as B1 anomaly from its location and shape.

c. An FE anomaly found in the depths below No. 11 to No. 15 on line BC corresponds to the western extention of B1 anomaly.

2) B2 anomaly

B2 anomaly is seen below No. 3 and No. 7.5 on line BC.

a. This is consisted of two FE anomalies, that is, one centered at No. 3.5–4, and the other centered at near No. 7. The former is inferred to be due to vertical anomalous sources, and the latter to be due to north dipping anomalous source.

b. Judging from the portion and the shape of anomaly, the former anomaly seems to be caused by the same anomalous source as FE anomalies detected between No. 2 5 and No. 4 on lines BA and BB. This anomaly becomes the biggest and strongest near line BC, however, it seems to have a trendency to decrease FE values toward line BD

c. On the other hand, the latter anomaly disappears at line BB.

d. On line BC, besides these two anomalies, two anomalies of more than 5% FE are seen from the surface to the depths below No. 7 to No. 11, and in the depths below No. 12 to No. 17.

3) B3 anomaly

B3 anomaly is detected below No. 3 to No. 9 on line BD.

a. This anomaly shows the most typical anomaly pattern within FE anomalies detected in this area, and the similar pattern with B2 anomaly mentioned at 2).

This B3 anomaly is consisted of two anomalies, namely, one centered below No. 3 and No. 4, and the other centered below No 6.5 and No. 8.5.

b. The former shows north dipping and seems to be due to the same source as northern anomaly (No. 3.5 and No. 4) of B2 anomaly.

c. The latter also shows north dipping and is seen from the surface to the depths, remaining high FE values. Although this anomaly seems to be a part of a large anomaly detected below No. 7 on line BC, this anomaly becomes broadest near line BD. This anomaly is seen in the depths on line BE, so it seems that this anomaly attenuates rapidly at the south side of line BD

4) B4 anomaly

This anomaly is seen below No 14 and No. 15.5 on line BE.

a. This anomaly is weaker than other FE anomalies mentioned at 1) to 3), but this anomaly is also one of typical FE anomalies in the Barrinha area

b. Any anomalies to be due to the same source can not be found on the neibouring survey lines so that this is called as 'local' FE anomaly. Especially, FE anomalies found on lines BF and BG seem to be typical local FE anomalies.

B) Apparent Resistivity

In Barrinha area, apparent resistivity range from 50 ohm-m to 2,500 ohm-m.

Low, middle and high apparent resistivity are found at similar portion on each survey line respectively, so the area may be classified into three types of zones, that is, low, middle and high apparent resistivity zones

Dense iso-contour lines found below No. 16 on line BB suggests the existence of the boundary of rock facies with different resistivity each other.

1) Low apparent resistivity zone (less than 250 ohm-m)

Two low apparent resistivity zones are found in the northwestern and the southern parts of the survey area. The former (northwestern) is located on the north sides of lines BA to BE. On the other hand, the latter (southern) at the south sides of lines BA to BG.

a) Northwestern low apparent resistivity zone

Low apparent resistivity are seen from the surface to the depths between No. 2 and No. 7 on lines BA to BD. This zone becomes the largest and the lowest on line BB, and it decreases its size and increases its value westward. It appears only in the depths on line BE and disappears on lines BF and BG.

b) Southern low apparent resistivity zone

Low apparent resistivity are found at the southern parts from No. 13 on all survey

lines, and especially, low resistivity of less than 10 ohm-m are distributed dominantly from the surface to the depths at the southern parts from No. 16 on lines BF and BG.

2) Middle apparent resistivity zone (250 ohm-m to 600 ohm-m)

This zone is found in the central part of the survey area. Middle apparent resistivity are seen from the surface to the depths between No. 7 and No. 13 on lines BA to BE. But apparent resistivity of more than 400 ohm-m are found wholly on lines BF and BG, so a little high apparent resistivity zone is formed at the southern part of the middle of the survey area.

3) High apparent resistivity zone (more than 600 ohm-m)

This zone is located mainly at the northwestern part of the survey area. On lines BA to BE, high apparent resistivity are found dispersedly within middle apparent resistivity zone of the central part of the survey area. High apparent resistivity anomaly detected below No. 7 to No. 13 on line BC, which shows north dipping and a remarkable contrast with surroundings, becomes small and weak on lines BD and BE. However high apparent resistivity are found dominantly at the northern parts of lines BF and BG.
and BG.

These high values may be induced by same kind of rock.

C) Relation of FE anomaly with apparent resistivity

Relations of remarkable FE anomalies mentioned at A) with apparent resistivity are described below.

1) B1 anomaly

This anomaly is distributed within low to middle apparent resistivity zone of less than 400 ohm-m. It may be called as 'low resistivity and high FE' anomaly.

2) B2 anomaly

This anomaly is located at the same portion of a low apparent resistivity zone. So it may be called as 'low resistivity and high FE' anomaly. It must be taken into consideration that FE values of more than 4% correspond to low apparent resistivity zone of less than 150 ohm-m in B2 anomaly.

3) B3 anomaly

This anomaly is distributed in a low apparent resistivity zone of less than 150 ohm-m and is thought to be caused by the same anomalous source as B2 anomaly. But, in this anomaly, metallic conduction factor shows higher values than one in B2 anomaly.

4) B4 FE anomaly

This anomaly is found within a middle apparent resistivity zone, so it seems to be due to different anomalous source with above-mentioned FE anomalies.

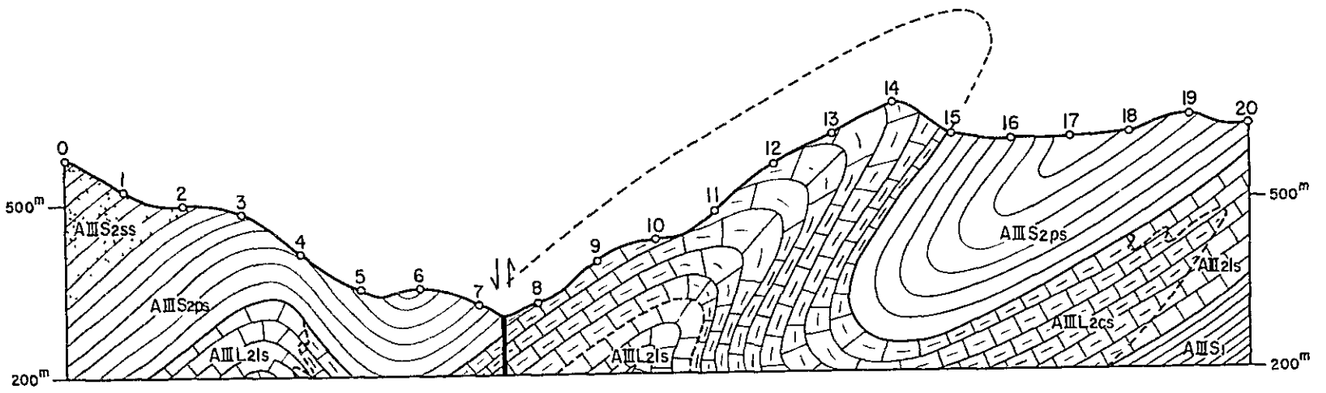

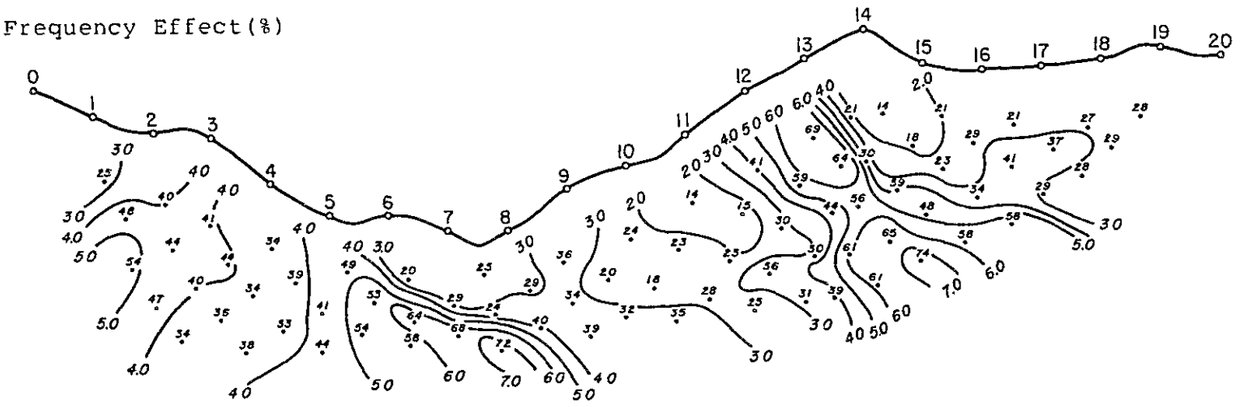

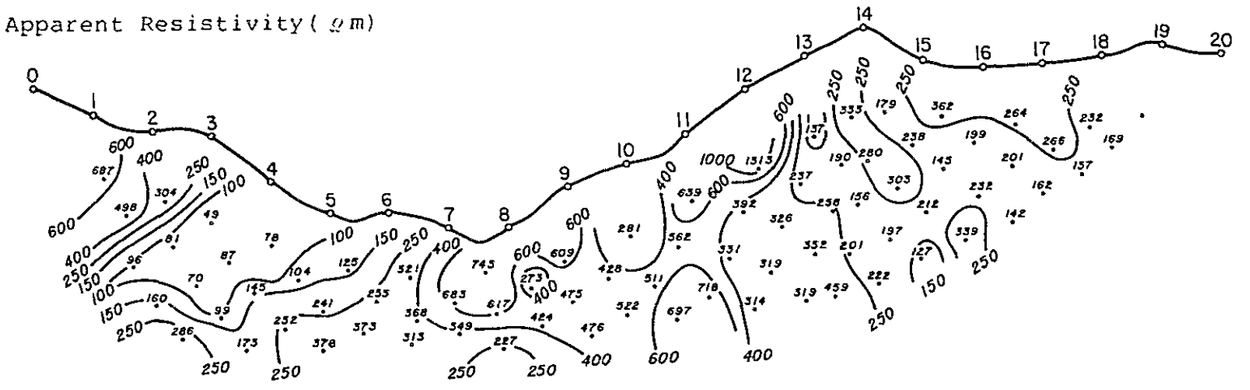

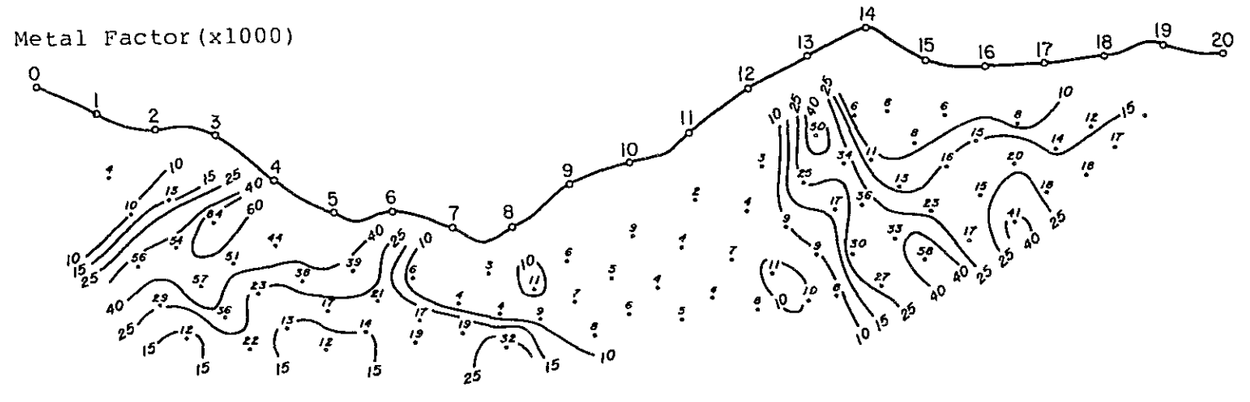

Fig. II－2－ 9 IP Pseudo-Section in Barrinha Area

(Line-BA)

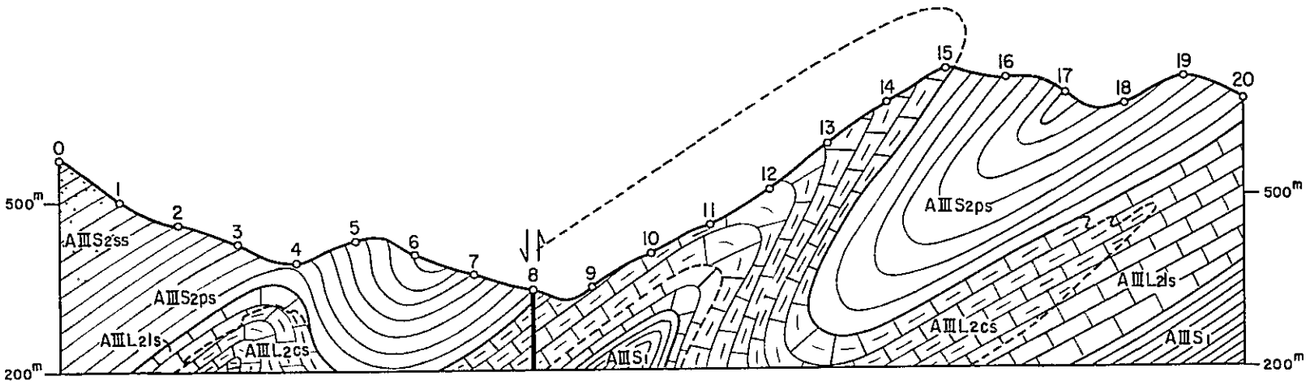

Frequency Effect(%)

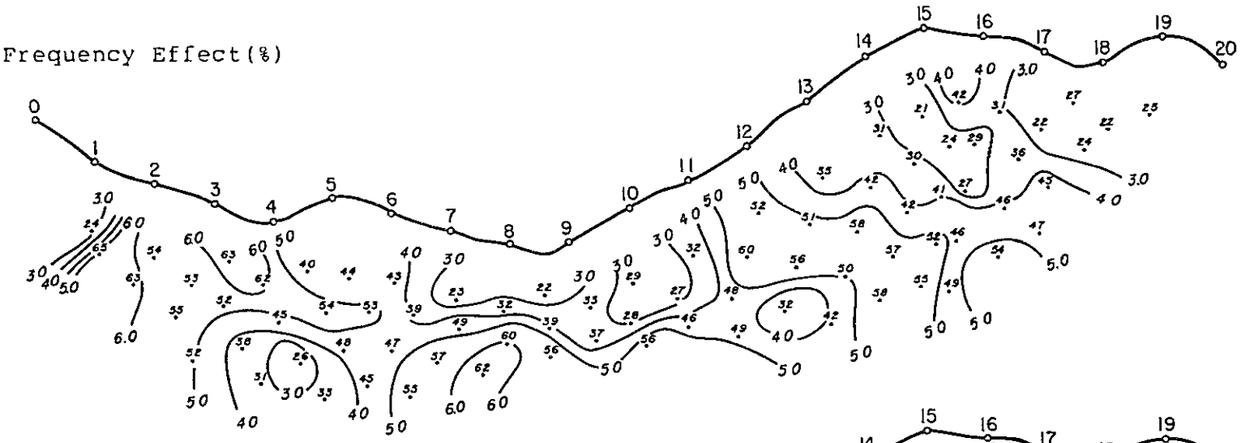

Apparent Resistivity(ϱ m)

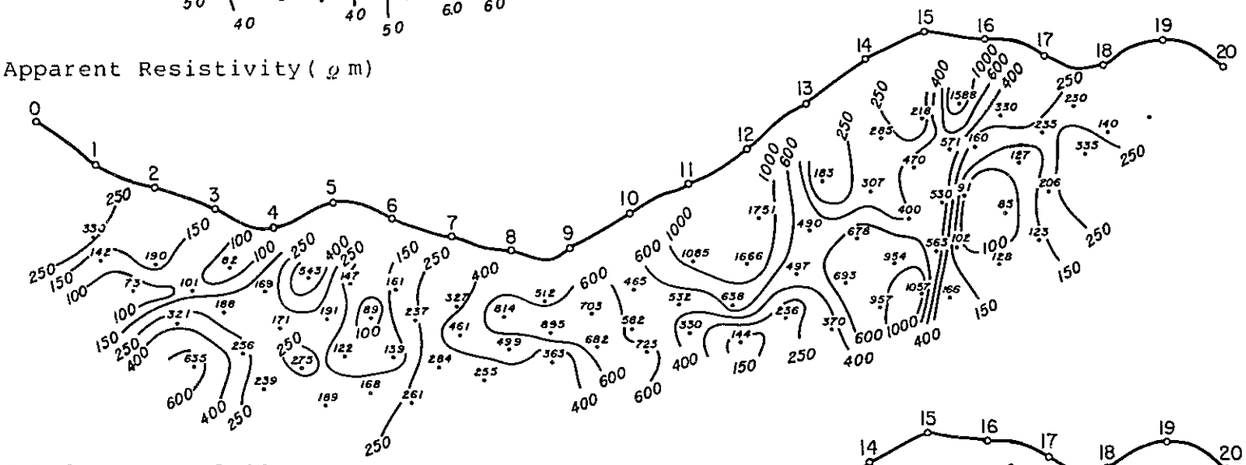

Metal Factor(x1000)

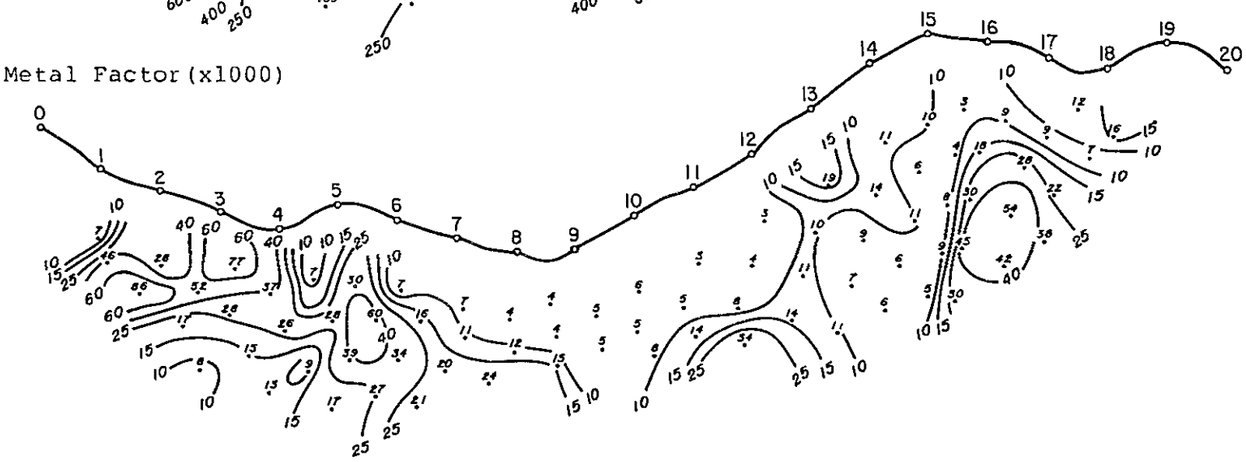

Fig. II－2－10 IP Pseudo-Section in Barrinha Area

(Line-BB)

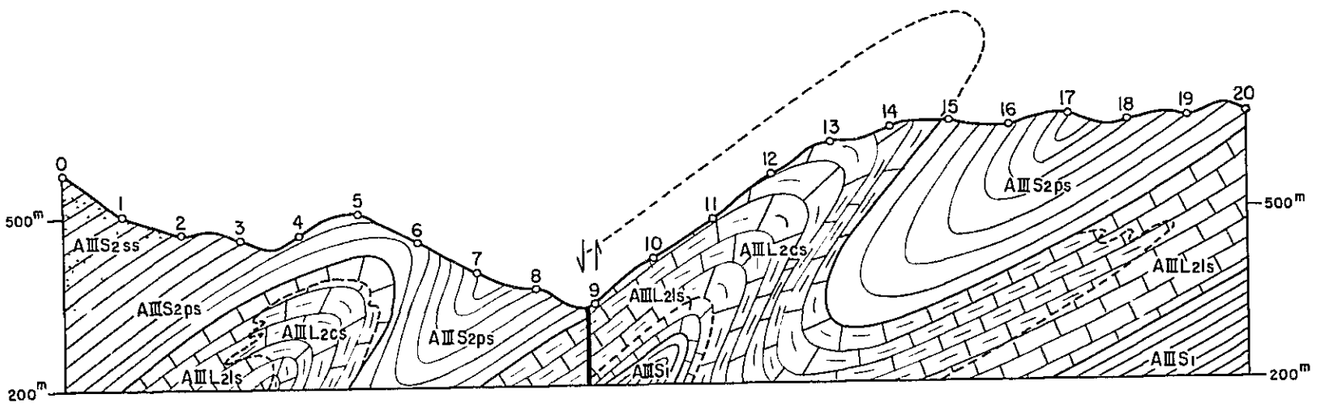

Frequency Effect(%)

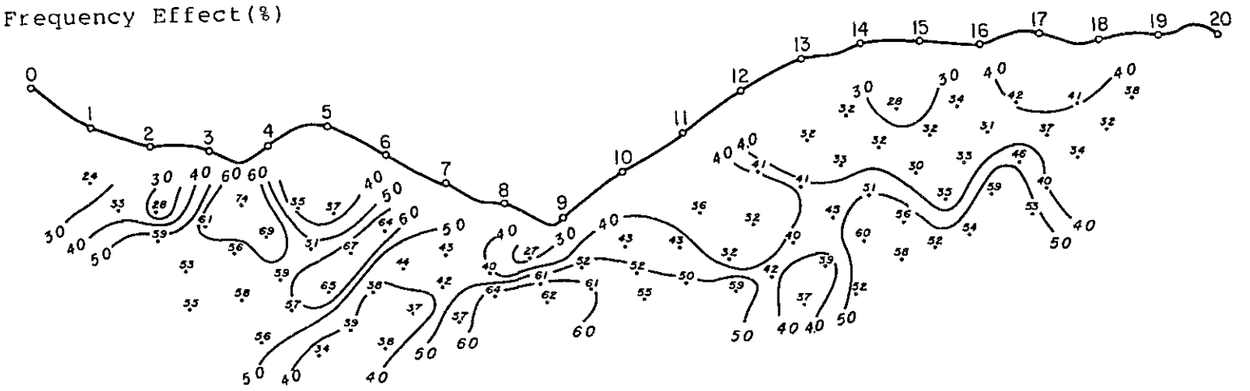

Apparent Resistivity(Ω m)

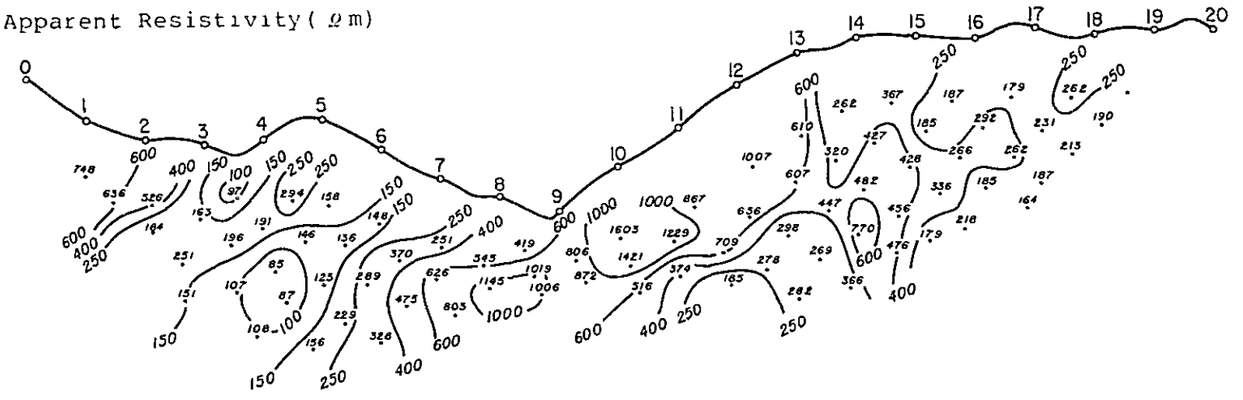

Metal factor(x1000)

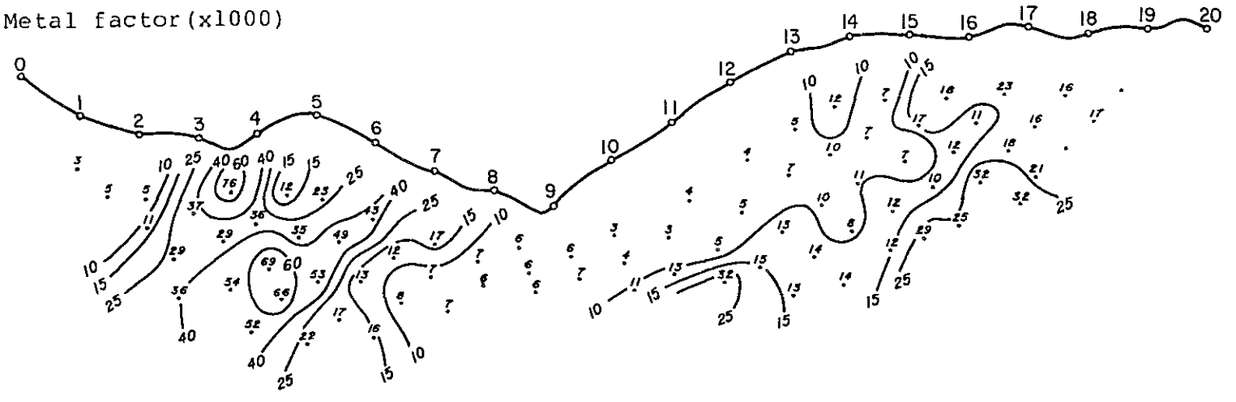

Fig. II－2－11 IP Pseudo-Section in Barrinha Area

(Line-BC)

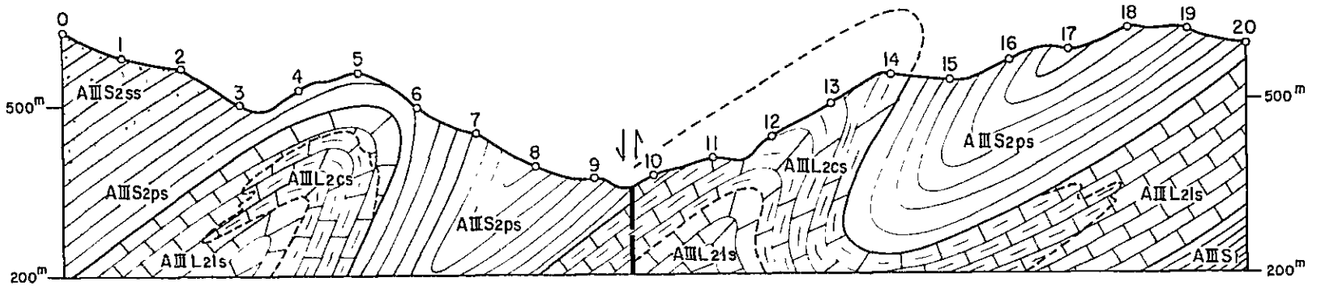

Frequency Effect(%)

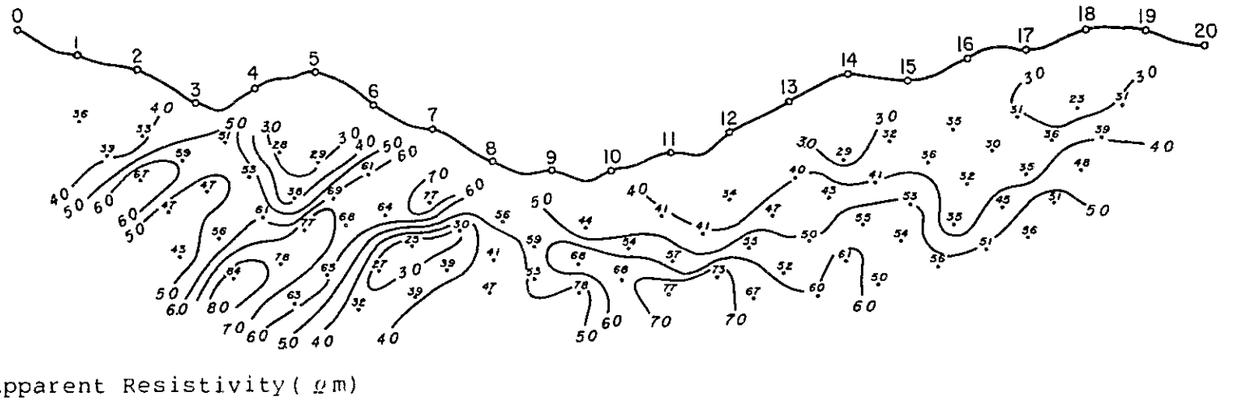

Apparent Resistivity(Ωm)

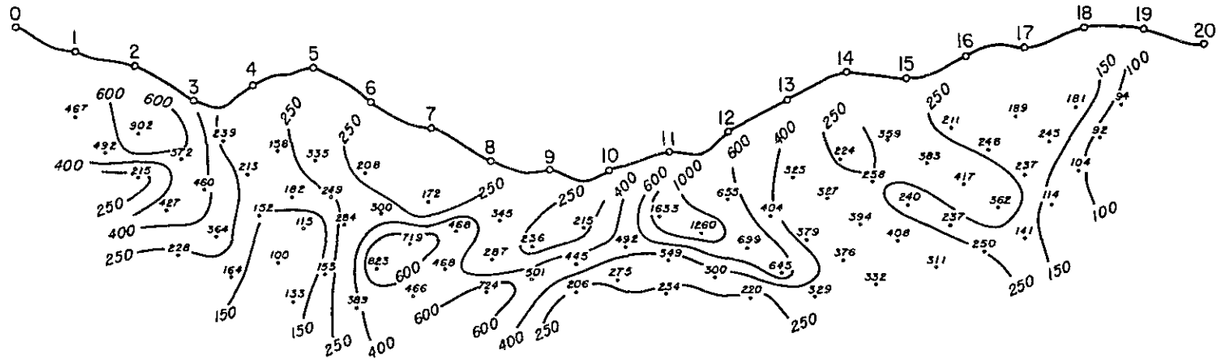

Metal Factor(x1000)

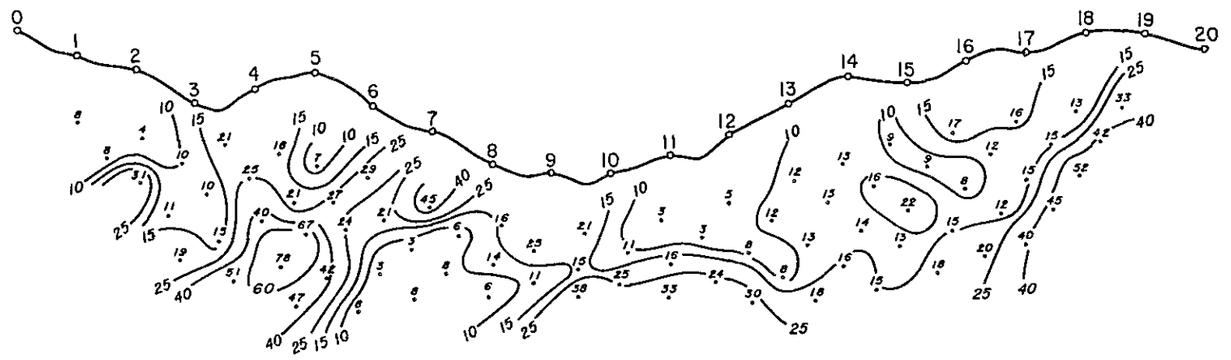

Fig. II－2－12 IP Pseudo-Section in Barrinha Area

(Line-BD)

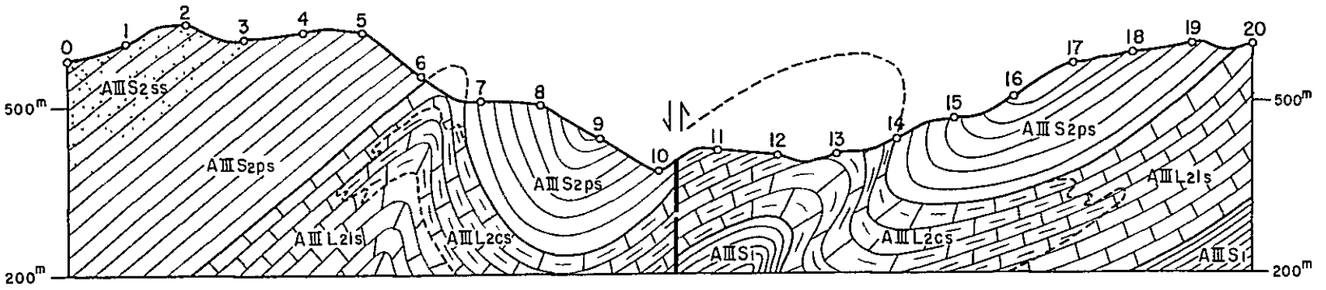

Frequency Effect(%)

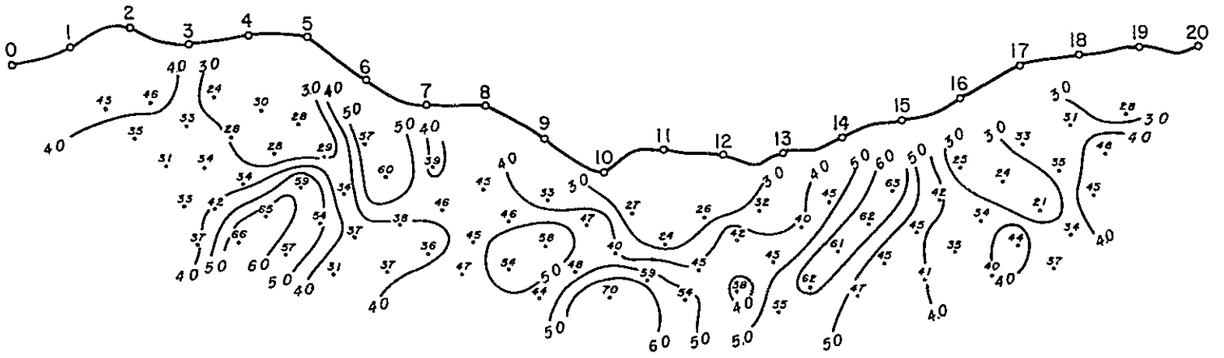

Apparent Resistivity(Ωm)

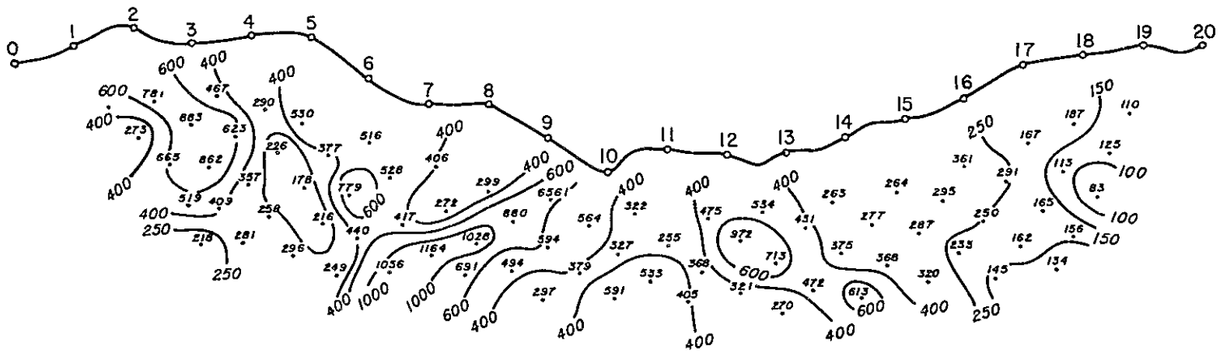

Metal Factor(x1000)

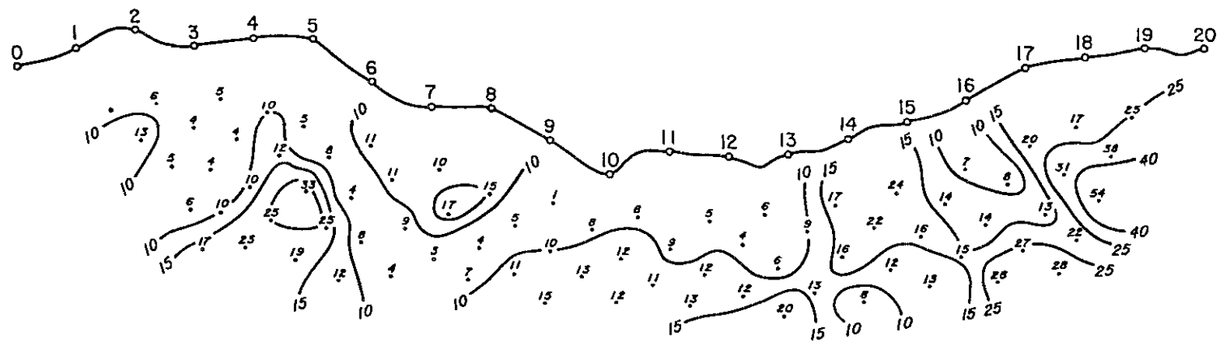

Fig. II－2－13 IP Pseudo-Section in Barrinha Area

(Line-BE)

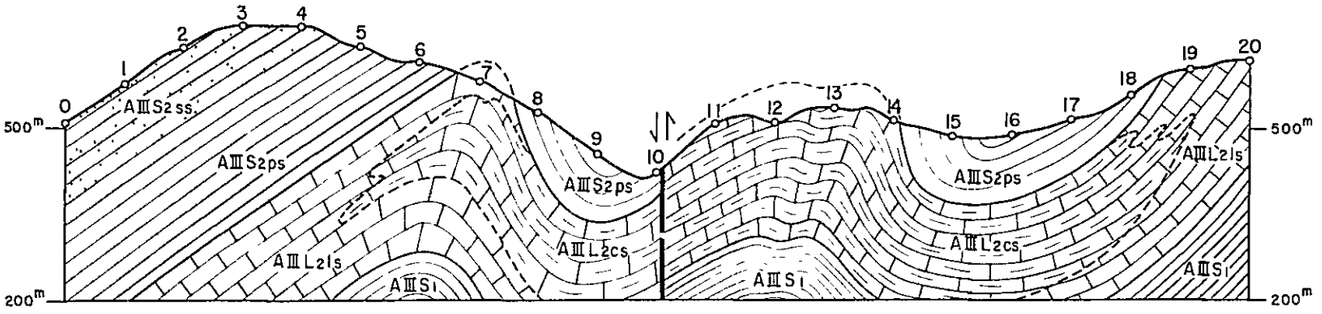

Frequency Effect(%)

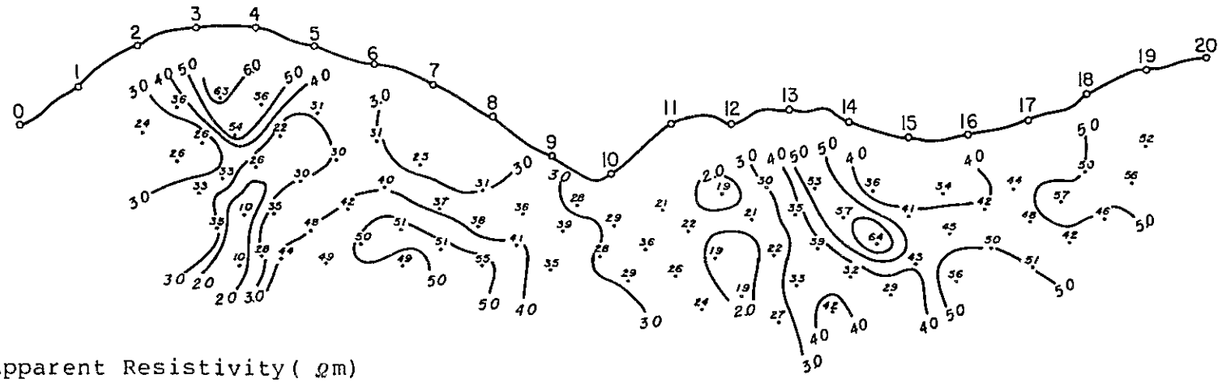

Apparent Resistivity(Ωm)

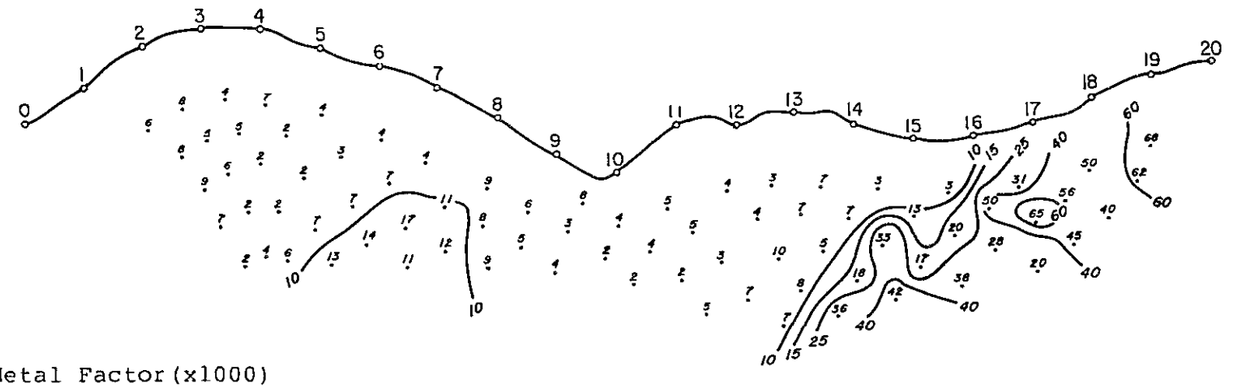

Metal Factor(x1000)

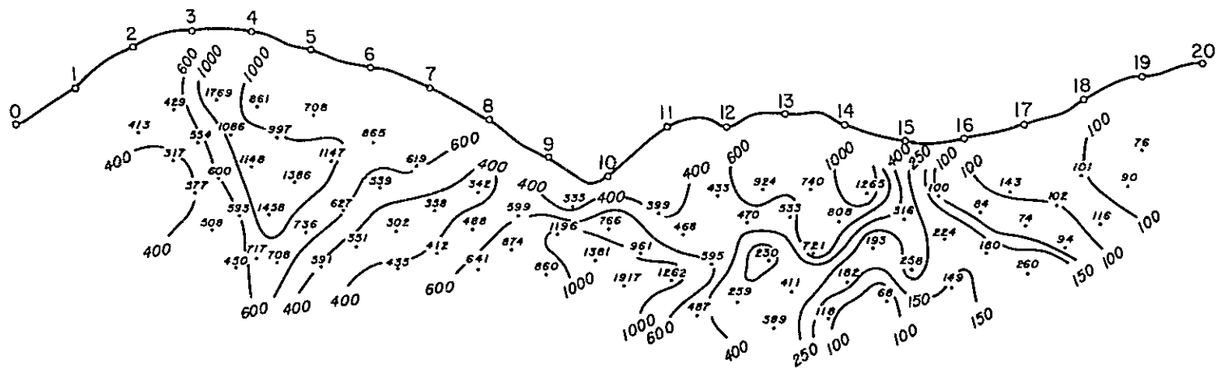

Fig. II－2－14 IP Pseudo-Section in Barrinha Area

(Line-BF)

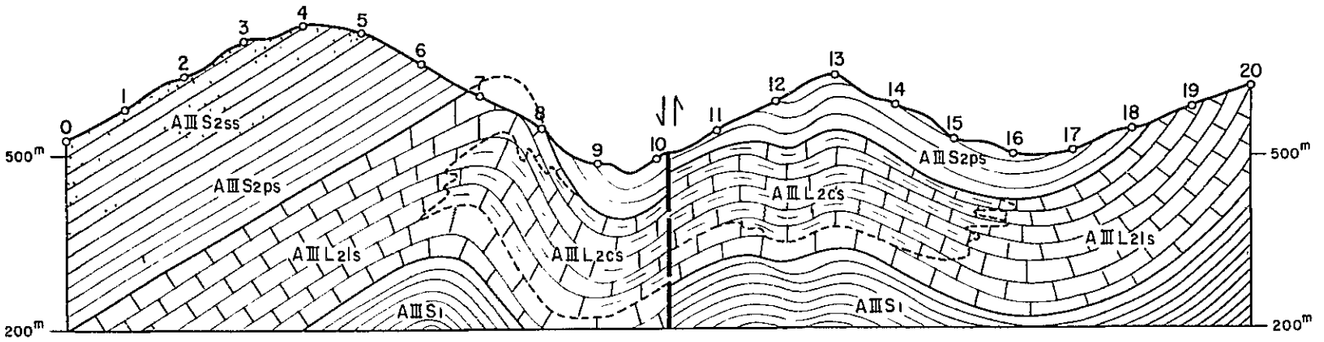

Frequency Effect(%)

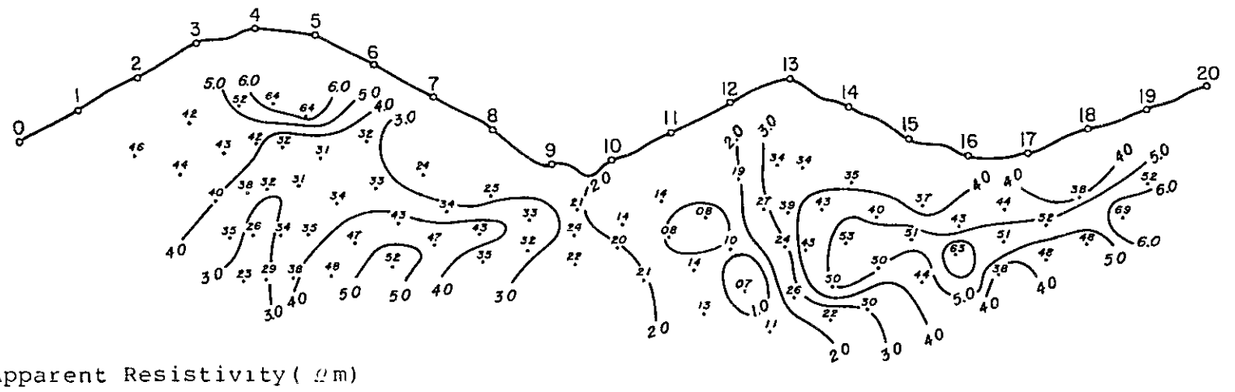

Apparent Resistivity(Ωm)

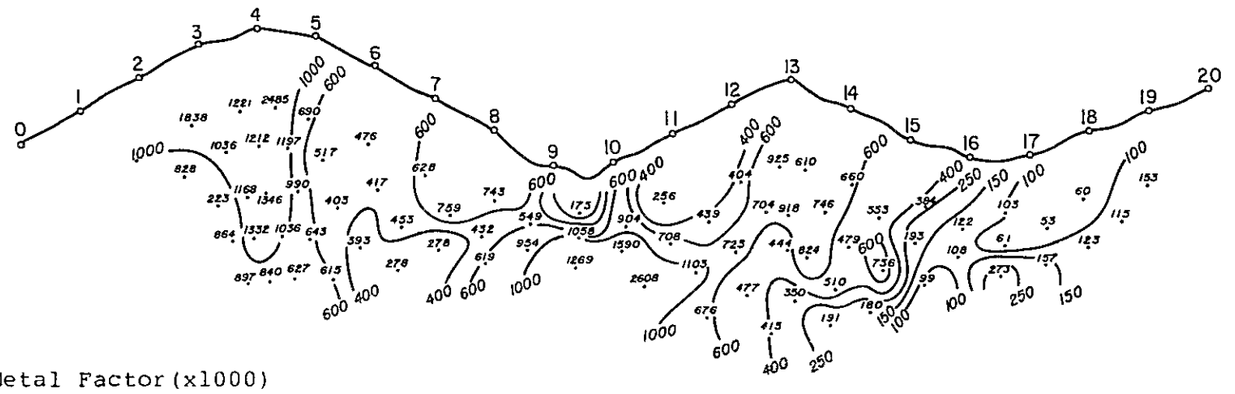

Metal Factor(x1000)

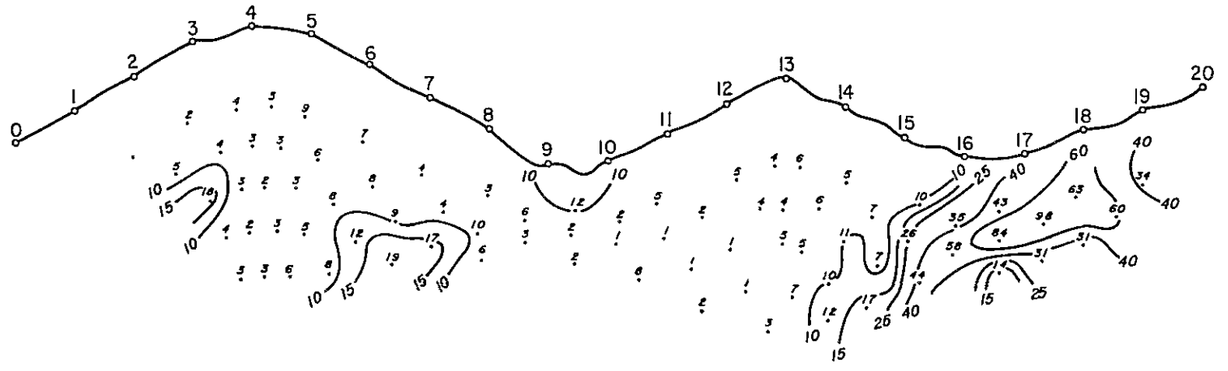

Fig. Ⅱ－2－15 IP Pseudo-Section in Barrinha Area

(Line-BG)

High values of metallic conduction factor are detected in this anomaly.

It must be taken into consideration that 'low resistivity and high FE' is one of good indicators for ore deposits or mineralization.

(2) Plan maps (PL. II–5)

Most of the FE and apparent resistivity anomalies detected in this area extend and increase towards depths with the eminent distribution in NE-SW and E-W direction. Interpretations on the plan maps are as follows:

n=1

FE anomalies more than 5% were detected in 6 places extending almost in N-S zone, in which the stronger anomalies were detected in nothern, southern and central part of the area.

Low to middle apparent resistivity zone are seen from the central to northeastern part of the area and in the southern part of the area in E-W direction with the tendency of extending towards south.

On the other hand, high resistivity zone are confirmed in the area surrounding the low resistivity zone detected in the middle of the area.

FE anomalies detected in the central and nothern part of the area generally correspond with low to middle resistivity zone except on lines BF and BG.

Another FE anomalies detected in the southern part of the area are only found on the southern end of lines BF and BG and the resistivity are rather high.

n=3

Three FE anomalies more than 5% are found in the northern area (north of No. 6 on lines BB-BD), and in central area (No. 8–11 on lines BC-BD) and in southern area (No. 14–16 on lines BA-BG). The distribution of apparent resistivity show the same tendency of NE-SW trending with n=1 and middle apparent resistivity is dominant in the central area.

FE anomaly detected in the northern area are in the zone of middle to low resistivity and considered to be the north dipping anomaly extending from the middle of the area on the surface.

FE anomaly in the middle of the area is not seen on n=1 which means it is due to the deeper sources and tends to extend towards south, but it may be a halo of the nothern anomaly.

Low resistivity in the northeastern part of the area distribute from line BE towards northeast in fan-shape spreading outside of the area surveyed. This low anomaly is also confirmed in the shallows.

Low resistivity in the south show the same E-W pattern with n=1 map but not very wide

in the depths.

High resistivity zones distribute in the northwest and central part of the area. The latter tends to extend in the depths by north dipping.

n=5

Two FE anomalies detected in the north (line BB-BE) are considered to be the deeper extension of n=1 and 3 anomaly detected in the north. The center of anomaly are far north than that of n=1 and 3 within the zone of low resistivity.

Broken arrow shaped FE anomaly seen from northeastern part towards south consist of two anomalous zones. Southern zone of No. 4 on line BA-BE and zone from No. 6–9 on line BA to line BE in NE-SW direction. The former one is considered to be the halo of the northern anomaly and the latter one is due to the deep sources.

(3) Correlation with geology

FE and apparent resistivity anomalies referred to in each plan map can be summerized as follows with the geological considerations.

(i) Eminent FE anomalies are found in the northeastern part of the area extending towards north in the depths.

(ii) FE anomalies detected in the middle of the survey area towards south seem to be due to the deep sources judging from the plan maps of n=1 and n=1

(iii) Vertical changes of apparent resistivity is not very clear and all resistivity anomalies tend to extend to the depths by north dipping.

(iv) Most interesting FE anomalies found in the northeastern part of the area coincide with the area of the steep change of resistivity.

(v) Judging from the apparent resistivity distribution dominant geological structure of this area is considered to be NE-SW or E-W.

(vi) Apparent resistivity suggests that the geology of this area reflect the big contrast of their physical properties.

(vii) Both high resistivity in the north and low resistivity in the south are detected in quartz selicite schist ($A\ III s_2$) which means the former selicite schist contain much quartz and the latter less quartz with strong weathering.

2–3–3 Physical property measurement

Resistivity of 50 rock samples collected in Barrinha were measured for four kinds of rocks; limestone, mica schist, carbonate schist and sand stone. One of the rock samples collapsed in the water during measurement so that the resistivity and FE were measured for 49 rock samples.

Results are shown in Table II–2–3 with PFE and Resistivity of Rock Samples in Barrinha Area.

One caution is that the results of physical property of the rock samples collected on the surface do not always represent the real property of the area. The following comment can be made for the samples of Barrinha area.

Limestone

Fifteen limestones were measured in which pure limestones are 11 and the rest are impure.

Resistivity of those samples range from 214 to 6,230 ohm-m with an average of 1,658 ohm-m. FE vary from −1.8 to 11.9% with an average of 4.7%, but it becomes 5.2% without an unusual value of −1.8% (BE−10).

As shown in Table II–2–3, resistivity of limestone can be separated into two groups; samples less than 1,000 ohm-m (BA−15, BD−13, BF−18.5 and BF−19) correspond with impure limestones, while more than 1,000 ohm-m ones with pure limestones.

Actual resistivity of limestones in this area would be from 1,000 to 2,000 ohm-m with FE values of 3 to 6%.

Calc-schist

Eleven rock samples of calc-schist were measured, and their average resistivity is 624 Ωm and average FE is 4.9%. 4.9% is the highest average FE value among all rock samples in which BA−8.2, BC−8.5 and BG−9 have high FE values.

Resistivity are generally low, in which BA−12, BC−13, BF−10 and BF−12 are especially low indicating less than 100 Ωm These samples are porous and strongly weathered.

In connection with alteration, the samples are classified as follows.

(1)	Strongly weathered and altered	80 Ωm
(2)	Weakly ∿ intermediately weathered and altered	400 Ωm
(3)	No alteration	1,340 Ωm

Resistivity of calc-schist may be more than 1,000 Ωm, which is a little lower than that of limestone.

Quartz sericite schist

Sixteen samples show the resistivity of 51 to 1,173 Ωm and FE of 1.1 to 6.1%. An average resistivity of these samples is 624 ohm-m which is the lowest value of four kinds of rocks in this area, and 4.9% of FE which is the highest of all. BA−8.2, BB−8.5 and BG−9 show high FE values and BA−12, BB−12, BC−13, BF−10 and BF−12 show low resistivity of less than 100 ohm-m, which are due to high porosity with strong weathering.

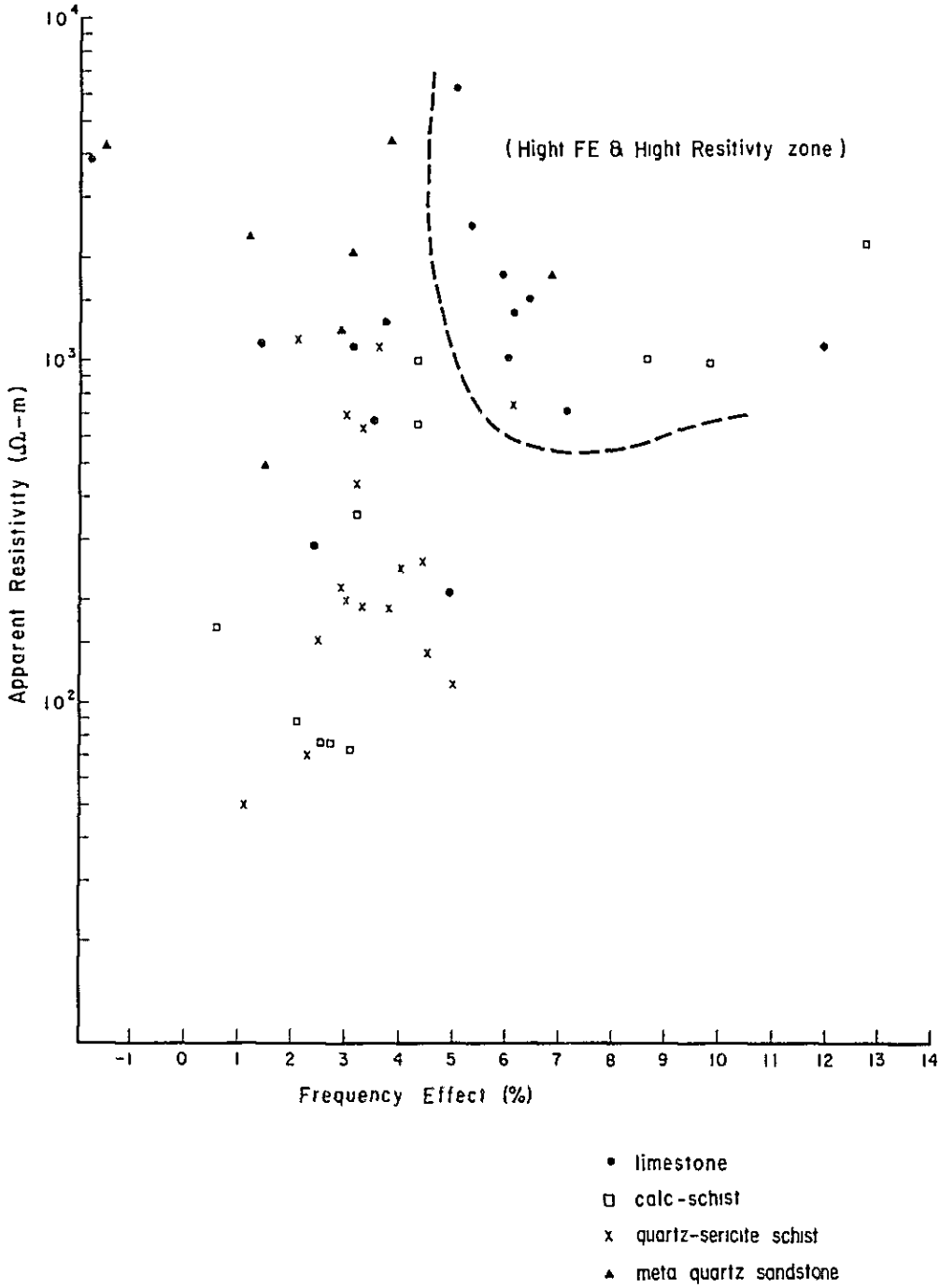

Fig. Ⅱ—2—16

Correlation between PFE and Resistivity of Rock Samples

Table II–2–3 PFF and Resistivity of Rock Samples in Barrinha Area

Limestone

Sample name	Resistivity (Ωm)	PEE (%)
BA - 8.5	1068	6.0
10.5	6230	5.0
15	722	7.1
BB - 9 5	1271	3.7
BC 10	1544	6.4
BC - 10	1362	6.1
11	1111	3 1
12	2453	5 3
13	670	3.5
BE - 10	3912	- 1.8
16	1778	5 9
BF - 7	1140	1.4
18 5 (B)	214	4.9
19	228	2.4
BG - 7	1105	11.9
15 pcs	2089	4.7

Calc-Schist

Sample name	Resistivity (Ωm)	PEE (%)
BA - 8 5	1026	8.6
12	76	2.7
BB - 11	1015	4 3
12	77	2 6
BC - 8 5	975	9 8
13	88	2.1
BF - 11	364	3 2
BF - 10	168	0 6
12	73	3 1
13	660	4.3
BG - 9	2341	12.7
11 pcs	624	4 9

Quartz Sericite Schist

Sample name	Resistivity (Ωm)	PEE (%)
BB - 2	249	4.0
BC 9	51	1.1
15	191	3 8
BD 6	116	5.0
8	201	3 0
15	71	2.3
BF 2	216	2 9
6 5	141	4 5
15.7	747	6.1
BI 4	259	4 4
16	1173	2.1
18 5 (S)	442	3.2
BG - 2.5	191	3 3
4.5	700	3 0
9 3	643	3.3
16	154	2.5
16 pcs	344	3.4

Meta quartz Sandstone

Sample name	Resistivity (Ωm)	PEE (%)
BA - 7.5	2105	3.1
BB - 3	2331	1.2
7	1839	6.8
BC - 3	512	1.5
BD - 3	4398	3.8
BI - 2	1253	2.9
6 5	4345	- 1.5
7 pcs	2398	2.5

Strong weathered rocks .....80 ohm-m

Weak weathered rocks ..... 400 ohm-m

No weathered rocks ..... 1,300 ohm-m

Quartz sacricite schist without weathering must be around 1,000 ohm-m which is almost same as limestone.

Meta quartz Sandstone

Only 7 samples show less deviation than the other rocks with an average of 2,398 ohm-m and 2.5%. BC–3 shows low resistivity as it is cracky, and BB–7 shows high FE anomaly as it contains pyrite.

Average value without anomalous values mentioned above is 2,712 ohm-m and 2.5%. Consequently, resistivity of quartz sandstone is more than 2,000 ohm-m and FE is around 2 to 3%.

2–3–4 Results of Model Simulation

The IP effect can be studied by simulation using digital model for the most interesting anomalies detected in the survey.

The following simulations shown in Fig. II–2–17 ∿ Fig. II–2–20 are adopted on four lines BA, BB, BC and BD.

The approximate values are close enough for geophysical purposes, considering that the earth is more complex than these models, and that data always have some noise.

However, because the full solution requires double the number of cells, and computer time increase as the cube of number of cells, the approximate solution is much less expensive.

Assumed model

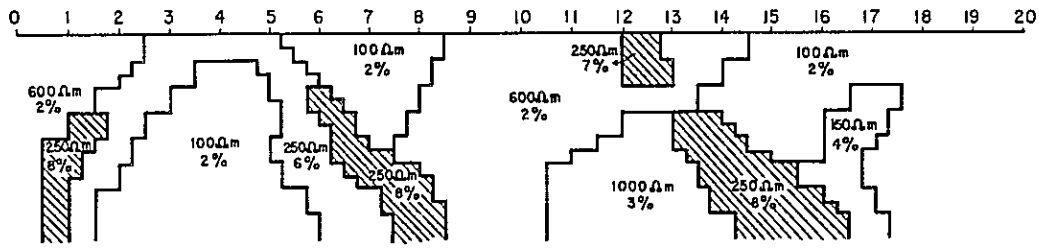

Calculated value

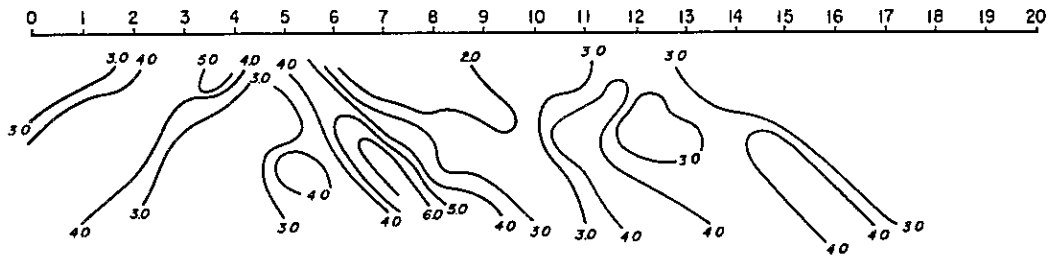

Observed value

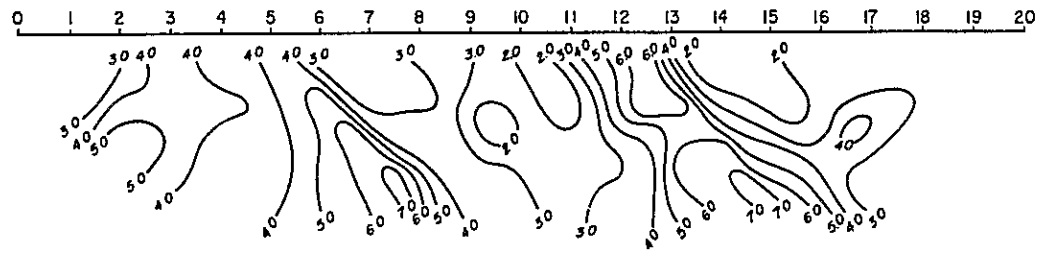

Fig. II－2－17 IP Model Calculation (Line-BA)

Assumed model

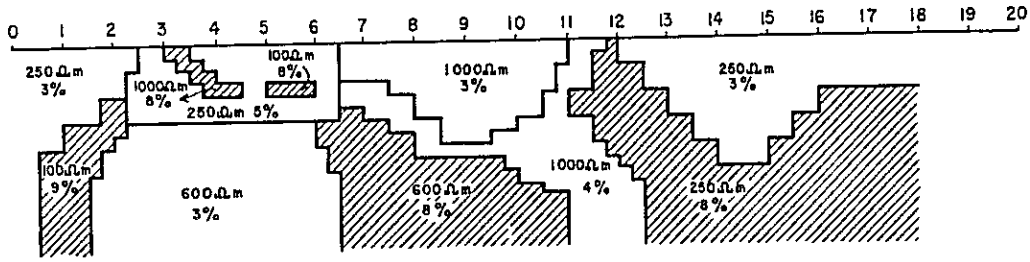

Calculated value

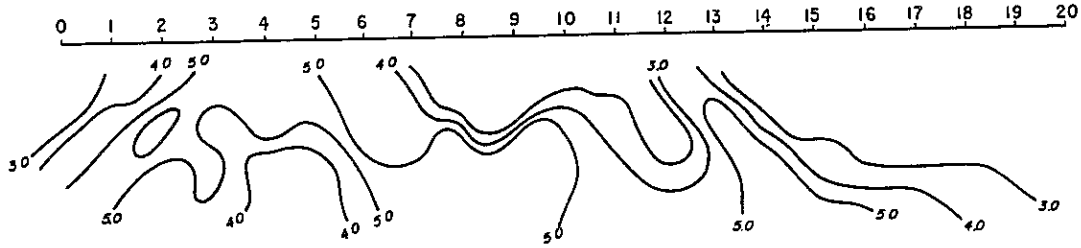

Observed value

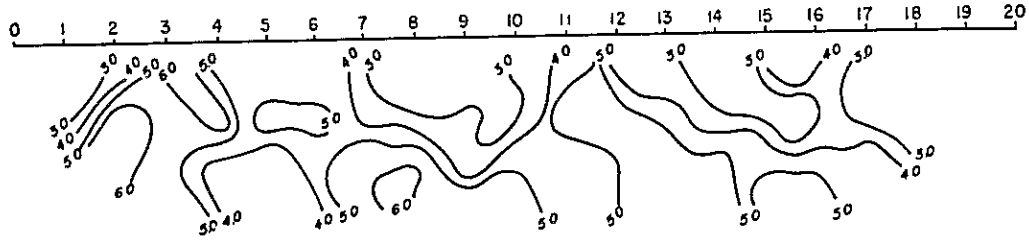

Fig. II－2－18 IP Model Calculation (Line-BB)

Assumed model

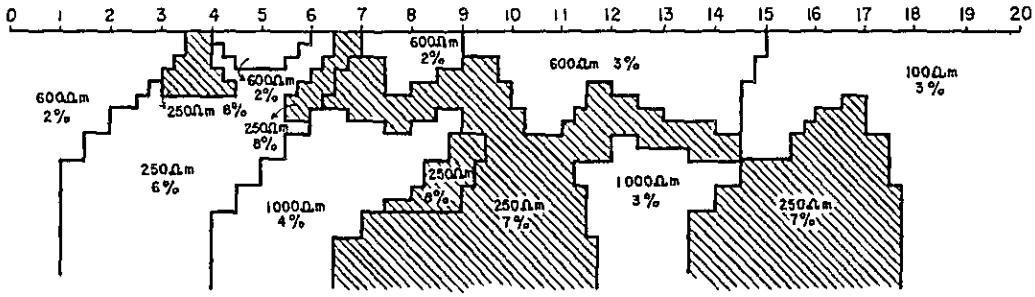

Calculated value

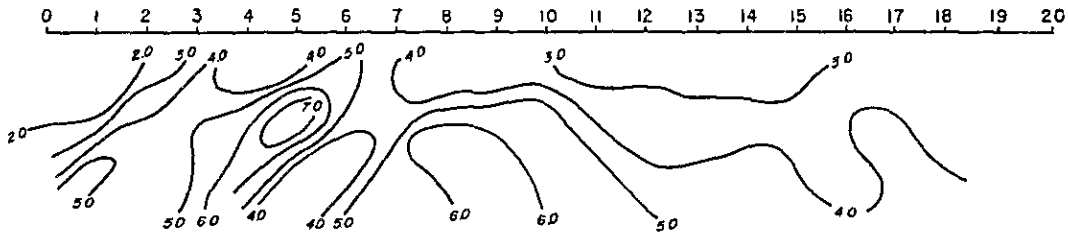

Observed value

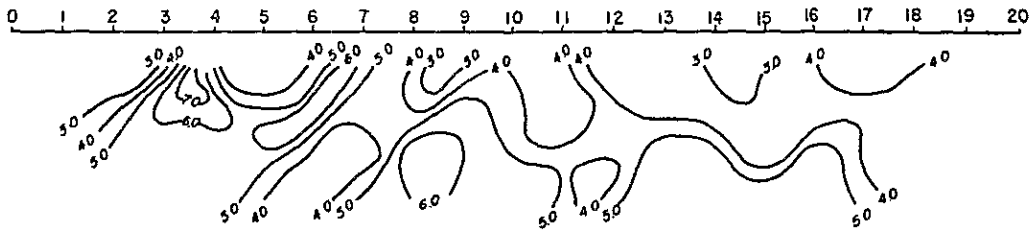

Fig. II－2－19 IP Model Calculation (Line-BC)

Assumed model

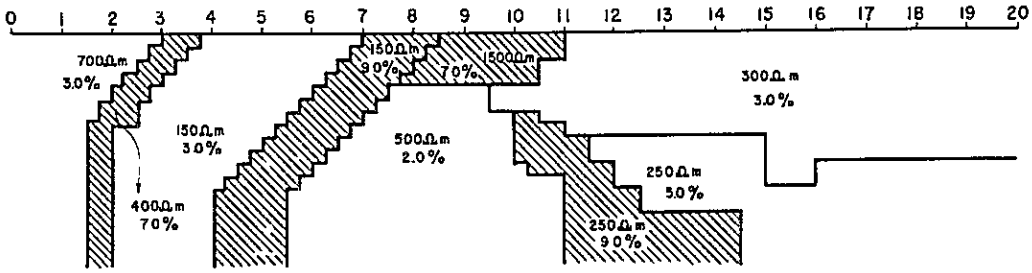

Calculated value

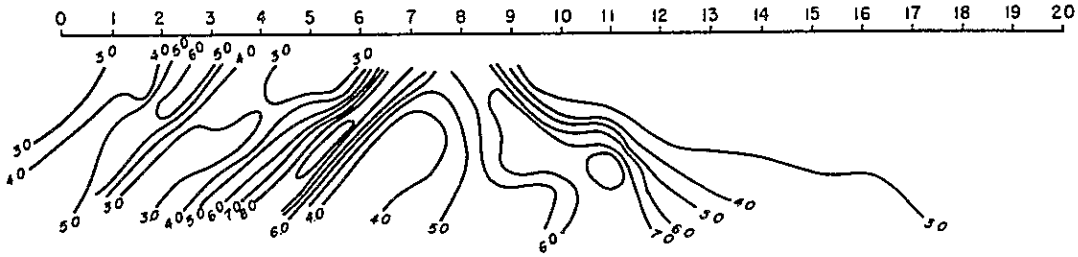

Observed value

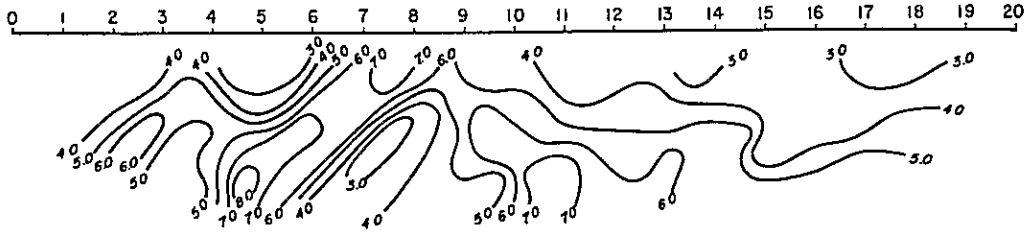

Fig. II－2－20 IP Model Calculation (Line-BD)

2–4 Summary of IP method

The results obtained by the IP survey are summarized here.

A) Perau Area

In this phase, IP electrical method was adopted in order to clarify the distribution of IP anomalous zones detected in Phase II survey and the relation between those IP anomalous zone and to know the mineralization in the south of the survey area of Phase II. The summary of result is presented here taking the drilling results into consideration.

1) FE values obrained by this survey range from 0.3% to 10%. Two FE anomalous zones with FE of more than 3% are found in the western and eastern parts of the survey area. FE anomalous zone detected at the western part shows NE-SW trending and the similar distribution with a low apparent resistivity zone. On the other hand, other zone detected at the eastern part, which is distributed in a middle apparent resistivity zone, shows NW-SE trending in the shallows but in the depths, it varies into weak anomaly from line N and extends southward beyond the survey area

2) Apparent resistivity range from 5 to 1,200 ohm-m. Dense iso-apparent resistivity lines are found in the whole area, which seem to reflect geological structure with strong contrasts of physical properties. Low, middle and high apparent resistivity zones are distributed laterally, that is, those are found from the surface to the depths respectively. High apparent resistivity are dominantly distributed at the southern part of the survey area.

3) Relation of FE anomaly mentioned above with IP anomalous zones detected in Phase II survey are described below.

a) IP anomalous zone (low resistivity and high FE) found at the western part is thought to be an extension of C anomalous zone detected in Phase II survey and distributed in AIPs (mica schist). This anomalous zone extends southward and its southern limit seems to be located at Perau anticlinal axis.

b) IP anomalous zone (middle resistivity and high FE) found at the eastern part is thought also as a southern extension of B anomalous zone detected in Phase II, which seems to be due to the Perau horizon. But in this area, as FE values are not high and apparent resistivity belong to middle range, mineralization in the Perau horizon seems to become rapidly weak southward from line M.

4) Resistivity of the Perau horizon may range from 300 to 500 ohm-m. And resistivity of AIPs is thought to be of less than 100 ohm-m, which is distributed in the southern part of the survey area where weak FE anomaly was detected.

B) Barrinha Area

1) Apparent resistivity observed in this survey range from 50 ohm-m to 1,800 ohm-m, and suggest that the geology in this area reflects the big contrast of their geophysical properties. High resistivity zones are found in the central and northern parts of this survey area. These high resistivity zones seem to be caused by meta-quartz sandstone and calc-schist ~ limestone sandstone and calc-schist ∿ limestone respectively.

On the other hand, low to middle resistivity zones are found in the northeastern and southern parts of the area. Low to middle resistivity zone in the northeastern part seems to be due to mica schist and limestone, and in the southern part to be due to weathered mica schist in the depth of 200 m below the surface and limestone in the depths.

These apparent resistivity are detected at north dipping and in the direction of NE-SW. These results coincide with the main geological structure in the survey area.

2) FE values obtained by this survey range from 0.7% to 8.4%. Remarkable FE anomalies of more than 4% are found in the northeastern part of the survey area, that is, the north from No. 8 on lines BB to BD. Another FE anomalies are detected at the north from No. 6 on lines BF and BG in the northwestern part of the area.

The former (northwestern anomaly) shows strong FE from the surface to the depths and its center increase its depth northward. As this anomaly is located in a low resistivity zone, this anomaly is classified as 'low resistivity and high FE' IP anomaly. This anomaly is distributed geologically in the upper part of calc-schist ∿ limestone, of which the upper layer is meta-quartz sandstone (partially mica schist). The geological structure in the vicinity of this anomaly shows overfold and north dipping, which coincides with the tendency of dips of FE anomaly. That is, two north dipping FE anomalies were detected on lines BC and BD. On the other hand, as geological structure near line BA shows a normal anticlinal structure, FE anomalies were found at both wings of its axis. In the vicinity of this anomaly, there exist mineral showings as like Saõ Joaquim etc. and this anomaly is located at the extension of these mineral showings, so that this anomaly seems to be related with these mineralization.

On the other hand, FE anomaly of the northwestern part is detected as 'high resistivity and high FE' anomaly at the shallow depth and shows north dipping as like northeastern anomaly. This anomaly is located in meta-quartz sandstone geologically. According to the results of the measurement of physical properties, meta-quartz sandstone shows high resistivity. In the vicinity of this anomaly, there are often floats of quartz-limonite vein, then this high resistivity and high FE anomaly may be caused by quartz-limonite vein. However, mineralization accompanying with quartz vein seems to be small scale.

3) FE anomaly found at the southern part of the survey area is presented as a local anomaly at the shallow depth, but it is distributed bloadly in the depths.

As, in the vicinity of this anomaly, there are mineral showings as like Celisa etc. which is enbeded in limestone, this anomaly may be related with these mineralization.

CHAPTER 3. SPECTRAL IP METHOD

3–1 The spectral IP

Conventional IP data contain essentially direct-current resistivity information, but if a maximum amount of electrical knowledge is desired, it is necessary to use additional alternating-current frequencies, looking at both the in- and out-of-phase components.

The spectral IP (SIP) or the complex-resistivity (CR) method is a variable-frequency, ground contact method of studying the electrical properties of the earth by which the both in-phase and out-of-phase components of the earth's total resistivity are analyzed. The spectral IP is a major step forward in electrical geophysical exploration inasmuch as it perceives the different parameters of the IP, resistivity, and related electrical and electromagnetic properties of the earth, separates their individual contribution, and presents a display for visual analysis and interpretation. Conventional IP survey has been used for many years and will be used in the field for many years to come, the future trend in electrical surveying seems to be in the direction of spectral IP surveying.

3–2 Results of Analysis

There are many known ore deposits and mineralization in Barrinha area, where the spectral IP was conducted in this phase.

The spectral IP was adopted in order to clarify the possibility of finding the deep ore deposit in this area with the active Quatro deposit as its center, and to know the effect of this method for the vein to layered type ore deposit.

It has been noticed that there is a predictable but as yet unexplained association between spectral signatures and different rock types. But, these phase spectrum are defined as followings, which are the different difinition from Zonge types. A, B and C responses are shown in an idealized form as follows:

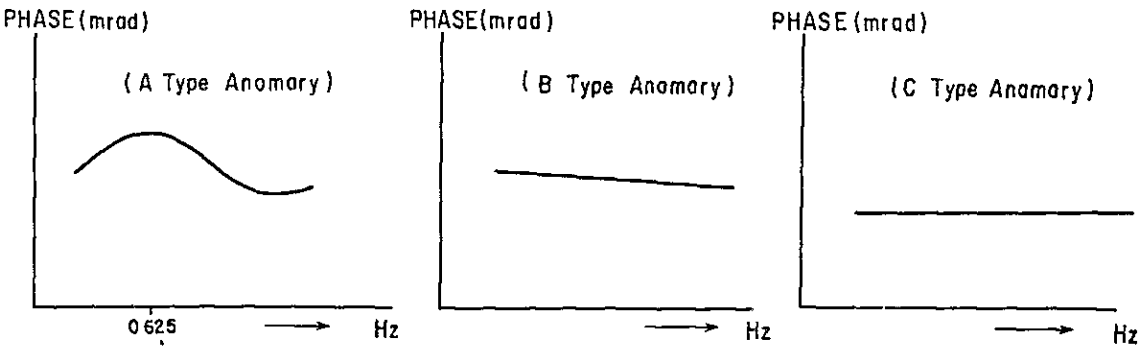

1) A type A response shows a phase spectrum with a peak of phase around 0.625 to 0.875 Hz.

2) A type B response is characterized by decreasing phase spectrum with increasing frequency in the frequency range less than 1 Hz.

3) A type C response is characterized by a constant or a slightly increasing phase spectrum with increasing frequency.

These spectral types mentioned above are all seen on line BH, so that the consideration on each spectral type are made as follows:

1) Type A anomaly;

This type of anomaly are seen at around No. 6.5 on line BH from the depth of n=1 increasing to the depths. But nowhere in this area are seen the same anomaly with this type. Apparent resistivity of the anomalous zone are less than 250 ohm-m, which tend to decrease with increasing IP anomaly.

2) Type B anomaly

This anomaly shows pants-leg shape and is a so-called "pipe line effect" detected as strong anomaly at No. 8 on line BH (south of type A anomaly). A typical pattern is seen on Cole-Cole map from n=1 to the depths at No. 8.5 by south dipping This kind of anomaly are sometimes found on the artificial buried pipes or the conductive layer, however, in this case, rails of the Quatro deposit excavation are so small that they would not affect too much. For this anomaly, phase response from 0.5 Hz to the lower frequency are extremely high which suggest the mineralized zone may exist in the depths.

Another type B anomalies are found in the following areas;

* On line BI, pants-leg shaped anomaly under No. 8 with n=2 as its top, and south dipping anomaly from n=1 to the depths at No. 11.5 are detected.
* On line BJ, some anomaly are found under No. 7 to No. 10, n=3 ~ 5, which are not stronger than that of No. 8 on line BI.
* On line BK, no anomaly is found at No. 8 as seen on the other lines, but there are strong phase response of more than 20 mrad at 0.125 Hz in the southern end of the line. Consequently, this anomaly must be an extension of the anomaly found on line BI.

3) Type C anomaly

This type shows the constant or slightly increasing phase spectrum with increasing frequency in the lower range than 1 Hz. This type of anomaly can be found around the Quatro and the Dito deposits, so that anomaly are due to their mineralization.

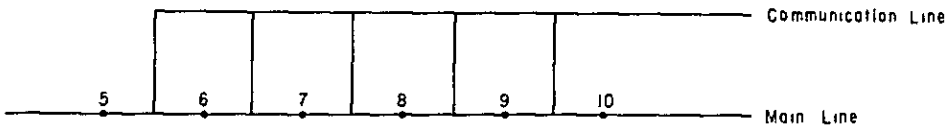

Fig. II–3–1 Survey and Communication Line

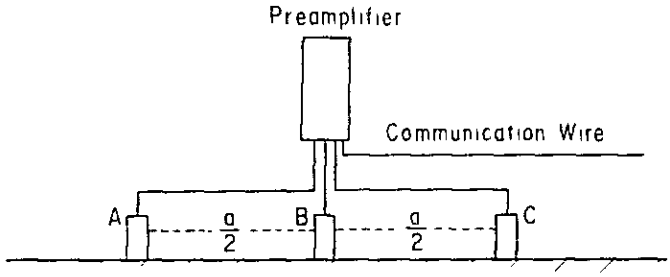

Fig. II–3–2 Arrangement of Potential Electrodes and Preamplifiers

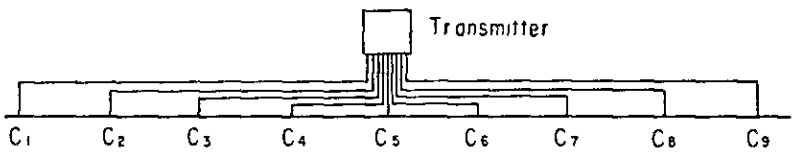

Fig. II–3–3 Arrangement of Current Electrodes and Wires

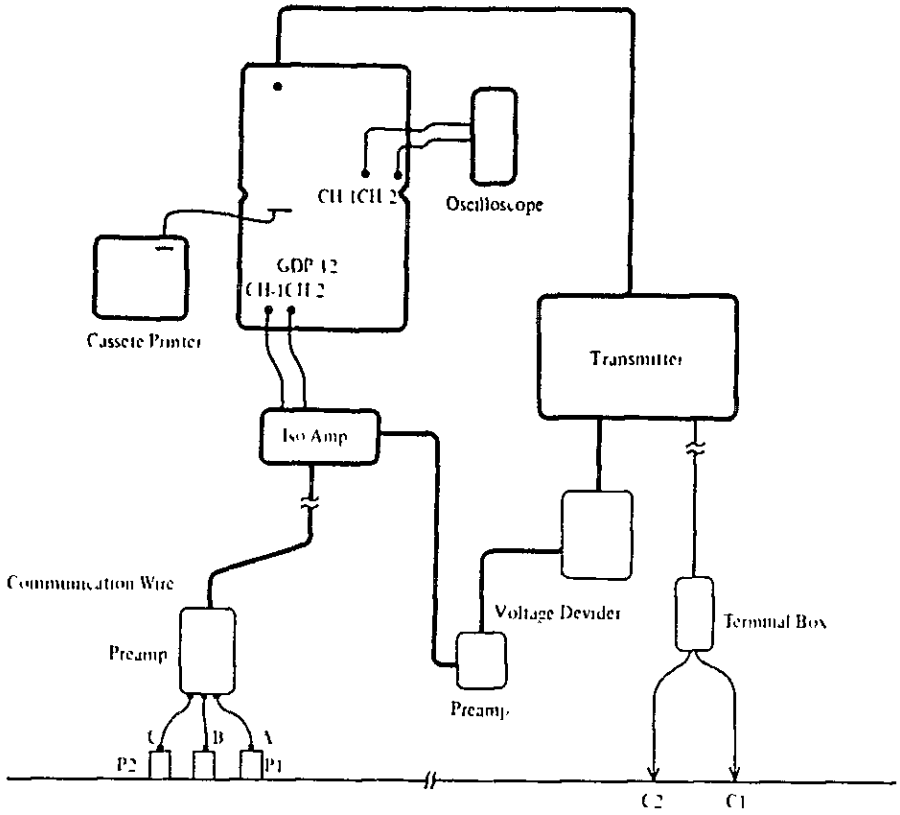

Fig. II–3–4 Block Diagram of Spectral IP Survey Instruments

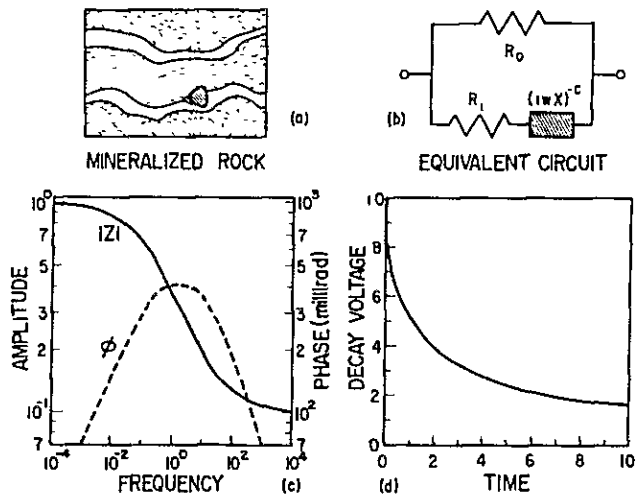

Fig. II–3–5 Spectral IP Effect

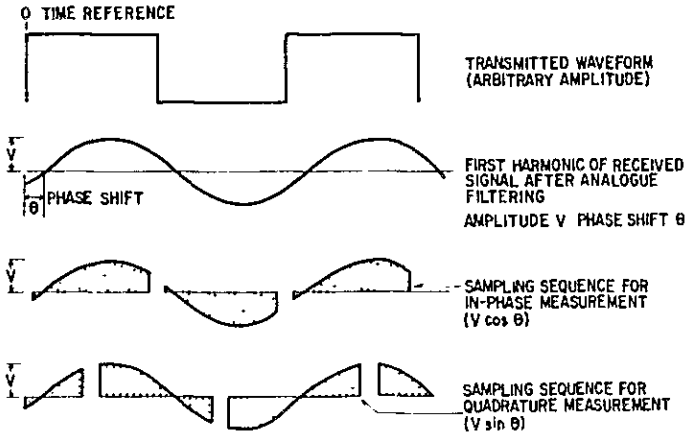

Fig. II–3–6 Transmitting and Receiving Wave-forms

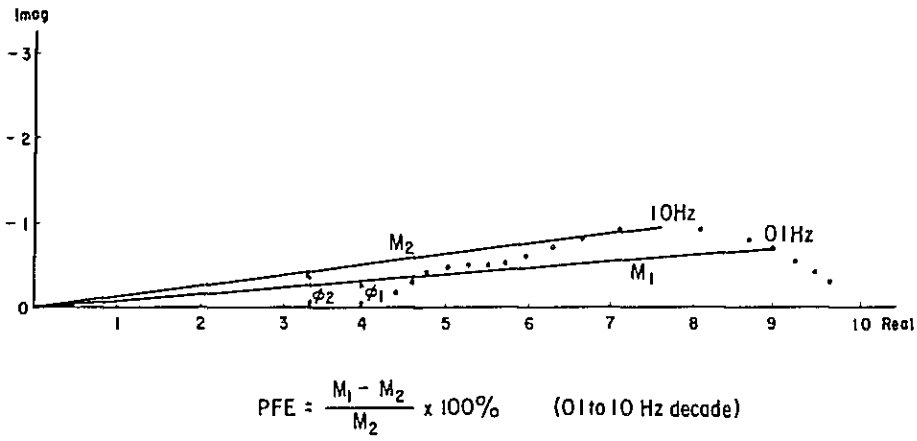

Fig. II–3–7 Relation between Frequency Effect and Phase Shift

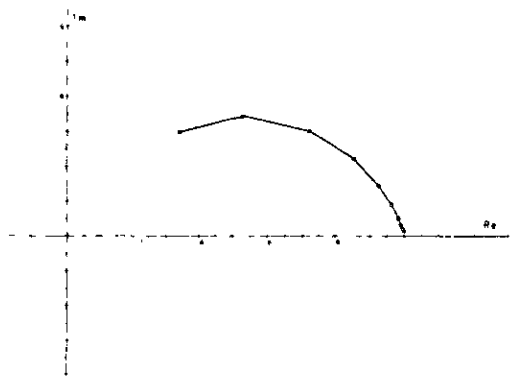

Fig. II–3–8 Example for Cole-Cole Diagram

1) C type anomaly due to the Dito deposit are seen in the following lines;

* On line BH, a weak phase anomaly of 17 mrad at 0.125 Hz was detected at No. 4~5 in the depth of N=1 and 2.
* On line BI, a weak pants-leg shaped anomaly was detected around No 4~5 with its top at n=1.
* On line BJ, no anomaly was detected in the shallow part around No. 4~5, however, in the depths phase response at 0.125 Hz of more than 20 mrad are seen.

This may be due to the other source extending from line BH to the depths of No. 4~5 on line BK. Therefore, C type anomaly due to the Dito deposit seem to disappear on line BJ.

2) C type anomaly due to the Quatro deposit on each line are as follows·

* On line BI, at No. 8.5 strong IP anomaly was detected dipping south n=1 to the depths.
* On line BJ, phase anomaly of more than 20 mrad at 0.125 Hz are seen at No. 4~5 at the depth of n=4 and 5. This anomaly is considered to be the deep extension from the anomalies detected on line BH and BI.
* On line BK, strong IP anomaly was confirmed around No. 6~9, especially at No. 6.5, at the depth of n=1. These anomalies are detected as wide spread anomaly on line BH and BI, deep anomaly on line BJ and shallow anomaly on this line.

An apparent resistivity and geological correlations are discussed in the next paragraph.

Apparent resistivity of each line show the same pattern each other, as the survey lines are planned to cut the geological strike perpendicularly.

High apparent resistivity zones are detected in the depths of No. 6~8, in the north of No 4 at the depth of n=2 and 3 around at No. 9.5~11.

High apparent resistivity of more than 600 ohm-m at No. 4 on line of line BH is considered to be due to meta-quartz sandstone.

This resistivity high which reflect the meta-quartz sandstone are seen all in the north of No. 3 on lines BA, BJ and BK.

Slightly north dipping resistivity high seen at No. 9.5~11 on line BH at the depth of n=2 and 3 seem to reflect lime schist~limestone lying under mica schist. The same resistivity high are seen at No. 10~11 on the other lines.

Furthermore, the resistivity high observed in the depths of No. 6 – No. 8 on each line is due to the same lime schist~limestone, which tend to be north dipping towards west Those high resistivity show the good coincidence with geological structure.

On the other hand, IP anomalous zone indicate the apparent resistivity of less than 600 ohm-m in the same pattern.

In the zone of apparent resistivity of less than 600 ohm-m locate the zone of lime schist ~ limestone which should indicate the higher indication than this value. Decrease of resistivity may be attributed to the fact that this formation is altered and mineralized, so that it could be said that the resistivity change would depend on the extent of mineralization.

3–3 Summary of Spectral IP Method

As IP survey lines were planned perpendicular to the geological structure, similar resistivity distribution are seen on each line reflecting the NE-SW structure.

Several eminent SIP anomalies were detected and it is seen that correlation between the types of anomaly and the known mineral deposits can be discussed as follows:

1) Type A anomaly

Type A anomaly shows an eminent IP effect with increasing intensity and decreasing resistivity towards depths. This type of anomaly are seen only on line BH which suggest the local mineralization, but it is difficult to discriminate the mineralization of the source.

2) Type B anomaly

This anomaly extend from line BH towards line BJ and dissappear around line BJ. It is also difficult to discriminate the mineralization, but it can be said that the strong IP anomaly detected on line BH would be due to the sulfide mineralization.

3) Type C anomaly

This type of anomaly were detected over the Quatro deposit and the Oito deposit. The anomaly due to the Quatro deposit seem to extend to southeast to the depths extending to the anomalous zone confirmed by the conventional IP method.

Furthermore, this anomaly may extend to the depths below No. 11~12 on lines BI, BJ and BK.

Another anomaly due to the Oito deposit tends to develop towards WSW, which would have no relation with the Quatro deposit. This anomaly may extend towards NE continueing to the nothern anomaly detected by conventional IP.

It is recommendable to conduct the detailed survey to confirm the distribution of this anomalies in the future.

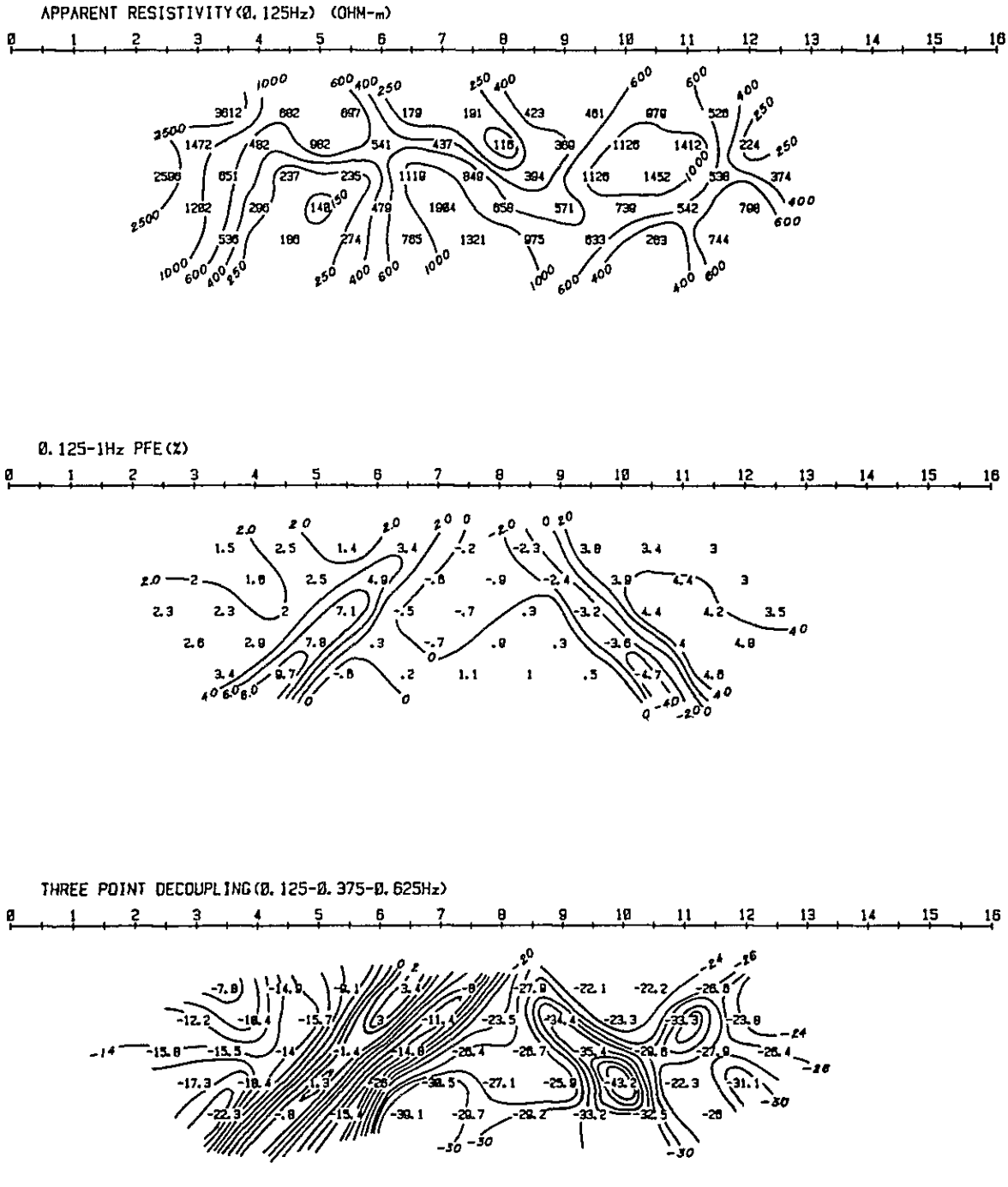

Fig. Ⅱ—3—9 Spectral IP Pseudo-Section

(Line-BH)

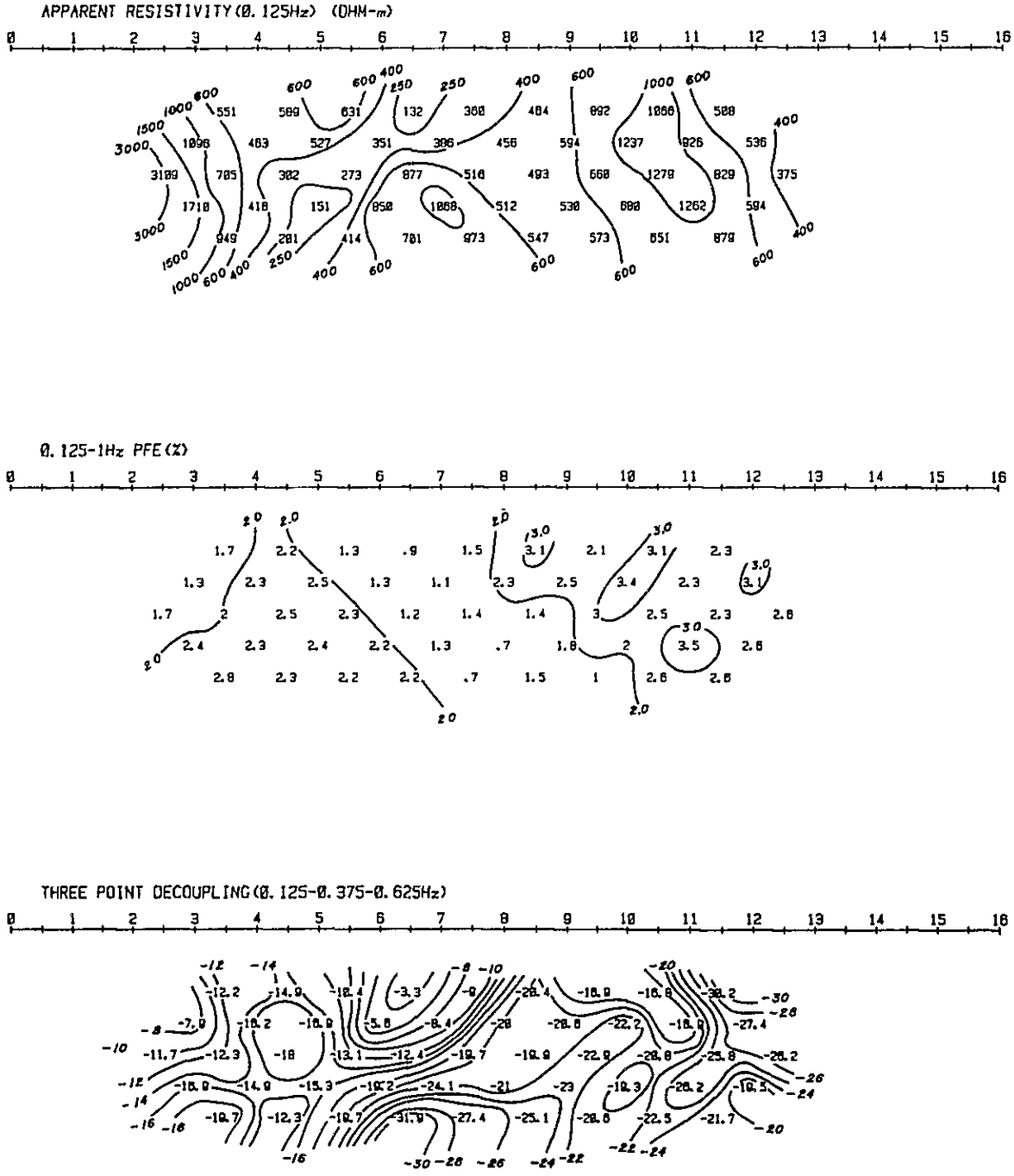

Fig. Ⅱ−3−10 Spectral IP Pseudo-Section

(Line-BI)

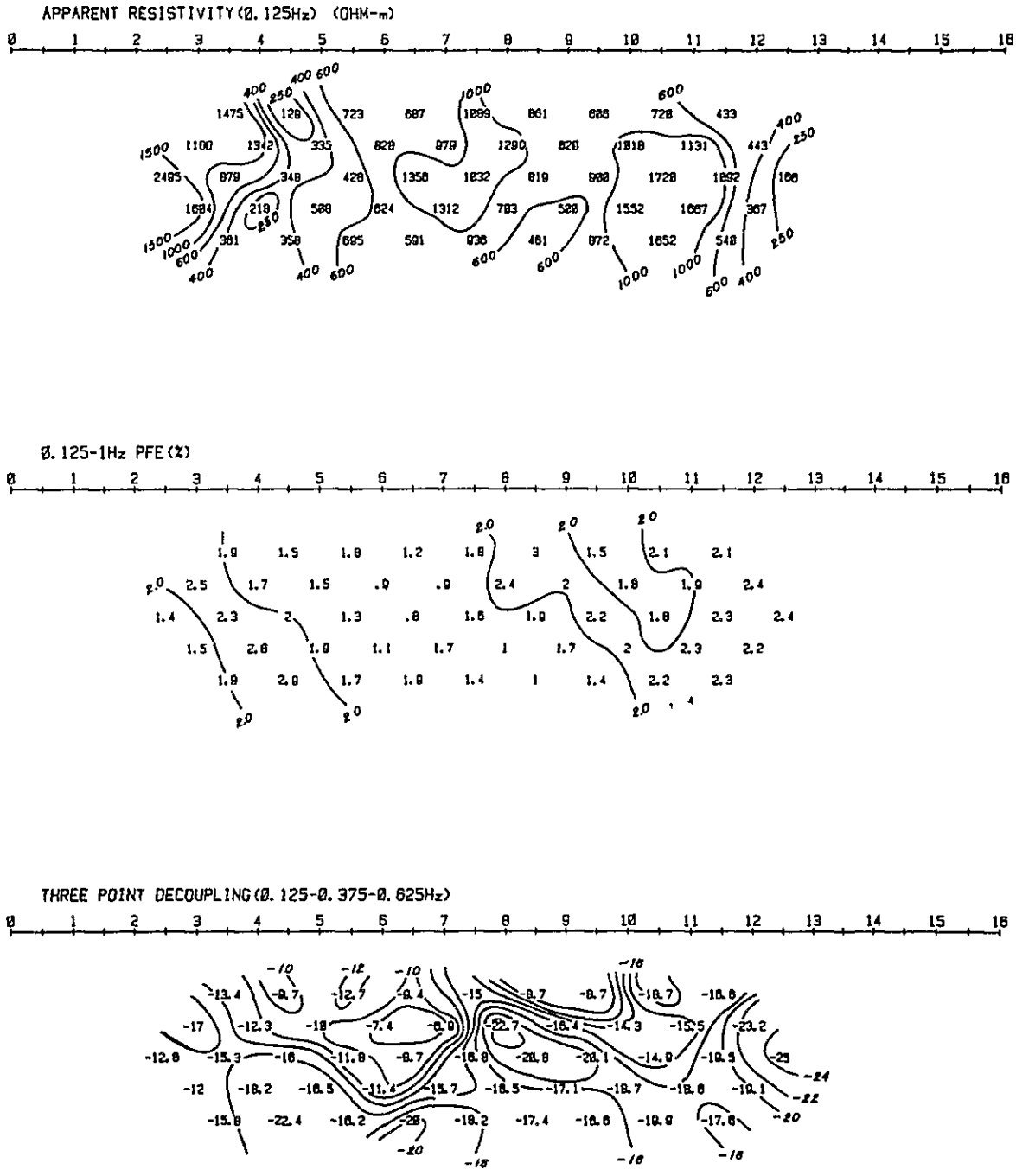

Fig. Ⅱ－3－11　　Spectral IP Pseudo-Section
(Line-BJ)

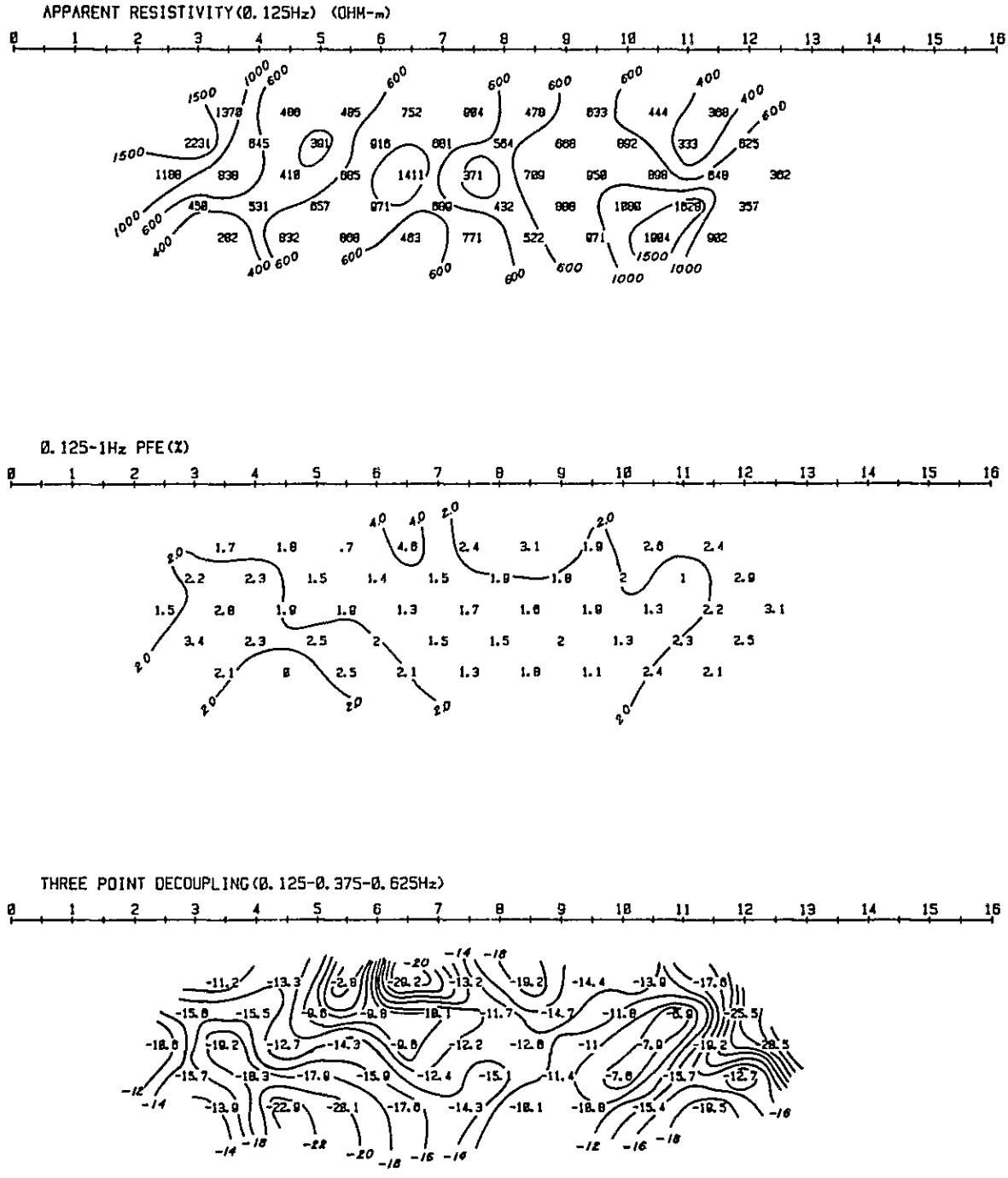

Fig. Ⅱ—3—12 Spectral IP Pseudo-Section

(Line-BK)

AREA BARRINHA
No BA-8 5
AR 1068 (Ohm-m)

FREQ	125	PHASE	-25 010
FREQ	250	PHASE	-24 150
FREQ	500	PHASE	-23 580
FREQ	1 000	PHASE	-23 510
FREQ	2 000	PHASE	-23 240
FREQ	4 000	PHASE	-23 220
FREQ	8 000	PHASE	-23 130
FREQ	16 000	PHASE	-23 450
FREQ	32 000	PHASE	-24 520
FREQ	64 000	PHASE	-26 670

AREA BARRINHA
No BA-15
AR 722 (Ohm-m)

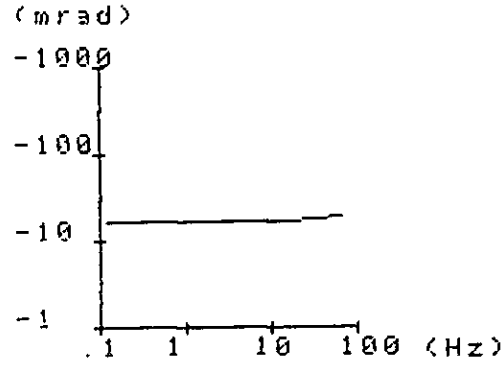

FREQ	125	PHASE	-16 169
FREQ	250	PHASE	-15 841
FREQ	500	PHASE	-16 036
FREQ	1 000	PHASE	-16 333
FREQ	2 000	PHASE	-16 379
FREQ	4 000	PHASE	-16 537
FREQ	8 000	PHASE	-16 529
FREQ	16 000	PHASE	-16 606
FREQ	32 000	PHASE	-16 930
FREQ	64 000	PHASE	-18 611

AREA BARRINHA
No BC-10
AR 1544 (Ohm-m)

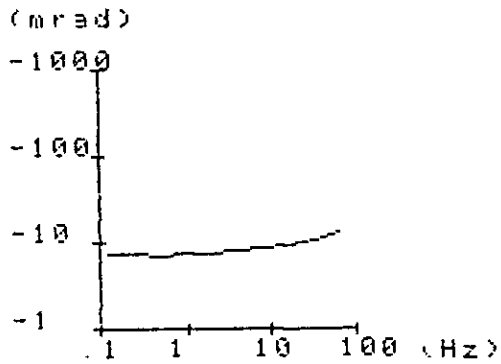

FREQ	125	PHASE	-7 274
FREQ	250	PHASE	-7 389
FREQ	500	PHASE	-6 287
FREQ	1 000	PHASE	-7 255
FREQ	2 000	PHASE	-7 350
FREQ	4 000	PHASE	-7 726
FREQ	8 000	PHASE	-8 349
FREQ	16 000	PHASE	-9 157
FREQ	32 000	PHASE	-10 462
FREQ	64 000	PHASE	-13 305

AREA BARRINHA
No BD-12-3
AR 2453 (Ohm-m)

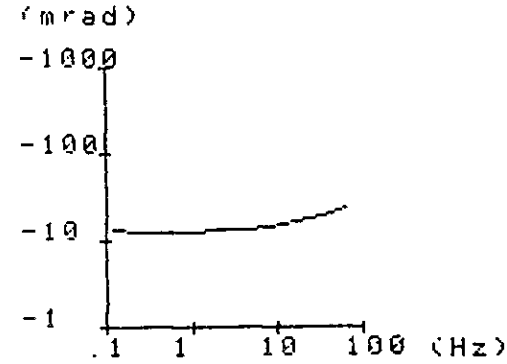

FREQ	125	PHASE	-12 686
FREQ	250	PHASE	-12 472
FREQ	500	PHASE	-11 952
FREQ	1 000	PHASE	-12 225
FREQ	2 000	PHASE	-12 545
FREQ	4 000	PHASE	-13 239
FREQ	8 000	PHASE	-14 153
FREQ	16 000	PHASE	-16 017
FREQ	32 000	PHASE	-18 916
FREQ	64 000	PHASE	-23 980

Fig. II－3－13 Phase Spectral of Rock Samples (limestone)

AREA: BARRINHA
No BA-12
AR: 76 (Ohm-m)

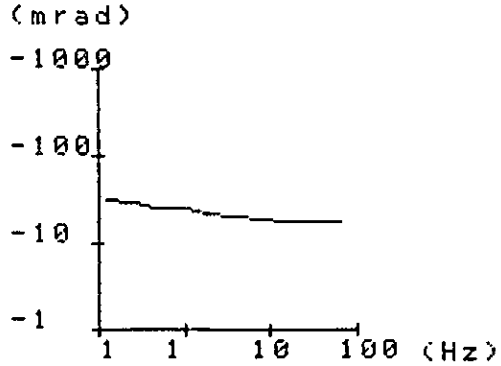

FREQ	125	PHASE	-1 590
FREQ	250	PHASE	-28 160
FREQ	500	PHASE	-25 080
FREQ	1 000	PHASE	-24 100
FREQ	2 000	PHASE	-22 020
FREQ	4 000	PHASE	-20 700
FREQ	8 000	PHASE	-18 386
FREQ	16 000	PHASE	-17 657
FREQ	32 000	PHASE	-16 854
FREQ	64 000	PHASE	-17 040

AREA: BARRINHA
No BC-8 5
AR: 975 (Ohm-m)

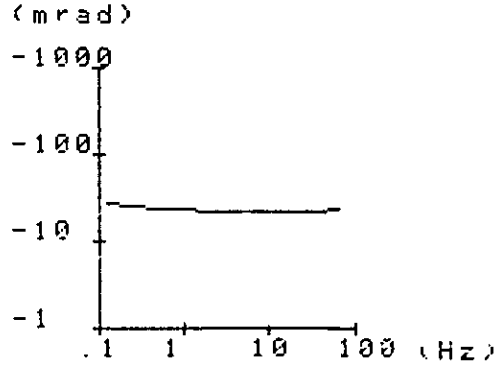

FREQ	125	PHASE	-26 490
FPEQ	250	PHASE	-25 350
FREQ	500	PHASE	-23 960
FREQ	1 000	PHASE	-23 100
FREQ	2 000	PHASE	-22 160
FREQ	4 000	PHASE	-21 340
FREQ	8 000	PHASE	-20 830
FREQ	16 000	PHASE	-20 980
FREQ	32 000	PHASE	-21 530
FREQ	64 000	PHASE	-23 970

AREA: BARRINHA
No: BE-11
AR: 364 (Ohm-m)

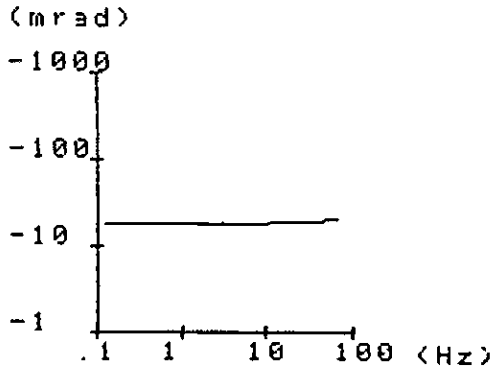

FREQ	125	PHASE	-17 109
FREQ	250	PHASE	-16 877
FREQ	500	PHASE	-17 157
FREQ	1 000	PHASE	-17 043
FREQ	2 000	PHASE	-17 266
FREQ	4 000	PHASE	-17 320
FREQ	8 000	PHASE	-17 523
FREQ	16 000	PHASE	-18 004
FREQ	32 000	PHASE	-18 834
FREQ	64 000	PHASE	-20 780

Fig. II－3－14 Phase Spectral of Rock Samples (calc-schist)

AREA: BARRINHA
No BB-2
AR: 249 (Ohm-m)

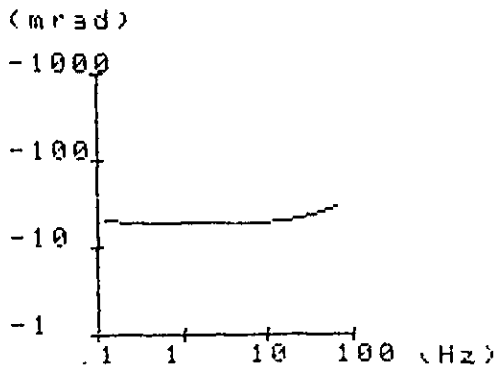

FREQ	125	PHASE	-19 740
FREQ	250	PHASE	-19 130
FREQ	500	PHASE	-19 850
FREQ	1 000	PHASE	-18 530
FREQ	2 000	PHASE	-18 280
FREQ	4 000	PHASE	-18 140
FREQ	8 000	PHASE	-18 330
FREQ	16 000	PHASE	-19 720
FREQ	32 000	PHASE	-23 530
FREQ	64 000	PHASE	-27 850

AREA: BARRINHA
No: BE-15 7
AR: 747 (Ohm-m)

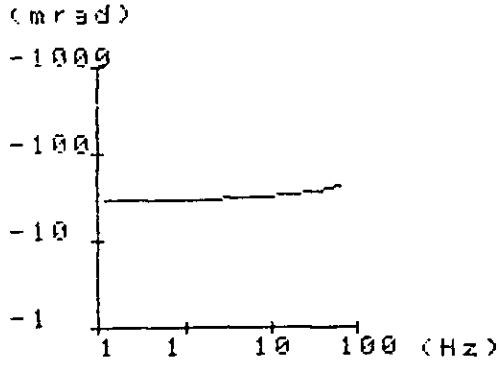

FREQ	125	PHASE	-29 440
FREQ	250	PHASE	-29 320
FREQ	500	PHASE	-28 640
FREQ	1 000	PHASE	-29 260
FREQ	2 000	PHASE	-29 420
FREQ	4 000	PHASE	-30 100
FREQ	8 000	PHASE	-31 080
FREQ	16 000	PHASE	-32 710
FREQ	32 000	PHASE	-35 420
FREQ	64 000	PHASE	-39 840

AREA: BARRINHA
No: BF-4
AR: 259 (Ohm-m)

FREQ	125	PHASE	-25 990
FREQ	250	PHASE	-26 370
FREQ	500	PHASE	-26 580
FREQ	1 000	PHASE	-26 550
FREQ	2 000	PHASE	-26 510
FREQ	4 000	PHASE	-26 540
FREQ	8 000	PHASE	-26 640
FREQ	16 000	PHASE	-26 890
FREQ	32 000	PHASE	-28 120
FREQ	64 000	PHASE	-30 170

AREA: BARRINHA
No: BF-18.5
AR: 442 (Ohm-m)

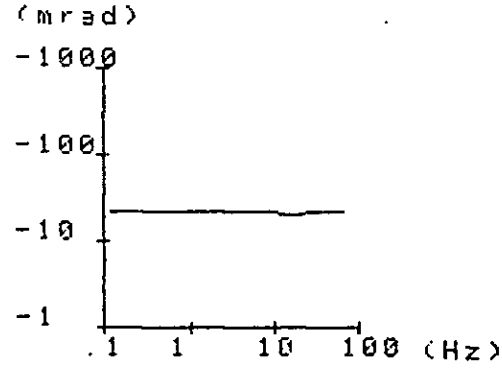

FREQ	125	PHASE	-21 270
FREQ	250	PHASE	-21 270
FREQ	500	PHASE	-21 630
FREQ	1 000	PHASE	-22 100
FREQ	2 000	PHASE	-21 490
FREQ	4 000	PHASE	-21 530
FREQ	8 000	PHASE	-21 080
FREQ	16 000	PHASE	-20 760
FREQ	32 000	PHASE	-20 890
FREQ	64 000	PHASE	-22 080

Fig. II－3－15 Phase Spectral of Rock Samples (quartz-sericite-schist)

AREA BARRINHA
No. BA-7 5
AR. 2105 (Ohm-m)

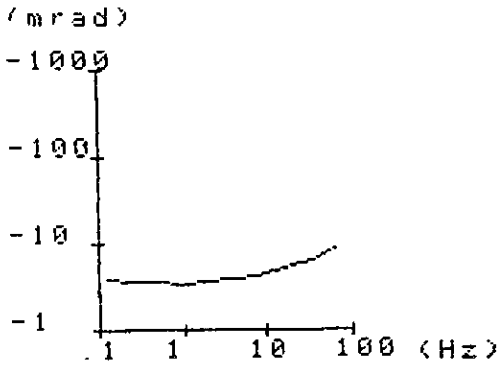

FREQ	125	PHASE	-3 680
FREQ	250	PHASE	-3 429
FREQ	500	PHASE	-3 484
FREQ	1 000	PHASE	-3 303
FREQ	2 000	PHASE	-3 520
FREQ	4 000	PHASE	-3 849
FREQ	8 000	PHASE	-4 124
FREQ	16 000	PHASE	-4 943
FREQ	32 000	PHASE	-6 217
FREQ	64 000	PHASE	-8 477

AREA: BARRINHA
No. BB-7
AR. 1839 (Ohm-m)

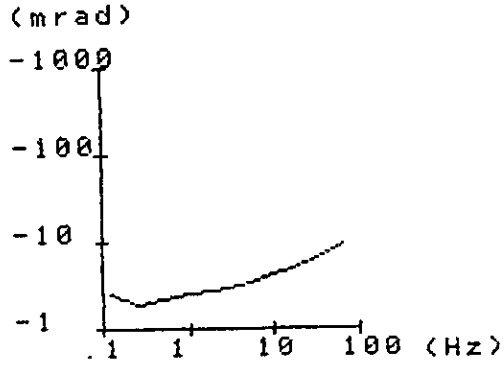

FREQ	125	PHASE	-3 387
FREQ	250	PHASE	-1 911
FREQ	500	PHASE	-2 061
FREQ	1 000	PHASE	-2 480
FREQ	2 000	PHASE	-2 707
FREQ	4 000	PHASE	-3 073
FREQ	8 000	PHASE	-3 737
FREQ	16 000	PHASE	-4 753
FREQ	32 000	PHASE	-6 531
FREQ	64 000	PHASE	-9 130

AREA. BARRINHA
No. BF-2
AR: 1253 (Ohm-m)

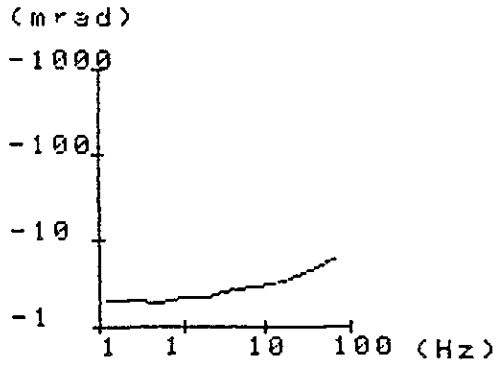

FREQ	125	PHASE	-2 004
FREQ	250	PHASE	-2 004
FREQ	500	PHASE	-1 873
FREQ	1 000	PHASE	-2 060
FREQ	2 000	PHASE	-2 162
FREQ	4 000	PHASE	-2 576
FREQ	8 000	PHASE	-2 784
FREQ	16 000	PHASE	-3 239
FREQ	32 000	PHASE	-4 310
FREQ	64 000	PHASE	-5 853

Fig. II－3－16 Phase Spectral of Rock Samples
(meta quartz sandstone)

AREA: BARRINHA
No: B0-1
AR: 4 (Ohm-m)

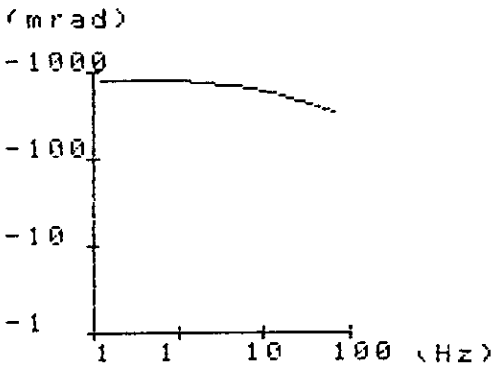

FREQ	125	PHASE	-773 600
FREQ	250	PHASE	-781 900
FREQ	500	PHASE	-825 300
FREQ	1 000	PHASE	-788 800
FREQ	2 000	PHASE	-752 100
FREQ	4 000	PHASE	-709 400
FREQ	8 000	PHASE	-662 800
FREQ	16 000	PHASE	-531 600
FREQ	32 000	PHASE	-430 900
FREQ	64 000	PHASE	-325 900

AREA BARRINHA
No G2+8N
AP 106 (Ohm-m)

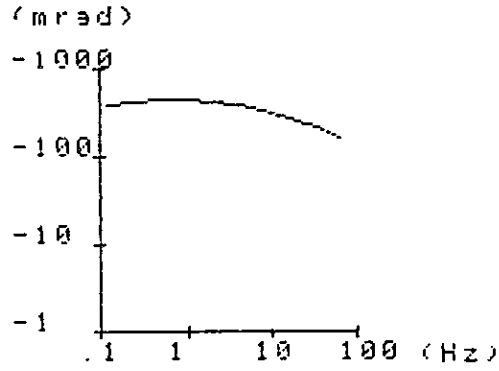

FREQ	125	PHASE	-792 500
FREQ	250	PHASE	-428 100
FREQ	500	PHASE	-448 600
FREQ	1 000	PHASE	-450 000
FREQ	2 000	PHASE	-431 000
FREQ	4 000	PHASE	-392 200
FREQ	8 000	PHASE	-339 400
FREQ	16 000	PHASE	-278 700
FREQ	32 000	PHASE	-219 160
FREQ	64 000	PHASE	-168 190

AREA: BARRINHA
No: G2-8S
AR: 404 (Ohm-m)

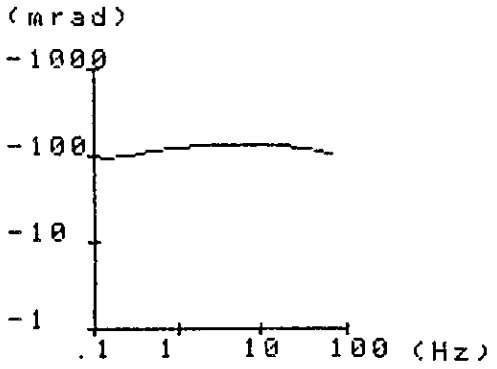

FREQ	125	PHASE	-88 210
FREQ	250	PHASE	-99 720
FREQ	500	PHASE	-111 390
FREQ	1 000	PHASE	-121 790
FREQ	2 000	PHASE	-129 190
FREQ	4 000	PHASE	-133 600
FREQ	8 000	PHASE	-133 930
FREQ	16 000	PHASE	-128 380
FREQ	32 000	PHASE	-118 930
FREQ	64 000	PHASE	-108 140

Fig. II－3－17 Phase Spectral of Rock Samples (ore)

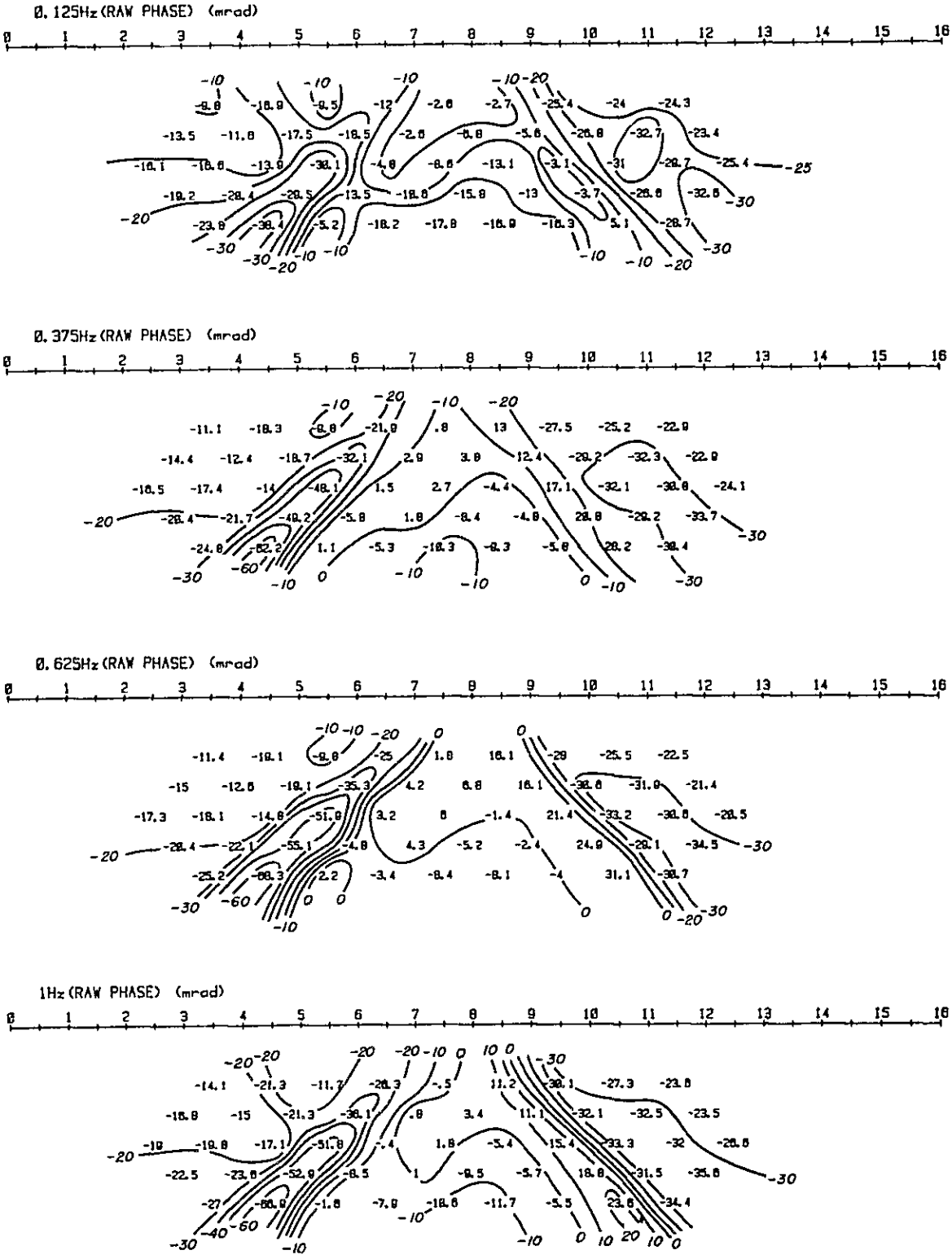

Fig. II－3－18 Phase Pseudo-Section

(Line-BH) －(1)

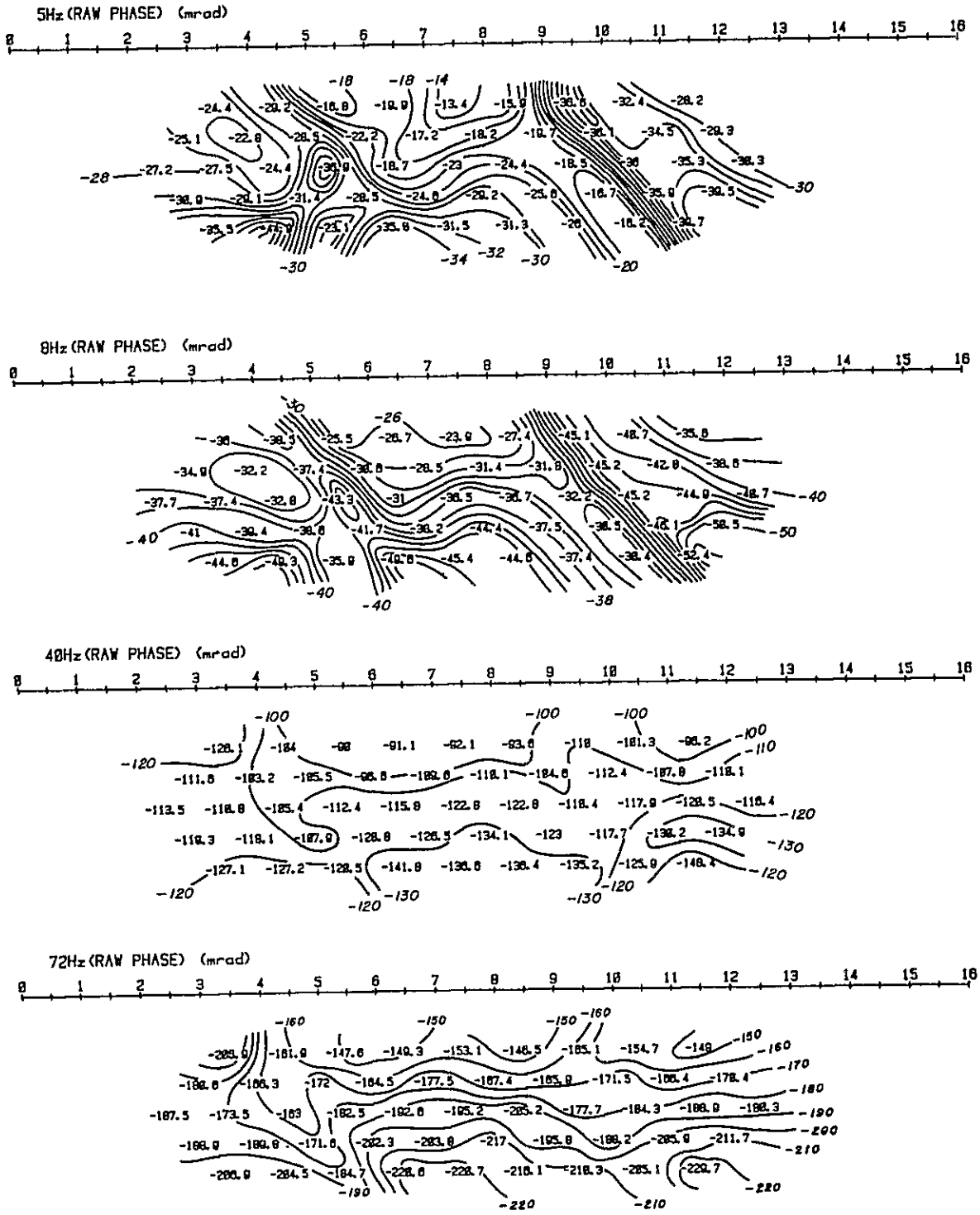

Fig. II－3－19 Phase Pseudo-Section

(Line-BH) －(2)

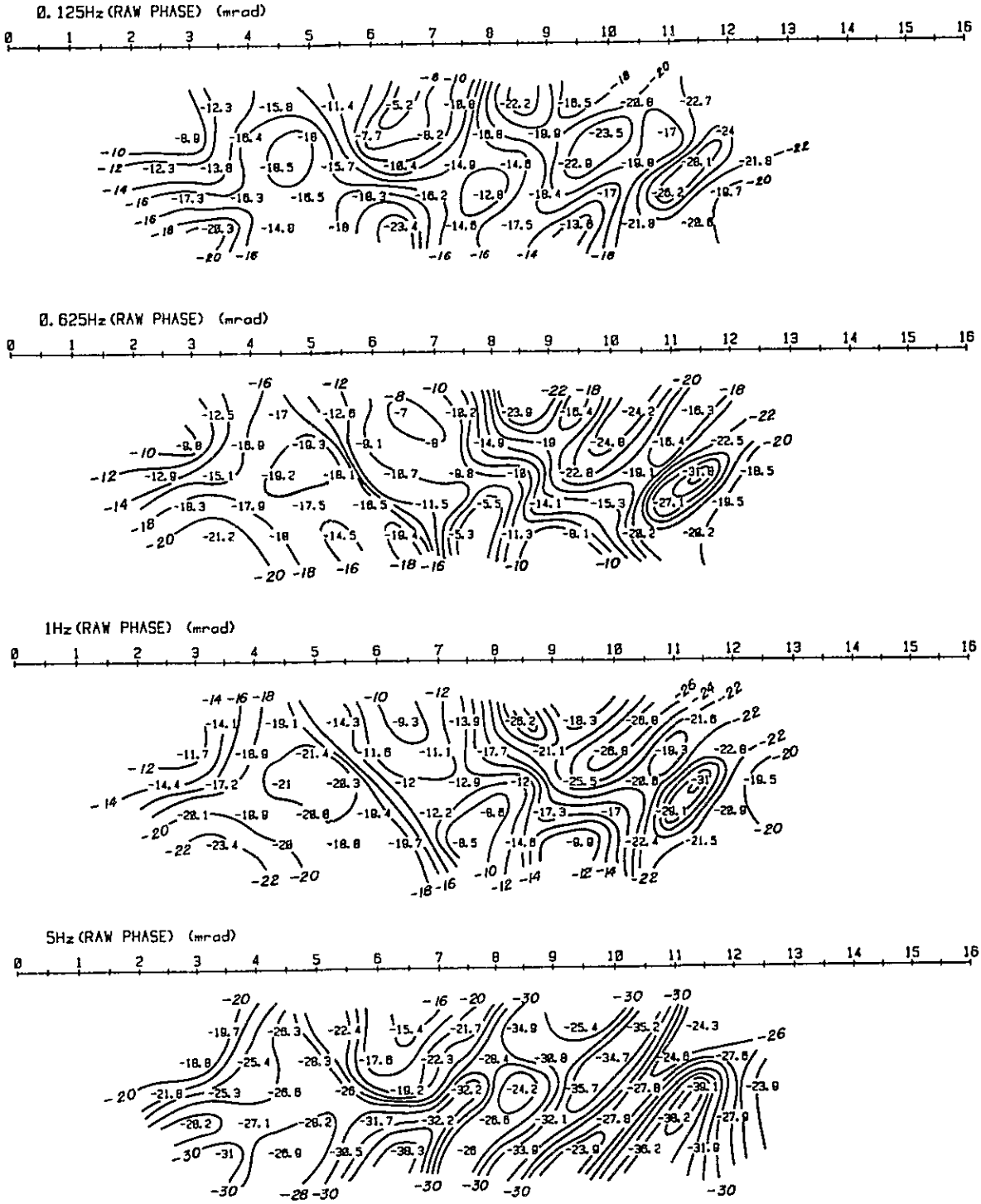

Fig. II－3－20 Phase Pseudo-Section

(Line-BI) －(1)

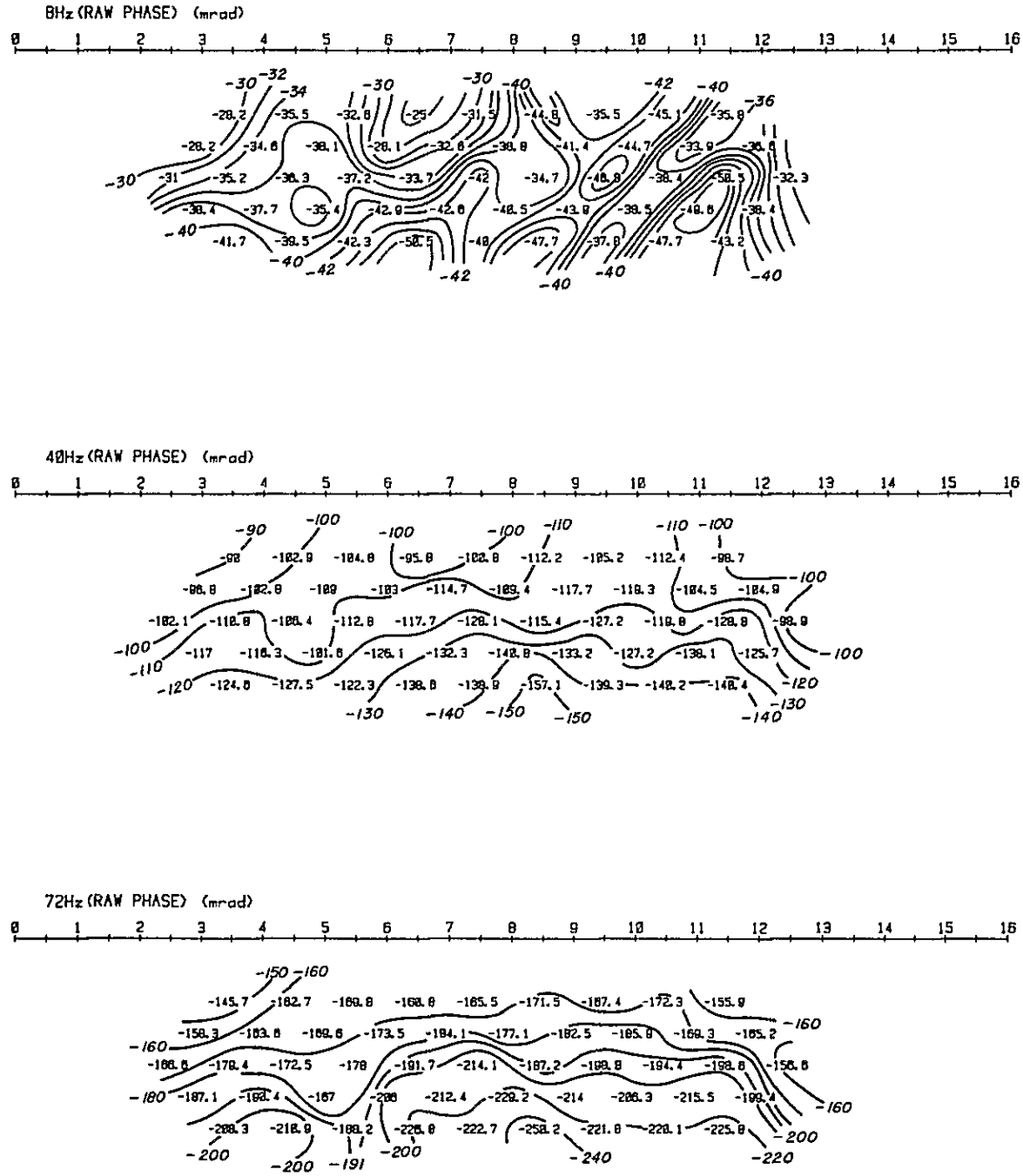

Fig. II－3－21 Phase Pseudo-Section

(Line-BI) －(2)

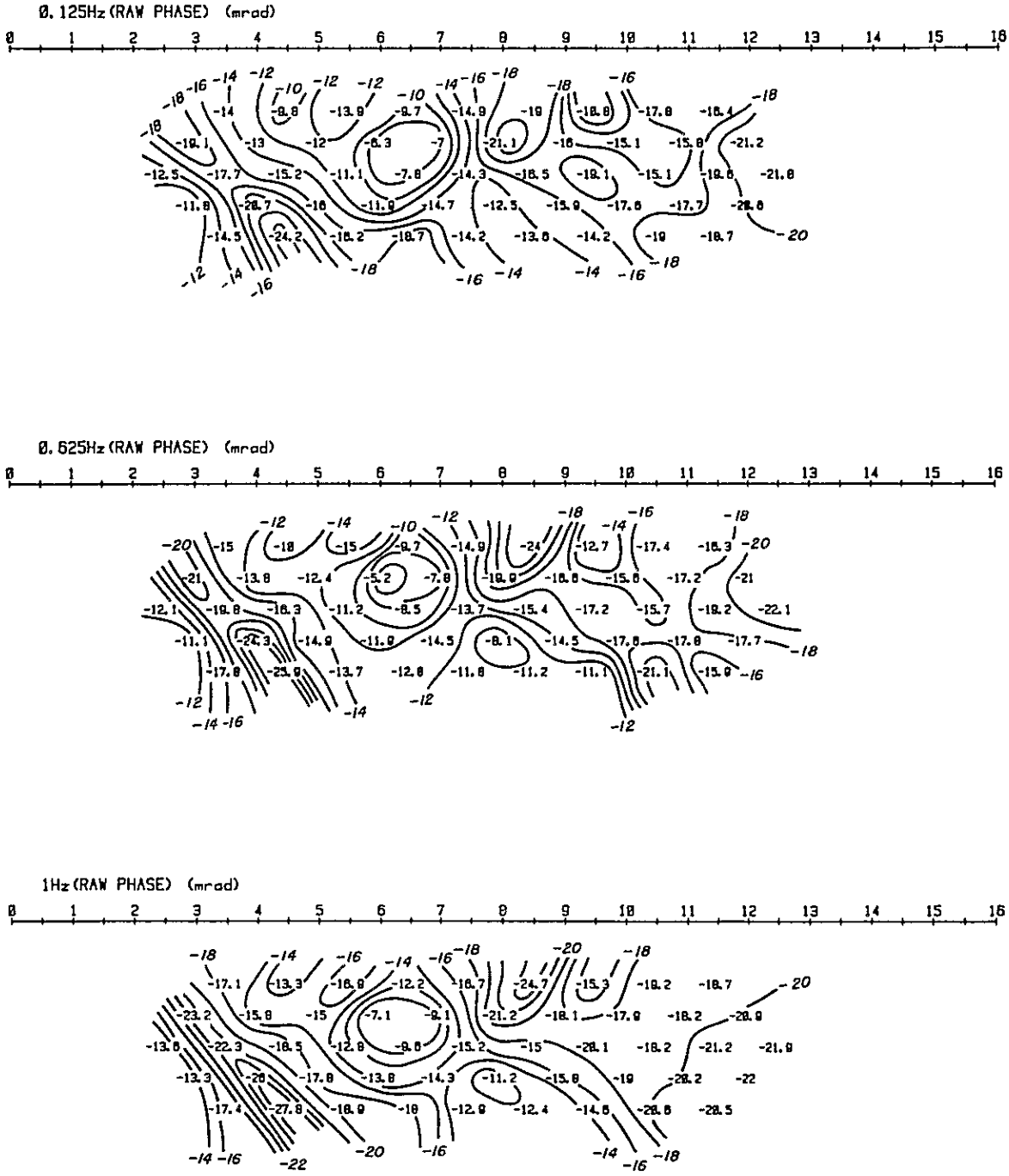

Fig. II－3－22 Phase Pseudo-Section

(Line-BJ) －(1)

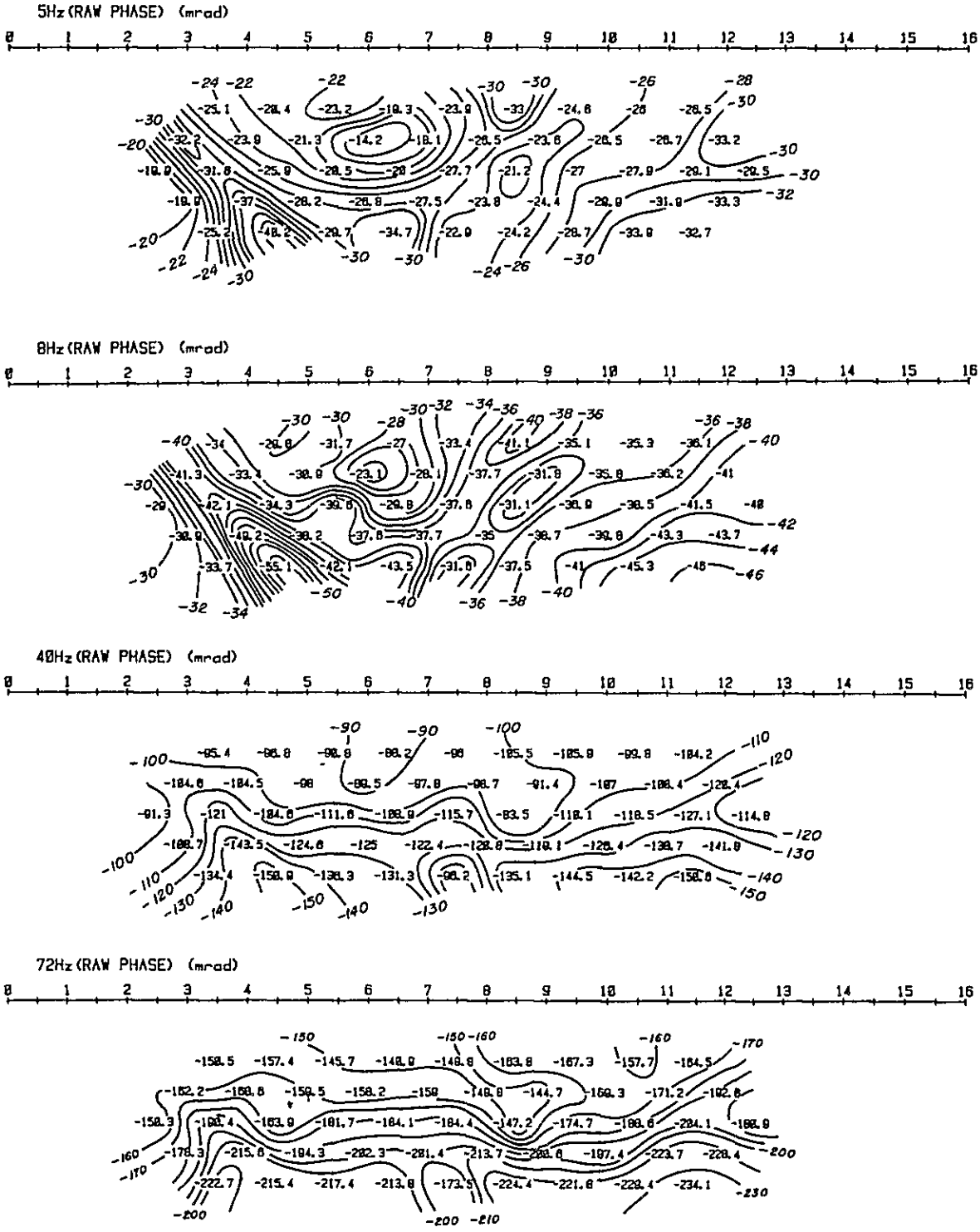

Fig. II－3－23 Phase Pseudo-Section

(Line-BJ) －(2)

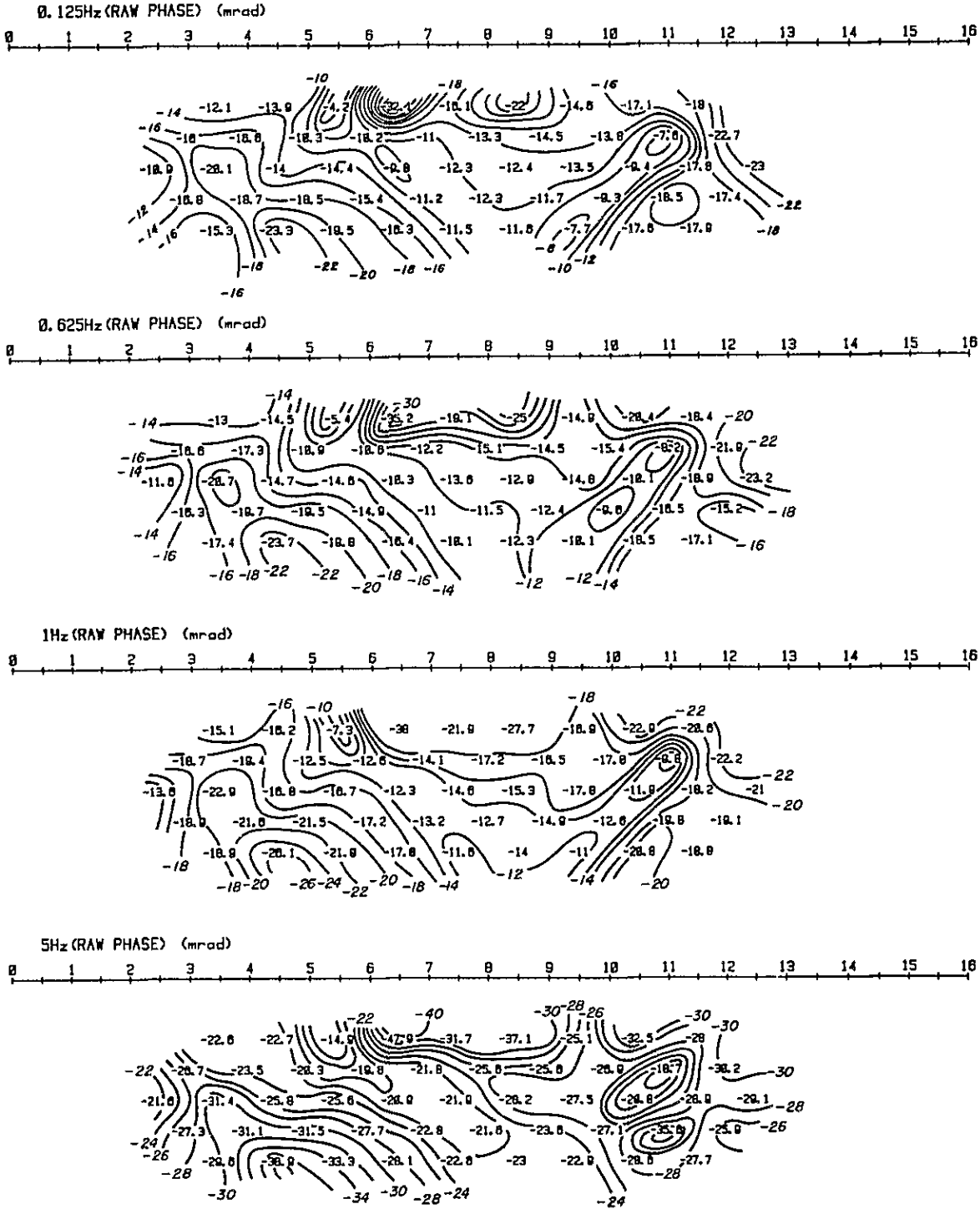

Fig. II－3－24 Phase Pseudo-Section

(Line-BK) －(1)

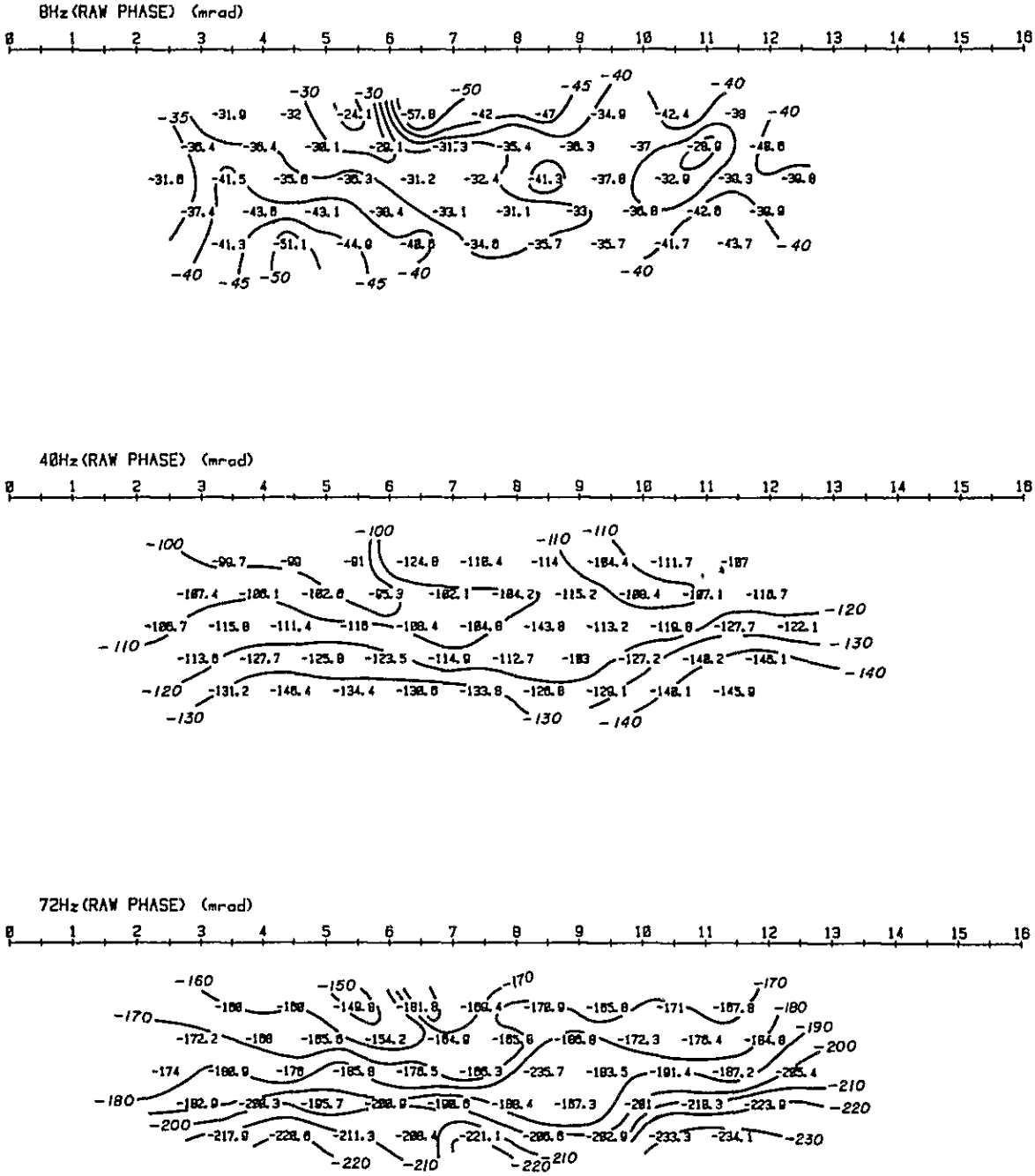

Fig. II－3－25 Phase Pseudo-Section

(Line-BK) －(2)

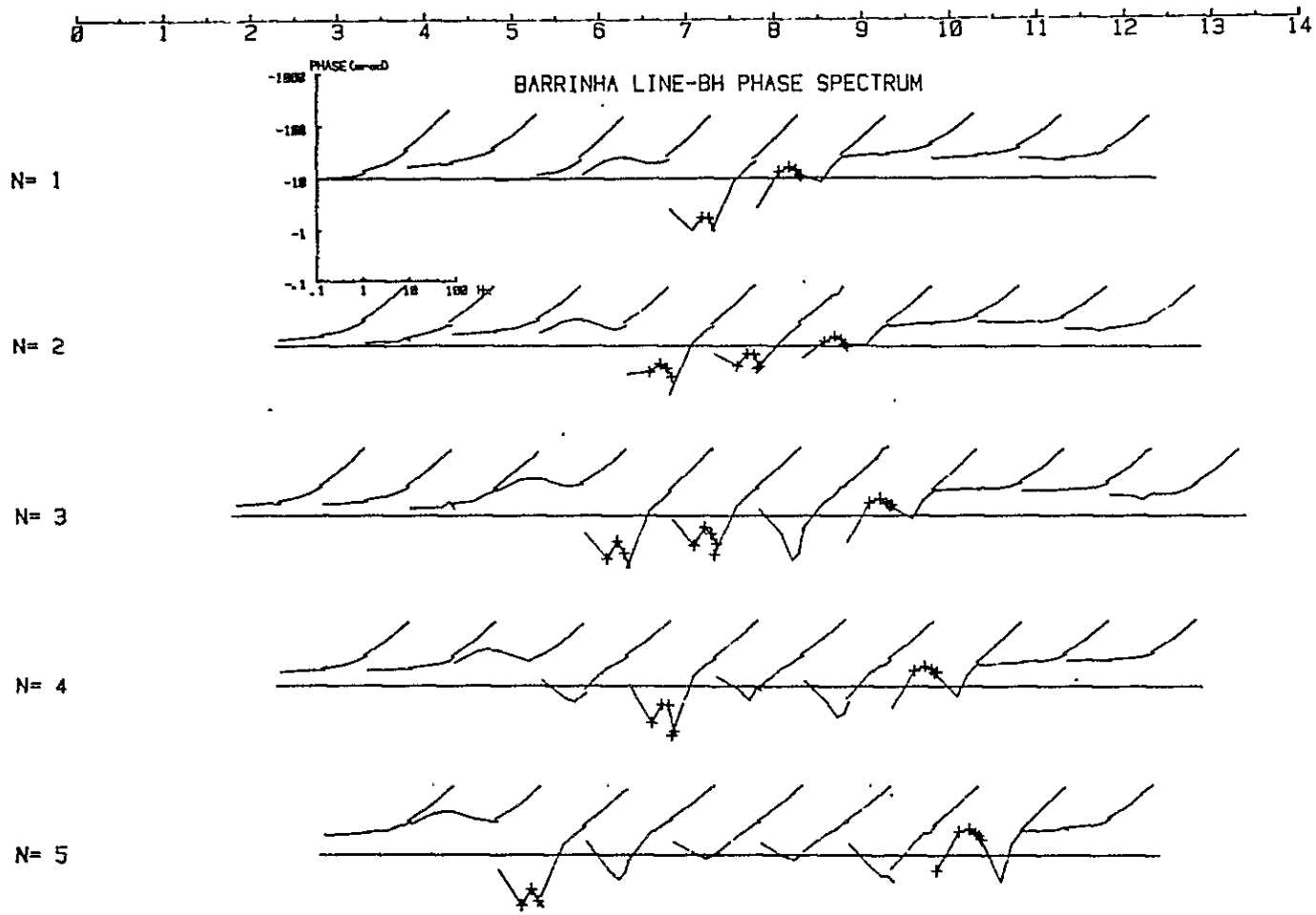

Fig. Ⅱ—3—26 Phase Spectrum (Line-BH)

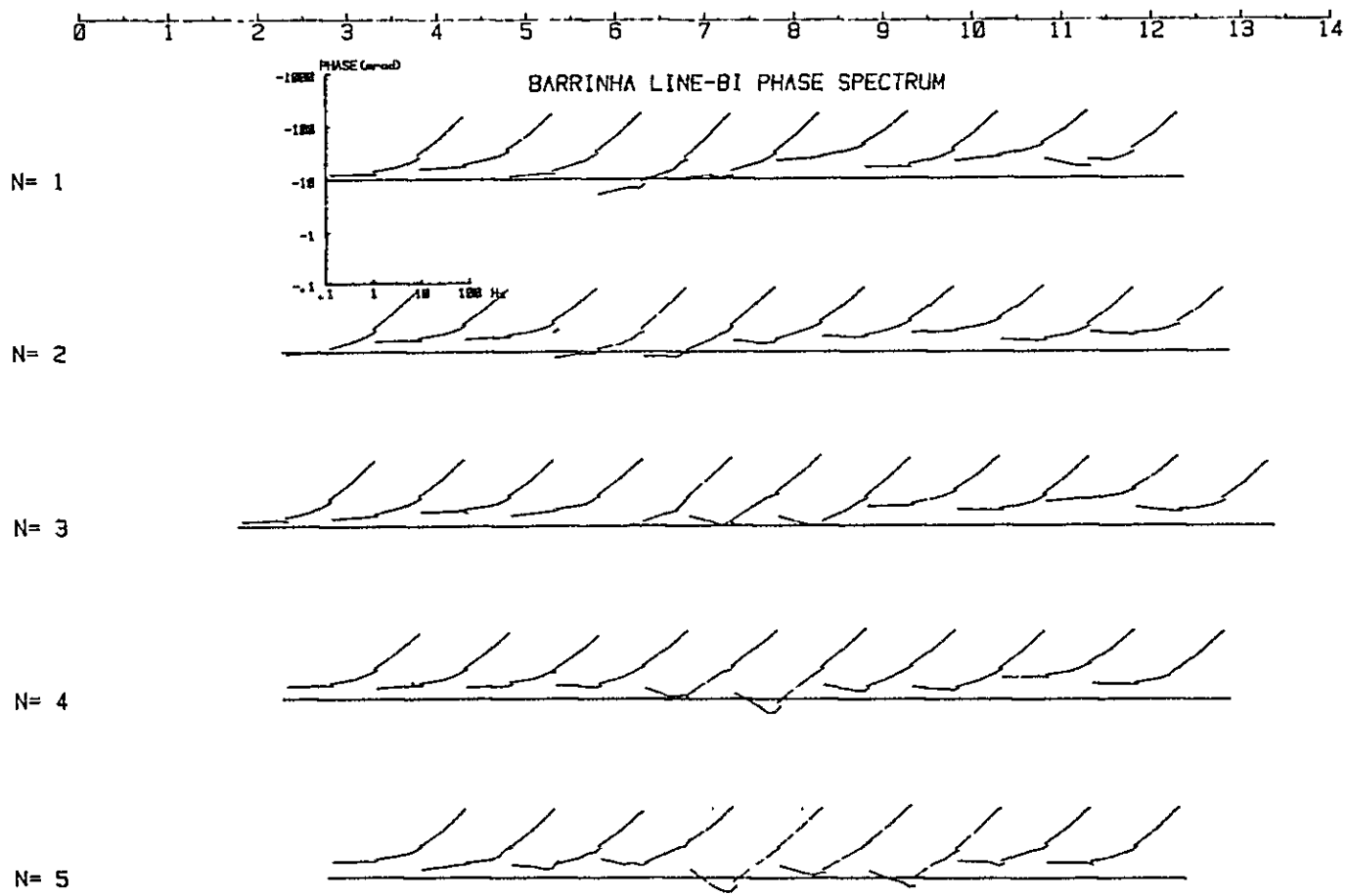

Fig. Ⅱ—3—27 Phase Spectrum (Line-BI)

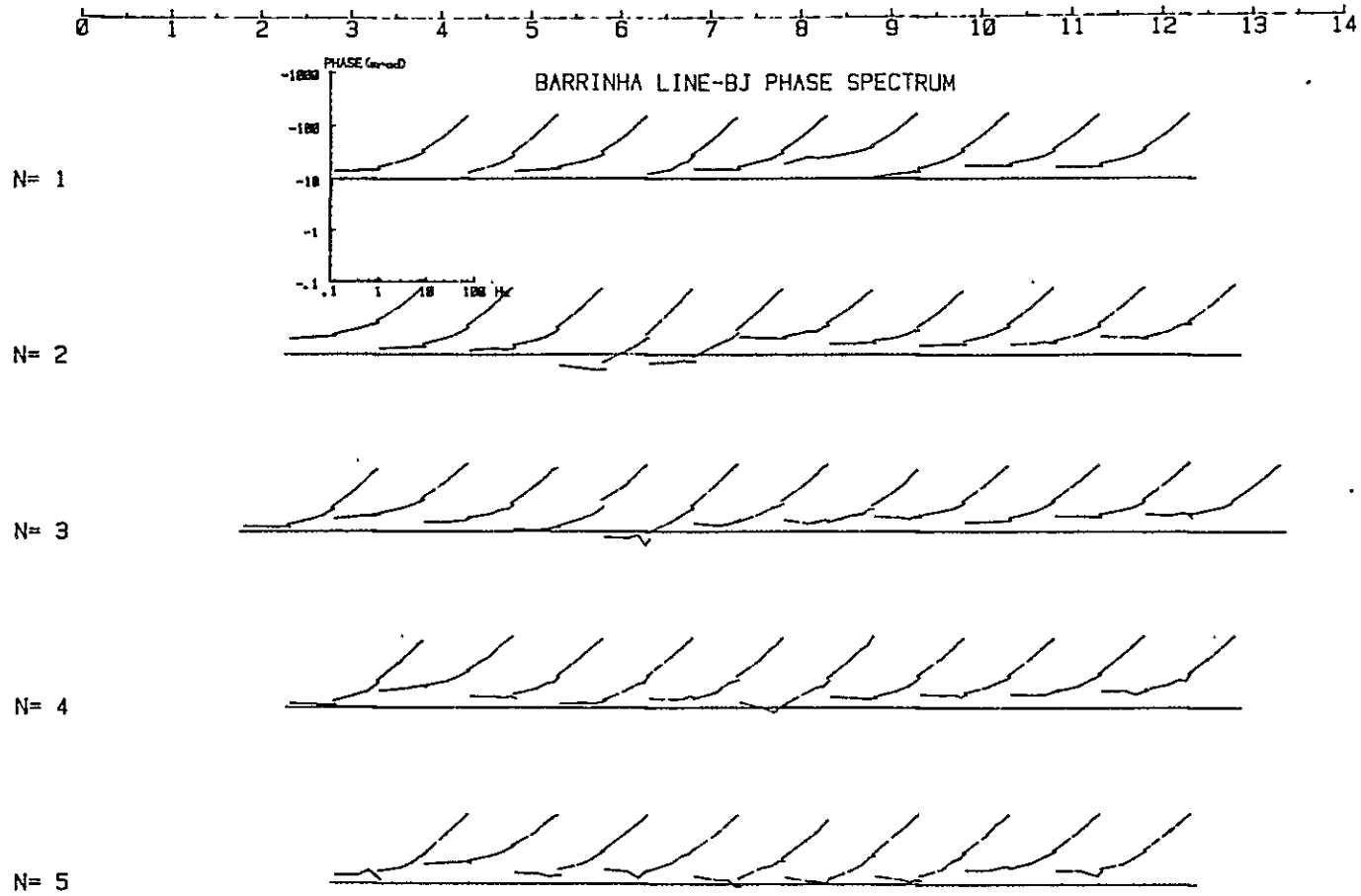

Fig. Ⅱ−3−28 Phase Spectrum (Line-BJ)

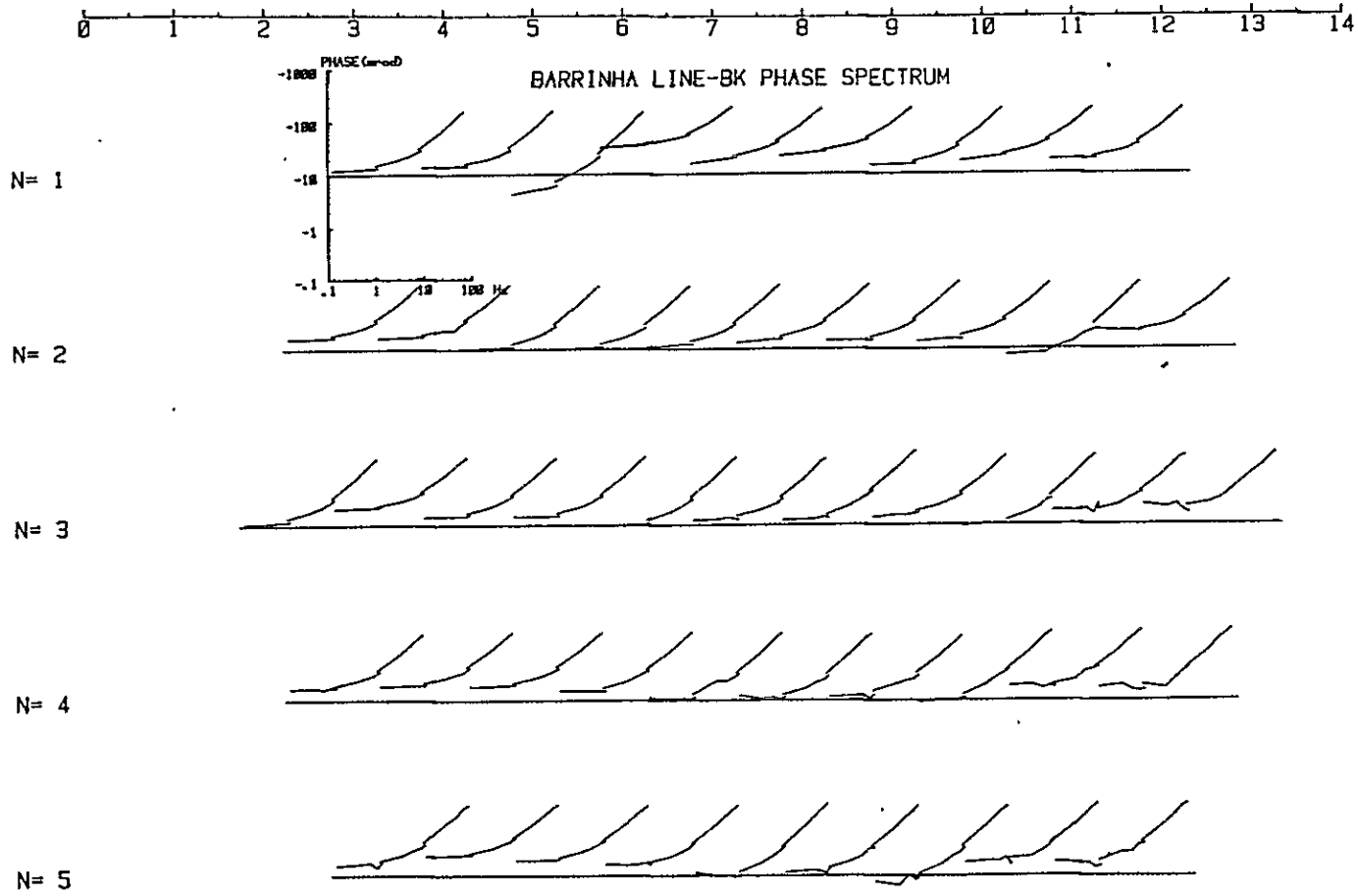

Fig. Ⅱ—3—29 Phase Spectrum (Line-BK)

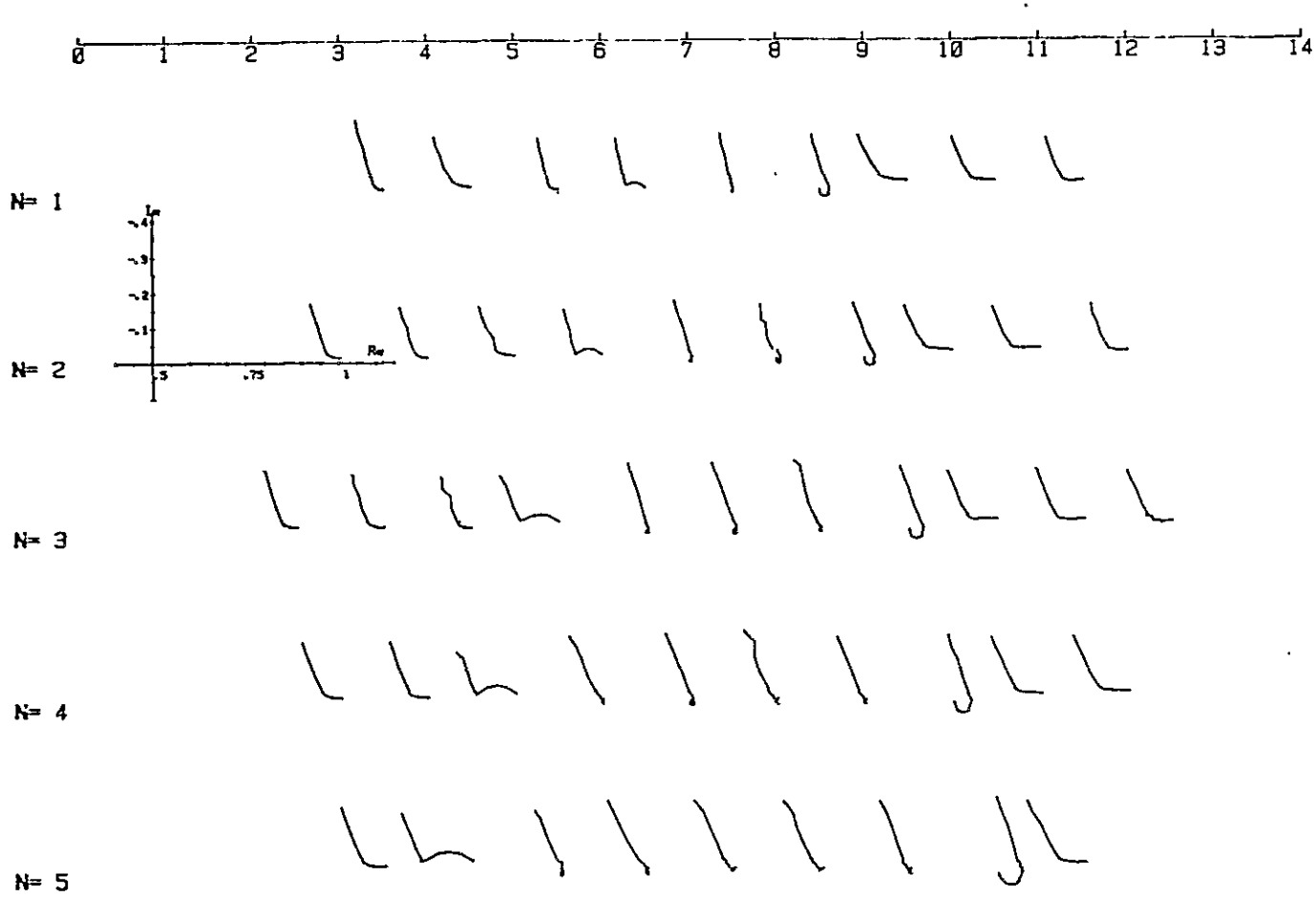

Fig. Ⅱ—3—30 Cole-Cole Diagram (Line-BH)

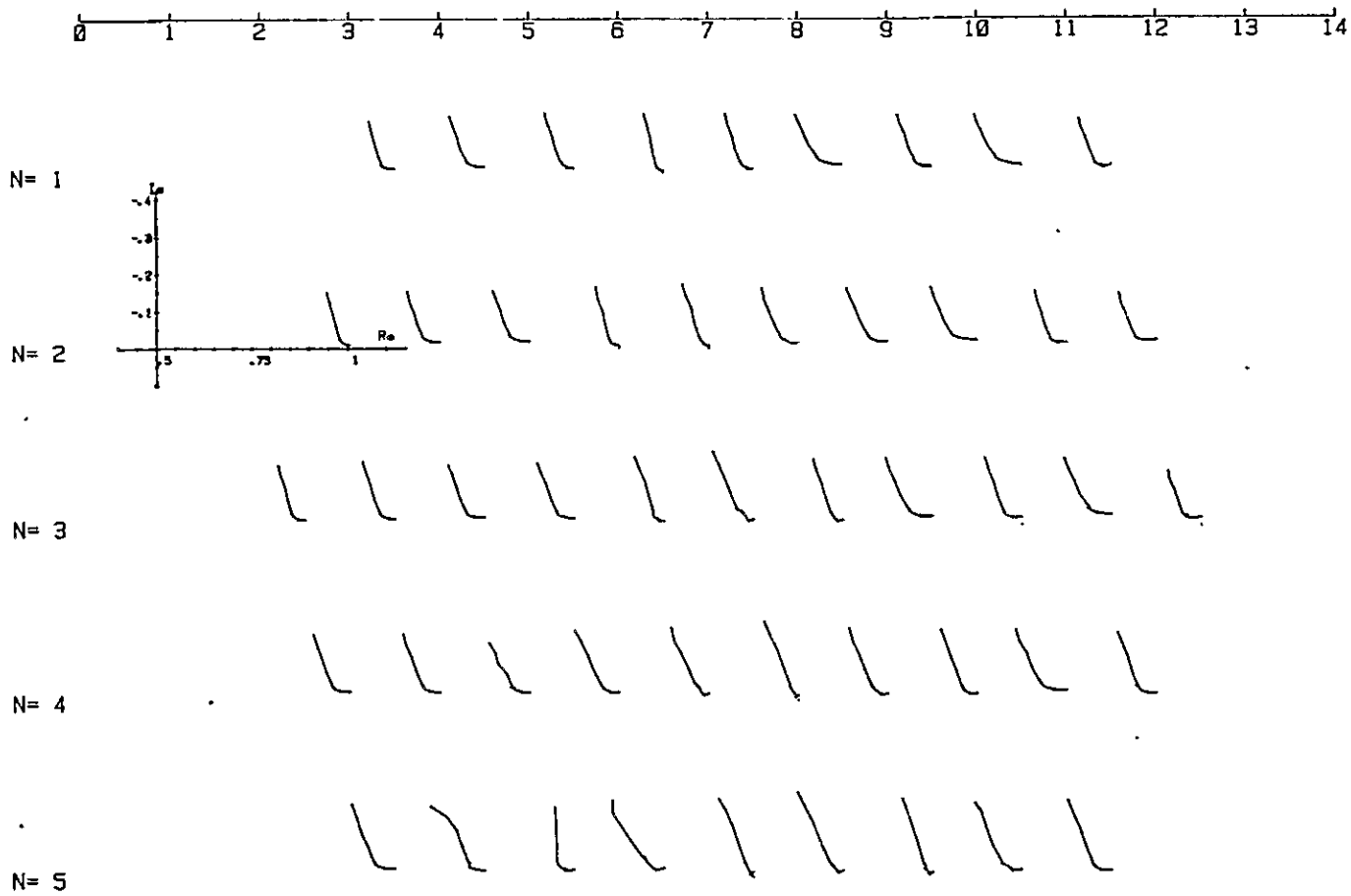

Fig. Ⅱ—3—31 Cole-Cole Diagram (Line-BI)

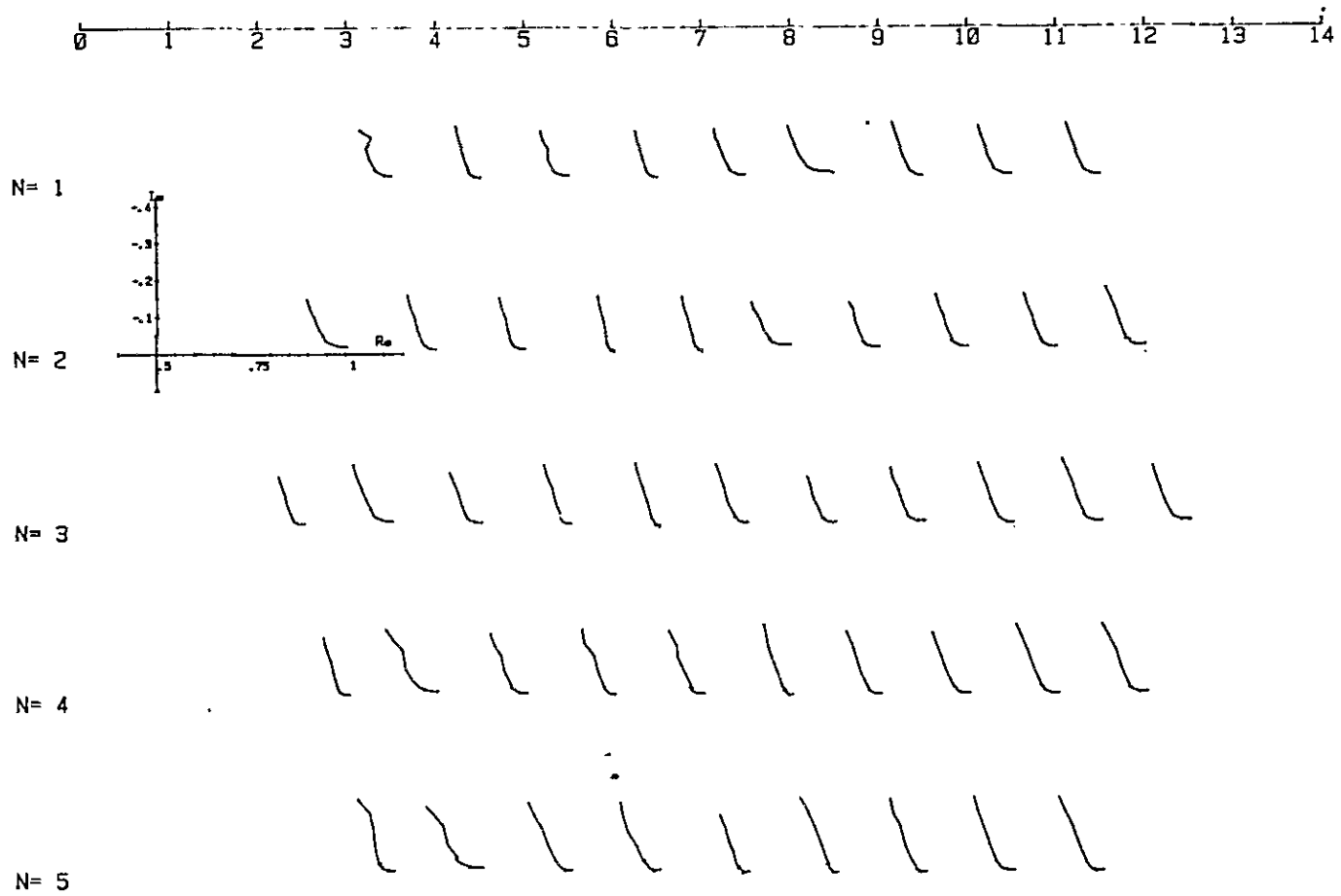

Fig. Ⅱ—3—32 Cole-Cole Diagram (Line-BJ)

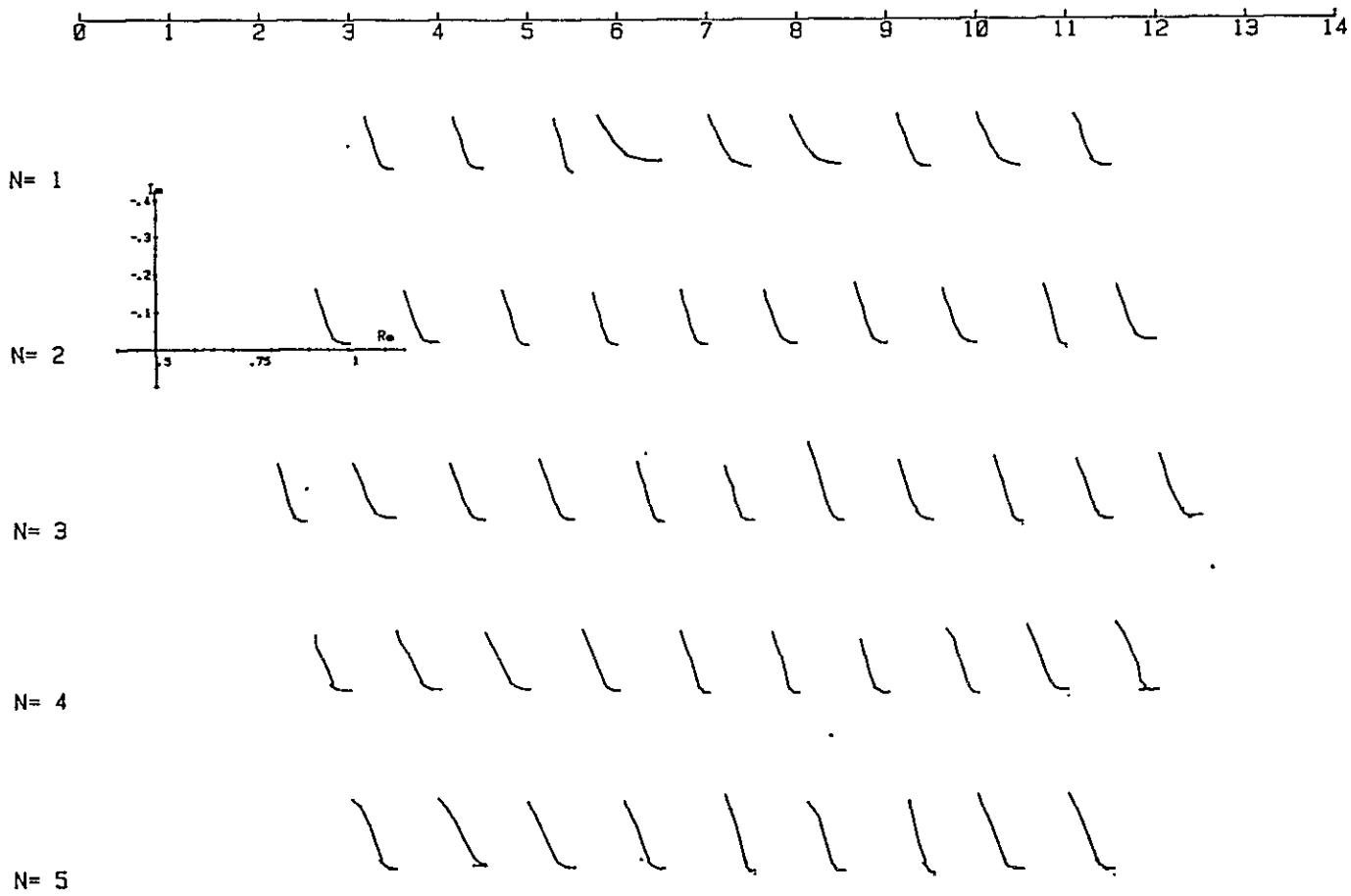

Fig. Ⅱ—3—33 Cole-Cole Diagram (Line-BK)

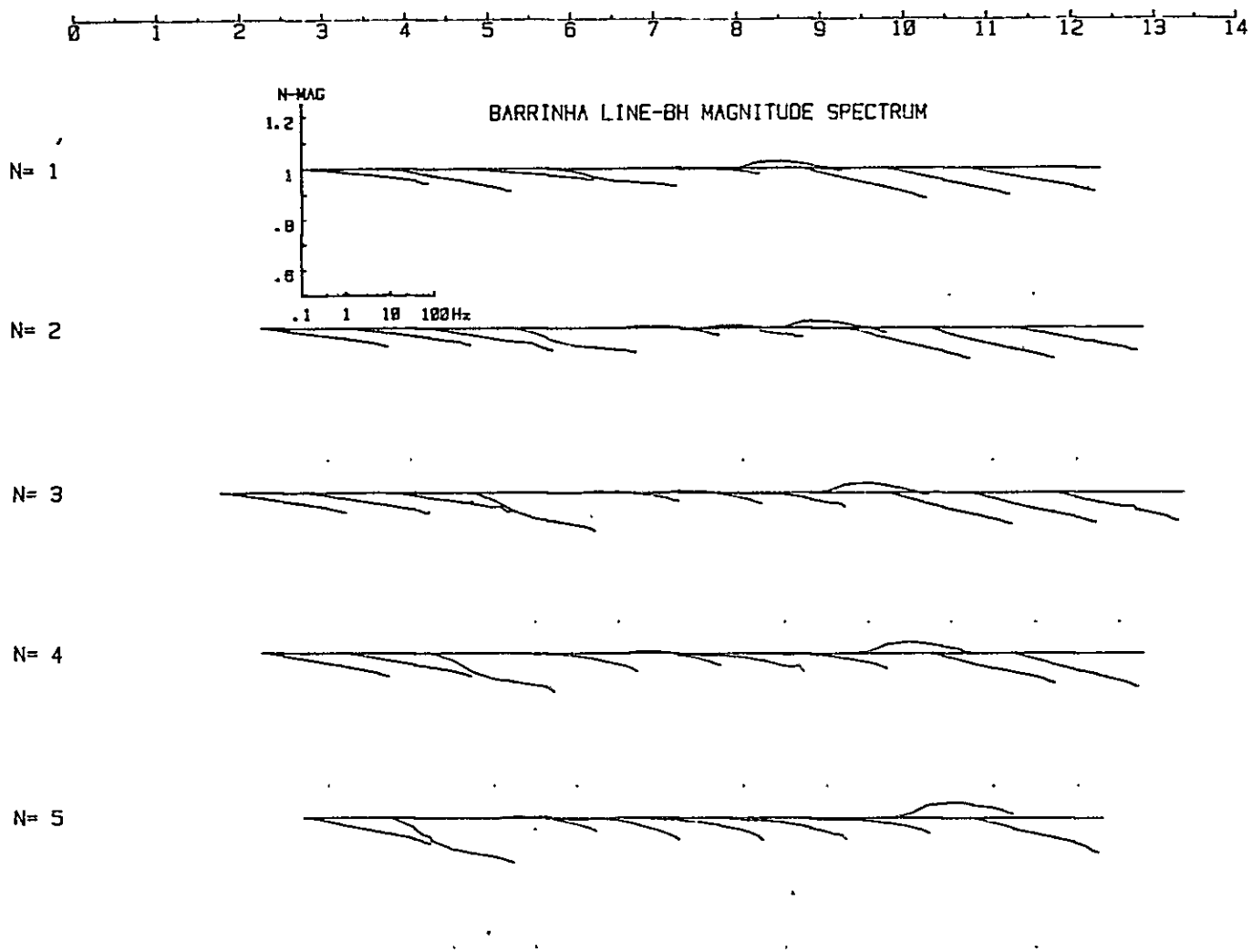

Fig. Ⅱ—3—34 Magnitude Spectrun m (Line-BH)

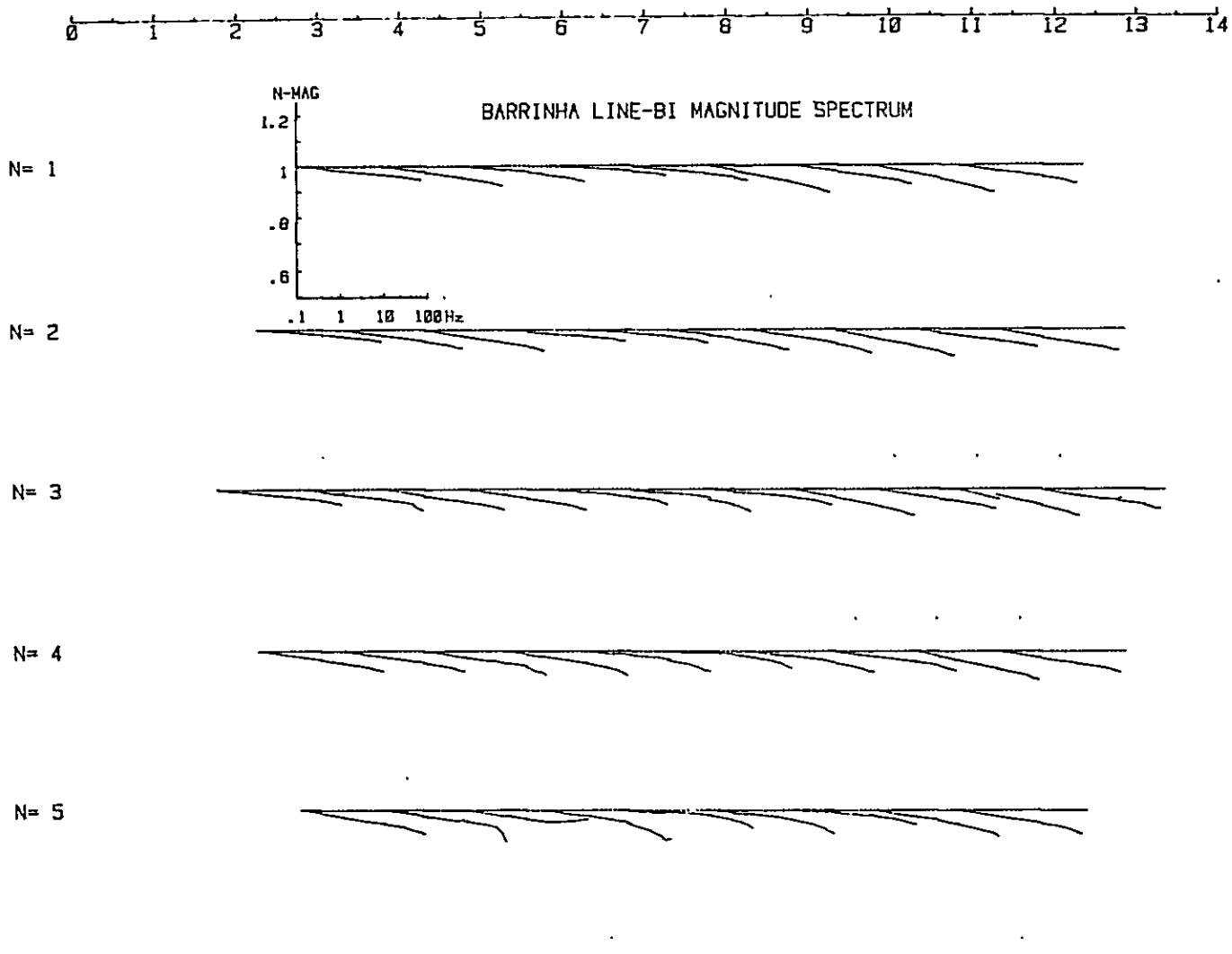

Fig. Ⅱ—3—35 Magnitude Spectrum (Line-BI)

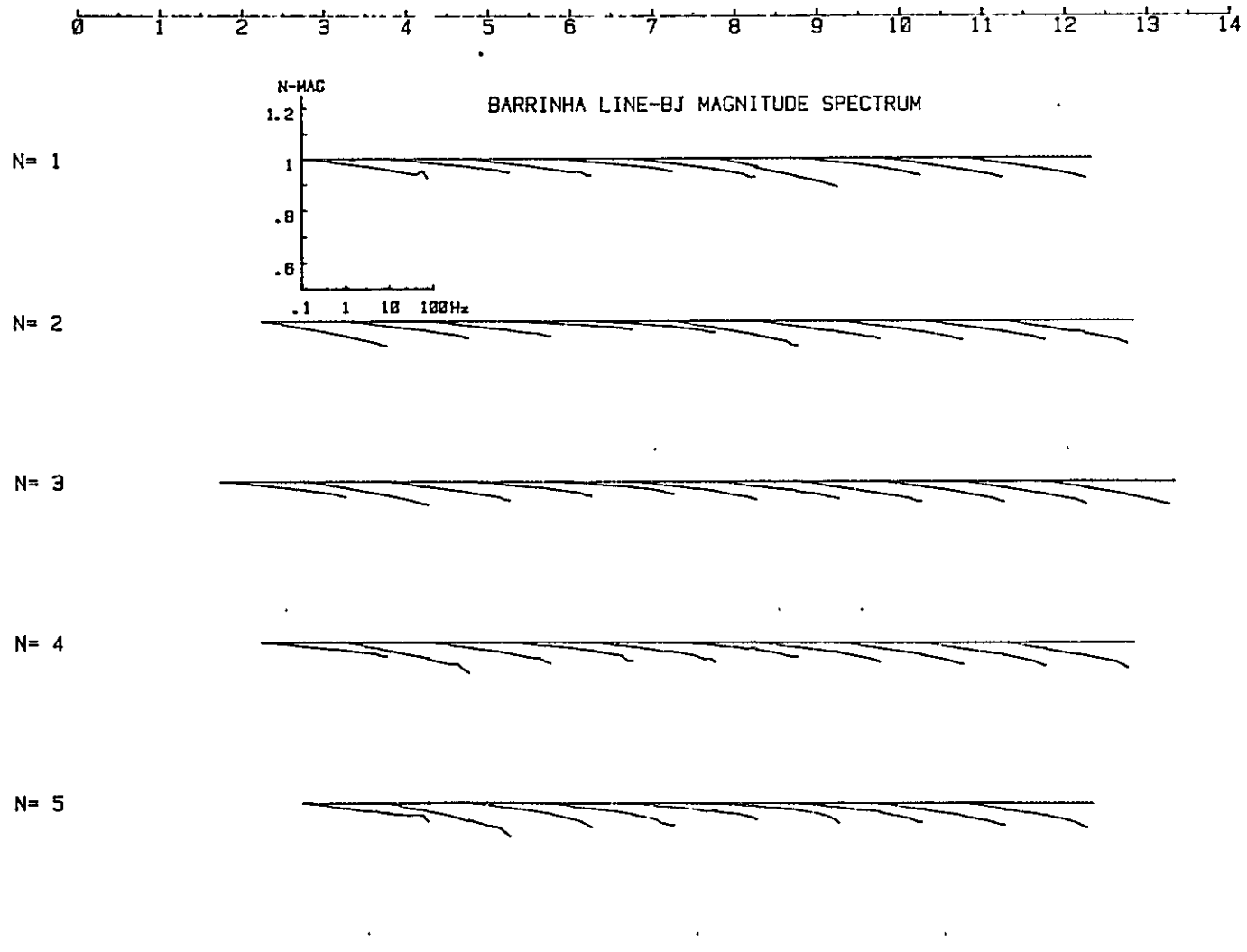

Fig. Ⅱ—3—36 Magnitude Spectrum (Line-BJ)

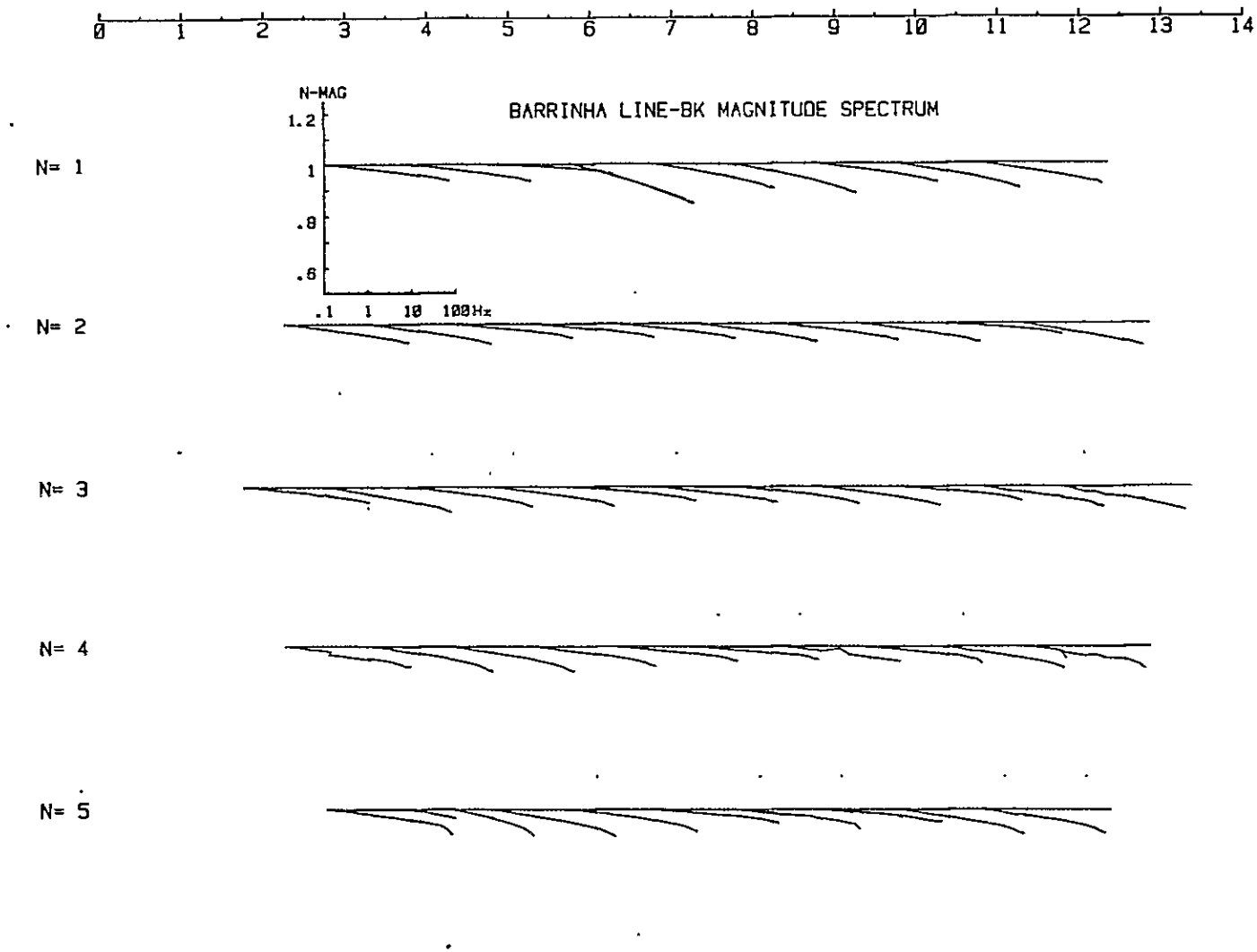

Fig. Ⅱ—3—37 Magnitude Spectrum (Line-BK)

PART Ⅲ DRILLING SURVEY

CHAPTER 1 SUMMARY OF DRILLING

1–1 Purpose of the Survey

As the result of geological survey and geophysical survey of the second year in the Anta Gorda area, the Perau area was extracted for the survey area in the third year.

The drilling survey was conducted to clarify the relation between the geologic structure and mineralization in the area.

1–2 Summary of Operation

The drilling of 500 meters at No.1 hole (AG–01) and 400 meters at No. 2 hole (AG–02) were initially planned. However, as the result that a promising mineralized zone was intersected in both holes, the length of both holes initially planned was changed and drilled an additional hole of No.3 (AG–03).

The depth of each hole drilled are 331.15 m. in the hole AG–01, 330.55 mm. in AG–02 and 250.50 m. in AG–03.

The drilling works of the survey at the site were carried out by Companhia de Pesquisa de Recursos Minerais (CPRM), a Brazilian company for exploration, and Bishimetal Exploration Co., Ltd. supervised the works at the site, and conducted logging and analytical research.

A Japanese member dispatched from Tokyo in advance of others on 2 July, 1982, entered the Perau area on 9 July to select the site for drilling.

Construction of the road of 2.5 kilometers for transportation of mechanical equipment and materials was commenced on 12 July by using bulldozer (Catapillar D5), and it was completed on 20 July.

Construction of the access road to the additional station of the Hole AG–03 of about 300 meters was completed on August 16. Two machines of Boyles-56 (drilling capacity of 600 m. by NQ size and 1,000 m. by BQ size) were used to drill three holes of total length of 912.20 meters.

The drilling works were carried out by two shifts of each 10 hours. Wireline method was used for drilling to improve core recovery and the progress of works.

The amount of drilling works was as follows.

Hole	Drill length	Core length	Core recovery*
AG–01	331.15 m.	326.20 m.	98.50%
AG–02	330 55	299.90	96.26
AG–03	250.50	238.35	98.69

The period of drilling was 63 days from July 27 to September 27.

1–3 Logging and Analysis Works

The investigation was carried out on rock facies, rock alteration and mineralization for all the core recovered, and these were compiled to the geological columnar section of 1 · 200 scale (PL. III–1 ~ 3).

The part of ore of the core was sampled by splitting it into halves using a rock cutter, and a half of them was prepared for chemical analysis. The analysis was made for the elements such as Cu, Pb, Zn, Ag, CaO, MgO, SiO_2, and BaO.

Thin sections of the rocks and polished section of the ore samples were observed under the microscope.

The contents of analytical research and the numbers are as follows.

(1) Microscopic observation of the thin sections 26

(2) Microscopic observation of the polished sections 13

(3) Chemical analysis of the ore samples (Pb, Zn, Cu, Ag, CaO, MgO, SiO_2, and BaO) 37

* Note.– The lenth of overburden is not included in the claculation of core recovery

CHAPTER 2 DIAMOND DRILLING WORK

2–1 Access Road for Transporting Equipment and Materials

A Japanese member left Tokyo on July 2, 1982 in advance of others arrived at Perau and made preliminary survey of the drill site. Based on the result of the survey, a preliminary arrangement was made as to the new construction of access road and the plan for maneuvering in cooperation with the staffs of CPRM in charge of the drilling.

For the access, a road of 2.5 kilometers long and 3.5 meters wide was constructed using a bulldozer (Caterpillar 5–D). Because of a steep topography in the mountainous area with the altitude of 400 to 700 meters above sea level and the heavily wooded hill, and because of the soft ground immediately after the rainy season, the work of the excavation of the road was considerably difficult.

2–2 Location of the Drill Holes

The site of drilling was situated to the West of the Perau mine, about 25 kilometers from Adrianopolis in Paranas State. It takes about an hour from there to the site by car.

The location of the drill holes and the altitude are shown in the following Table.

Hole	Distance in longitude	Distance in latitude	Altitude a.s.l.	Survey line (IP)
A–01	701.29 E	7251.10 N	490 m.	G–line – 8.3
AG–02	701.49 E	7251.21 N	592 m.	G–line – 10.5
AG–03	701.50 E	7251.03 N	548 m.	9.8, midway between the lines of G and H

2–3 Preparation Works

2–3–1 Transportation of Mechanical Equipment and Material

Mechanical equipment and materials, and the operators were transported by a truck of a large size and a pick-up truck from Poço de Cardas and Belo Horizonte to the drill site on July 20 and August 30 respectively.

2–3–2 Preparation

The preparation was started at AG–01. Leveling of ground for setting of the drill machine was made by a bulldozer. Leveling for the hole AG–02 was made during the drilling of AG–01, and construction of the access road to AG–03 and the leveling of the ground there were made after the completion of drilling work at AG–01.

2–3–3 Water Supply for Drilling

Water supply for drilling was obtained from a tributary of Ribeirão Grande which runs northward through the area of drill site, by damming up the stream and pumping up water to feed it for drilling.

The heads of pumping at each hole were 10 meters at AG–01, 112 meters at AG–02 and 68 meters at AG–03.

2–4 Drilling Works

Since the overburden of the area is relatively thin, the drilling was commenced by HQ wireline method. After encountering the bedrock, NQ wireline was used and the final diameter was BQ wireline.

The situations of each hole are described as follows (Fig. III–1–1~3).

2–4–1 AG–01

Drill length : 331.15 m.

Core length : 326.20 m.

Core recovery : 98.5% (excluding the overburden)

Commencement : July 26, 1982

Completion : September 1, 1982

0 – 0.55 m.

Overburden was drilling by HQ wireline method.

0.55 – 200.15 m.

Mica schist and amphibolite were penetrated by HQ–WL diamond bit using bentonite mud water.

Although the rock was stable in general, clay zones were encountered at the two sections of 186.60 m. ~ 187.70 m. and 189.60 m. ~ 189.90 m.

These clay zones caused jamming when drilling was being in progress at the depth of 200.15 meters, and the trouble suspended the drilling operation.

NQ–WL diamond bit was replaced at 157.30 m.

200.15 – 222.50 m.

The works for restoration such as pulling out of the pipe, washing of the hole, reaming of cement, and drilling were repeated. It took 11 days to restore the trouble.

The bit was changed to BQ–WL diamond bit at 222.50 m.

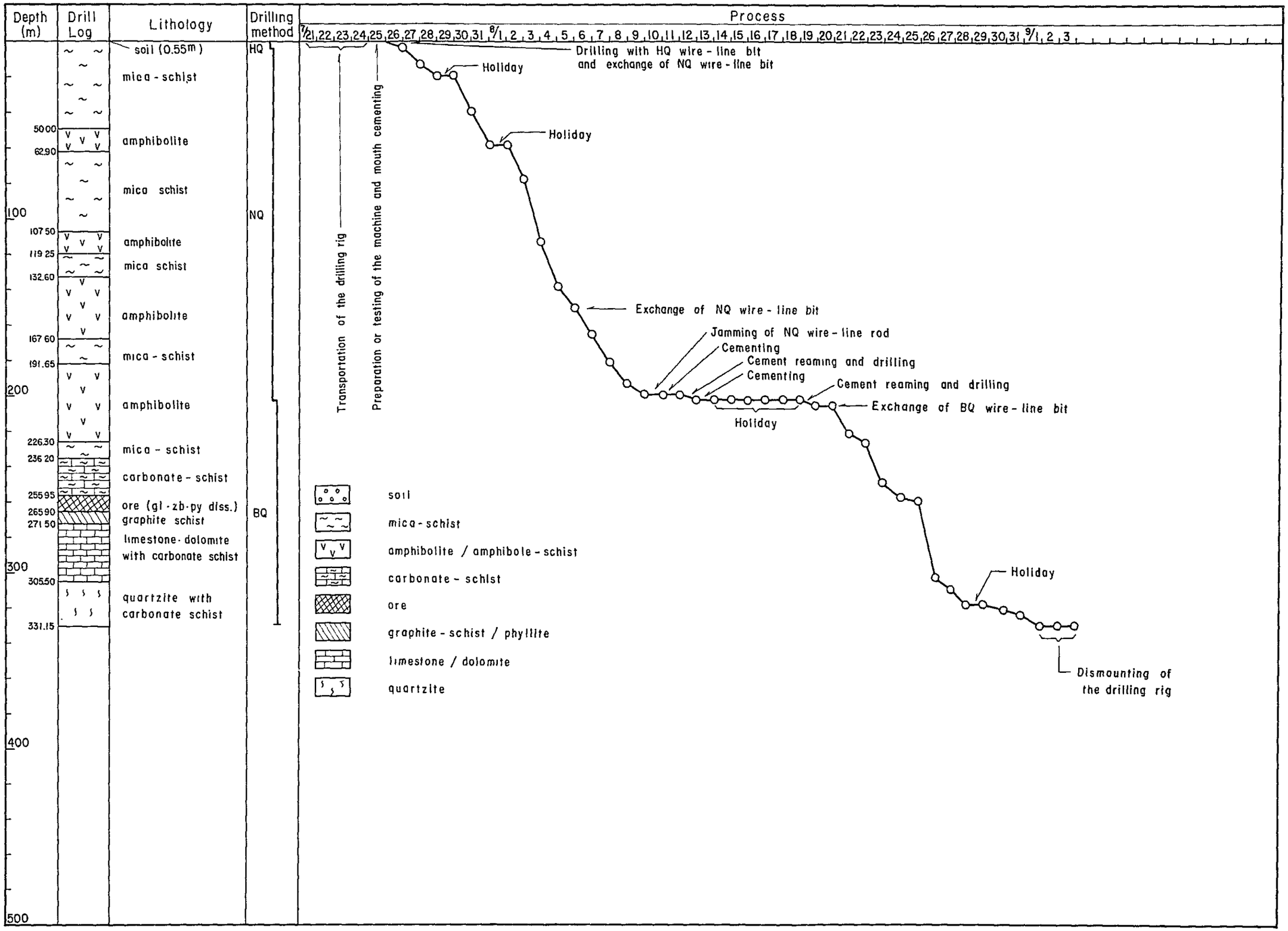

Fig. Ⅲ−1−1 Progress Record of Diamond Drilling AG-01

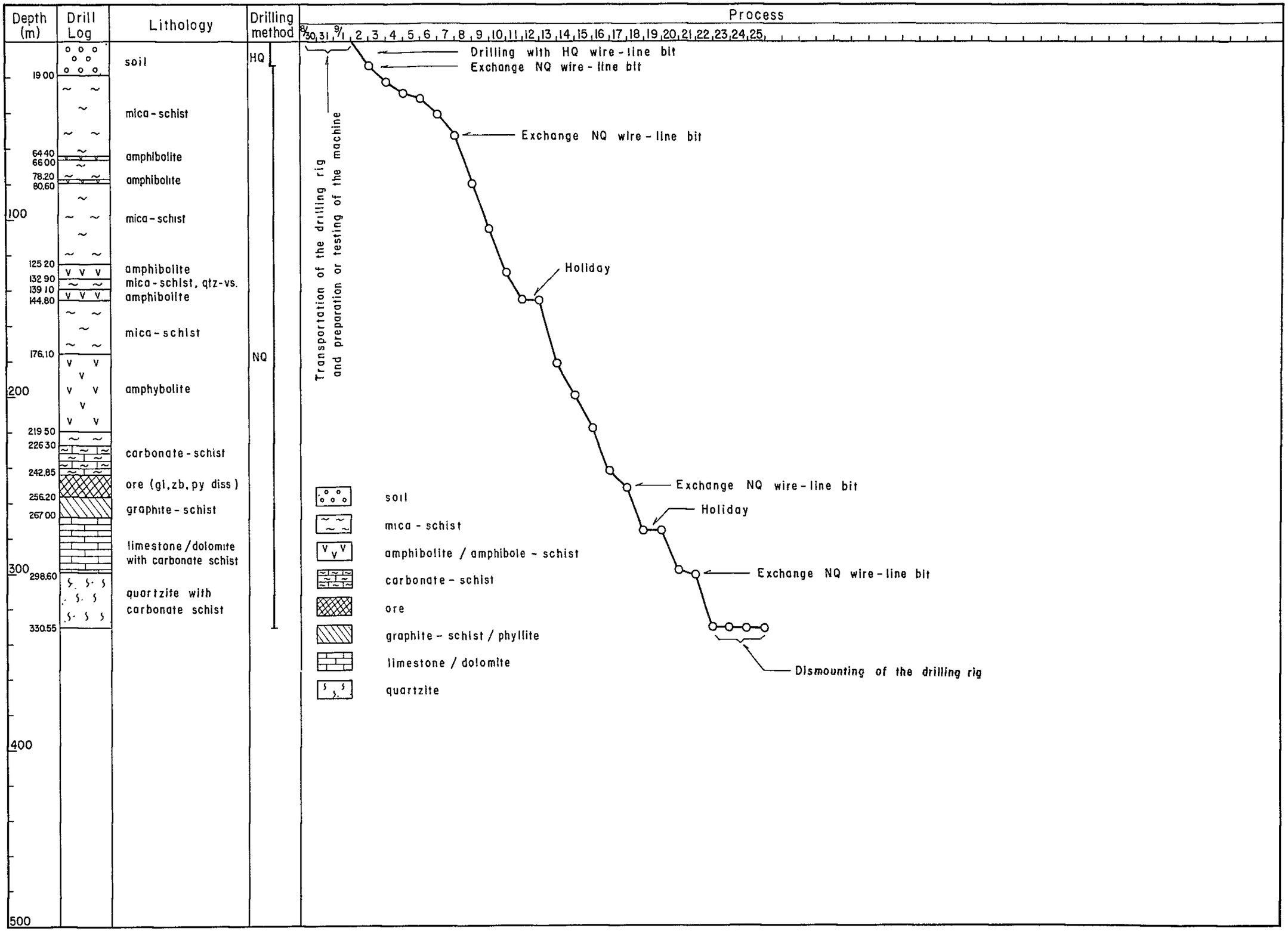

Fig. Ⅲ—1—2 Progress Record of Diamond Drilling AG-02

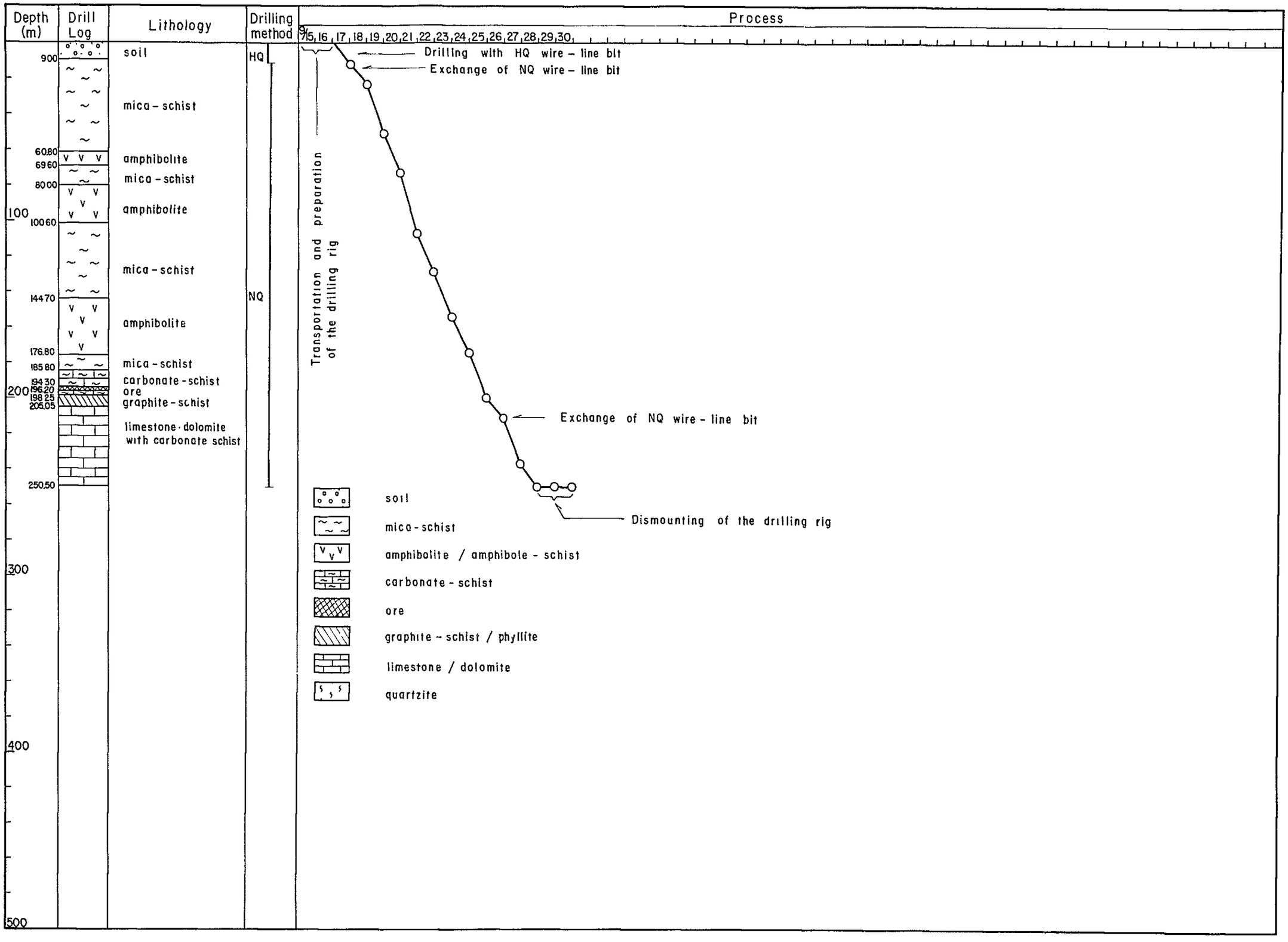

Fig. Ⅲ—1—3 Progress Record of Diamond Drilling AG-03

222.50 – 331.15 m.

Mica schist, amphibolite and carbonate rocks were drilled up to 255.95 m. by using BQ–WL diamond bit and bentonite mud water. Lead and Zinc ore zone was encountered at the section from 255.95 m. to 265.90 m.

After that, graphite schist to phyllite and limestone were drilled, and from 305.50 m., alternating beds of limestone and quartzite were commenced. Drilling was stopped when quartzite became more predominant.

2–4–2 AG–02

Drill length :	330.55 m.
Core length :	299.90 m.
Core recovery :	96. 26%(excluding the overburden)
Commencement :	September 2, 1982
Completion :	September 22, 1982

0 – 19.00 m.

Overburden was excavated by HQ–WL method using bentonite mud water. HQ casing was inserted and set since the rock became stable at 19 m.

19 – 330.55 m.

A stable rock facies of mica schist, amphibolite, carbonate rocks, graphite schist, limestone to dolomite and alternating beds of limestone and quartzite were drilled by using NQ–WL diamond bit and bentonite mud water. At the section of 242.85 to 252.50 m., lead and zinc ore zone was intersected.

It is considered that this zone is the extention of the ore zone intersected in AG–01 some days before.

NQ–WL diamond bit was replaced at 80.00 m., 251.90 m. and 298.70 m.

2–4–3 AG–03

Drill length :	250.50 m.
Core length :	238.35 m.
Core recovery :	98.69%(excluding the overburden)
Commencement :	September 17, 1982
Completion :	September 28, 1982